

# Geochemical and Petrographic Analysis of the Sparks Hill Diatreme and Its Relationship to the Illinois-Kentucky Fluorspar District

F. Brett Denny,<sup>1</sup> Anton H. Maria,<sup>2</sup> Joseph L. Mulvaney-Norris,<sup>3</sup> Renald N. Guillemette,<sup>4</sup> Richard A. Cahill,<sup>1</sup> Richard H. Fifarek,<sup>5</sup> Jared T. Freiburg,<sup>1</sup> and Warren H. Anderson<sup>6</sup>

<sup>1</sup>Illinois State Geological Survey, Prairie Research Institute, University of Illinois at Urbana-Champaign, <sup>2</sup>University of Southern Indiana, Department of Geology and Physics, Evansville, Indiana, <sup>3</sup>Washington State University, School of the Environment, Pullman, Washington, <sup>4</sup>Texas A&M University, Department of Geology and Geophysics, College Station, Texas, <sup>5</sup>Southern Illinois University, Department of Geology, Carbondale, Illinois, and <sup>6</sup>Kentucky Geological Survey, University of Kentucky, Lexington, Kentucky

Circular 588 2017



ILLINOIS STATE  
GEOLOGICAL SURVEY  
PRAIRIE RESEARCH INSTITUTE



ILLINOIS STATE GEOLOGICAL SURVEY  
Prairie Research Institute  
University of Illinois at Urbana-Champaign

**Front cover:** *Cathodoluminescence image of a fluorite vein transecting a dolostone clast (see Figure 9). Euhedral quartz crystals (dark gray) can be observed protruding into the vein, which is infilled with calcite (orange) and fluorite (purple).*

# Geochemical and Petrographic Analysis of the Sparks Hill Diatreme and Its Relationship to the Illinois-Kentucky Fluorspar District

F. Brett Denny,<sup>1</sup> Anton H. Maria,<sup>2</sup> Joseph L. Mulvaney-Norris,<sup>3</sup>  
Renald N. Guillemette,<sup>4</sup> Richard A. Cahill,<sup>1</sup> Richard H. Fifiarek,<sup>5</sup>  
Jared T. Freiburg,<sup>1</sup> and Warren H. Anderson<sup>6</sup>

<sup>1</sup>Illinois State Geological Survey, Prairie Research Institute, University of Illinois at Urbana-Champaign, <sup>2</sup>University of Southern Indiana, Department of Geology and Physics, Evansville, Indiana, <sup>3</sup>Washington State University, School of the Environment, Pullman, Washington, <sup>4</sup>Texas A&M University, Department of Geology and Geophysics, College Station, Texas, <sup>5</sup>Southern Illinois University, Department of Geology, Carbondale, Illinois, and <sup>6</sup>Kentucky Geological Survey, University of Kentucky, Lexington, Kentucky

Circular 588 2017



**ILLINOIS STATE GEOLOGICAL SURVEY**  
Prairie Research Institute  
University of Illinois at Urbana-Champaign  
615 E. Peabody Drive  
Champaign, Illinois 61820-6918  
<http://www.isgs.illinois.edu>

**Suggested citation:**

Denny, F.B., A.H. Maria, J.L. Mulvaney-Norris, R.N. Guillemette, R.A. Cahill, R.H. Ficarek, J.T. Freiburg, and W.H. Anderson, 2017, Geochemical and petrographic analysis of the Sparks Hill Diatreme and its relationship to the Illinois-Kentucky Fluorspar District: Illinois State Geological Survey, Circular 588, 51 p.

# CONTENTS

<b>Abstract</b>	1
<b>Introduction</b>	1
Background	1
Regional Geologic Setting	1
The Illinois-Kentucky Fluorspar District	4
Carbonatite and Rare Earth Elements in the Study Area	6
<b>Methods</b>	6
<b>Results</b>	7
Energy-Dispersive X-ray Fluorescence Spectrometry	9
Cathodoluminescence and Scanning Electron Microscopy–Energy-Dispersive X-ray Analyses of a Fluorite Veinlet	9
Electron Microprobe	10
Geochemical Analyses (Inductively Coupled Plasma Mass Spectrometry)	10
<b>Discussion</b>	17
Lamprophyre and Diatremes	17
Fluorite and the Illinois-Kentucky Fluorspar District	19
<b>Conclusions</b>	19
<b>Acknowledgments</b>	20
<b>References</b>	20
<b>Appendixes</b>	25
Appendix 1	25
Appendix 2	51
<b>Tables</b>	
1 Radiometric age determinations of ultramafic rock and breccia in southeastern Illinois and northwestern Kentucky	4
2 Generalized classification of lamprophyres with key mineral constituents	7
3 Energy-dispersive X-ray fluorescence spectrometry (ED-XRF) analyses of barium (Ba), lanthanum (La), and cerium (Ce) from the Sparks Hill Diatreme	10
4 Electron microprobe analyses of minerals within lamprophyres in the study area	12
5 Geochemical analyses of lamprophyres in the study area	14
6 Geochemical analyses of calcite and fluorite in the study area	15
A1 Legend	25
<b>Figures</b>	
1 Map showing the location of the Illinois-Kentucky Fluorspar District and the major tectonic relationships (adapted from Denny et al. 2008)	2
2 Map showing the crustal plate boundaries and Cretaceous-Tertiary alkalic magmatism proposed by Duke et al. (2014)	3
3 Geologic map of the Illinois-Kentucky Fluorspar District (adapted from Denny et al. 2008) with locations of the Sparks Hill Diatreme and sample locations for the rare earth element (REE) analyses contained in this report	5
4 Core photograph of lamprophyre with calcite veining	8
5 Core photograph of clast-supported diatreme containing primarily brecciated sedimentary autoliths	8
6 Core photograph of globular segregations composed of fine-grained igneous material enclosing occasional brecciated to rounded sedimentary clasts	9
7 Core photograph of diatreme showing a mixture of textures, including globular segregations	9
8 Plot of barium, cerium, and lanthanum concentrations in 2 ft (0.6 m) intervals from the Sparks Hill Diatreme core (2 cm <sup>2</sup> spots)	11
9 Core photograph of white dolostone bisected by a mineralized vein	11
10 (a) False-colored backscattered electron image from the sample at 1,344 ft (410 m). (b, c) Florencite with dolomite and quartz associated with open spaces or voids	13

11	Backscattered electron image showing apatite from 1,344 ft (410 m) in the Sparks Hill Diatreme with zonation along the edges	13
12	Plot of rare earth element (REE) concentrations from (a) igneous rock, (b) fluorite, (c) mixed fluorite and calcite, and (d) fluorite from the Cave-in-Rock subdistrict-bedded replacement ore	16
13	Binary plots of phlogopite titanium dioxide ( $\text{TiO}_2$ ) and aluminum oxide ( $\text{Al}_2\text{O}_3$ ) contents from ultramafic lamprophyres from the region and ultramafic lamprophyres within the Sparks Hill Diatreme (compositional fields and trends from Mitchell 1995)	18
A1	Photographs of the areas scanned for each energy-dispersive X-ray fluorescence spectrometry (EDX) analysis	25
A2	Graphic log of borehole USSH-3S	51

## ABSTRACT

Rock core from a drilling project that penetrated the Sparks Hill Diatreme was studied through several geochemical and petrographic methods in an effort to determine its provenance. The Sparks Hill Diatreme is primarily composed of rounded to subangular clasts of various sedimentary rocks set in a fine-grained igneous groundmass. A clast of igneous material is sometimes observed, but sedimentary clasts are dominant. Several intrusive phases are present in the core, and the intrusion is likely multiphase and related to the Permian ultramafic intrusions in the region. The Permian intrusions have commonly been classified as ultramafic lamprophyre, and several intrusions in the region have been described as explosive. Electron microprobe analyses indicate that rare earth element (REE) minerals (synchysite and florencite) are present, mainly as micrometer-size aggregates of crystals along the boundaries of other minerals crystalizing in open spaces. A calcite-quartz-pyrite-fluorite vein bisecting a well-rounded dolostone clast was observed. Fluorite crystalized only within the confines of the dolostone clast in the vein. To relate the REE minerals and fluorite, we compared REE plots of fluorite and an assemblage of igneous intrusive rocks from the Illinois Kentucky Fluorspar District (IKFD). The fluorite REE pattern for the Cave-in-Rock subdistrict within the IKFD exhibits a light REE (LREE)-depleted or convex-up shape, whereas the igneous rocks show an LREE-enriched pattern similar to those of other ultramafic igneous provinces. The mixed calcite and fluorite ore REE pattern occurs intermediate between the igneous and fluorite REE patterns. This relationship may indicate that the fluorite was originally sourced from the ultramafic igneous rocks and that the LREE-depleted pattern evolved through time and or distance from the source. Previous isotopic studies and fluid inclusion microthermometry and salinity investigations suggest that the ore within the IKFD precipitated from a fluid mixture that included a Mississippi Valley-type (MVT) brine. However, the anomalous concentration of fluorite in the IKFD ore is difficult to explain from a solely sedimentary brine source.

Primarily because of the REE minerals present in the diatreme and in fluorite at Hicks Dome, we suggest that the fluorine and REE minerals are linked with the ultramafic lamprophyre. The LREE-depleted pattern in fluorite in the Cave-in-Rock subdistrict may indicate a hydrothermal fluid of igneous origin, as proposed by Huang et al. (2007) for late-stage fluorite associated with carbonatite in China. Alternatively, the fluorine and REEs may have been leached by circulating groundwater migrating through a deep bedrock rift, which, studies indicate, may have been active toward the end of the Precambrian in this region. Because mixing of fluids is well documented in this ore district, the fluorine-rich IKFD ore fluids were likely formed through the mixing of multiple sources, including NaCl-rich "MVT brine" and hydrothermal and magmatic fluids associated with the ultramafic intrusions.

## INTRODUCTION

The Karbers Ridge Quadrangle lies along the northern edge of the Illinois Kentucky Fluorspar District (IKFD). The IKFD is commonly classified as a Mississippi Valley-type (MVT) deposit (Ohle 1959). By definition, MVTs are not associated with concurrent igneous activity (Leach et al. 2010). However, ultramafic igneous rocks are documented in several places within the IKFD and have been observed in several mines within the IKFD. An igneous intrusion, named the Sparks Hill Diatreme, is located southeast of Sparks Hill, Illinois, in the Karbers Ridge Quadrangle. Outcrop samples of the Sparks Hill Diatreme, analyzed by whole-rock methods for trace element geochemistry, contain anomalous concentrations of rare earth elements (REEs). The source of the REE anomaly was determined to be rare earth fluorocarbonate and rare earth phosphate minerals residing within the fine-grained igneous matrix between autolithic sedimentary clasts (Denny et al. 2010, 2015). This report describes the results of analyses of drill core through the Sparks Hill Diatreme and compares these results with ultramafic rocks and with fluorite ore from the IKFD.

## Background

The Sparks Hill Diatreme is located in Hardin County in southeastern Illinois, approximately 1.5 mi (2.4 km) southeast of Sparks Hill at latitude 37.568 and longitude -88.267. In the early 1900s, Sparks Hill was a small community with a post office, but presently only a cluster of houses remain. The namesake hill, located on the U.S. Geological Survey (USGS) Karbers Ridge 7.5-minute quadrangle map, forms a gentle east-west-trending cuesta capped by indurated Upper-Mississippian Period units.

During the fall of 1984, Ozark Mahoning Inc. drilled borehole USSH-3S through the Sparks Hill Diatreme to explore for fluorite. The hole was drilled 1,346 ft (410 m) in length and at a bearing of N 29° W on a 66° angle from horizontal. The Illinois State Geological Survey (ISGS) records indicate that three holes (USSH-1S, USSH-2S, and USSH-3S) were drilled from the same location but at different bearings. No core was found for holes USSH-1S and USSH-2S, but a map indicates that USSH-2S intercepted a series of dikes that strike northwesterly. The ISGS has only a portion of core USSH-3S, spanning the interval from 1,108 to 1,346 ft (338 to 410 m), consisting of approximately 236 ft (72 m) of core. The core is approximately 1.5 in. (38 mm) in diameter and is probably (BQ) size. The core description supplied by Ozark Mahoning subdivided the diatreme into gray and green dike, altered dike, and diatreme facies.

## Regional Geologic Setting

The study area lies in southern Illinois along the intersection of the Neoproterozoic to Early Paleozoic Era Reelfoot Rift and the Rough Creek Graben (Figure 1). Near-surface bedrock is composed of Devonian rocks at the apex of Hicks Dome with younger Carboniferous rocks along the periphery of the dome and even younger Tertiary and Cretaceous rocks to the southwest near the Illinois-Kentucky border. The Sparks Hill Diatreme is situated on the northeast flank of Hicks Dome, a large structural uplift cored by ultramafic alkaline dikes and intrusive breccias. The region has been structurally affected by several events from Cambrian through Quaternary

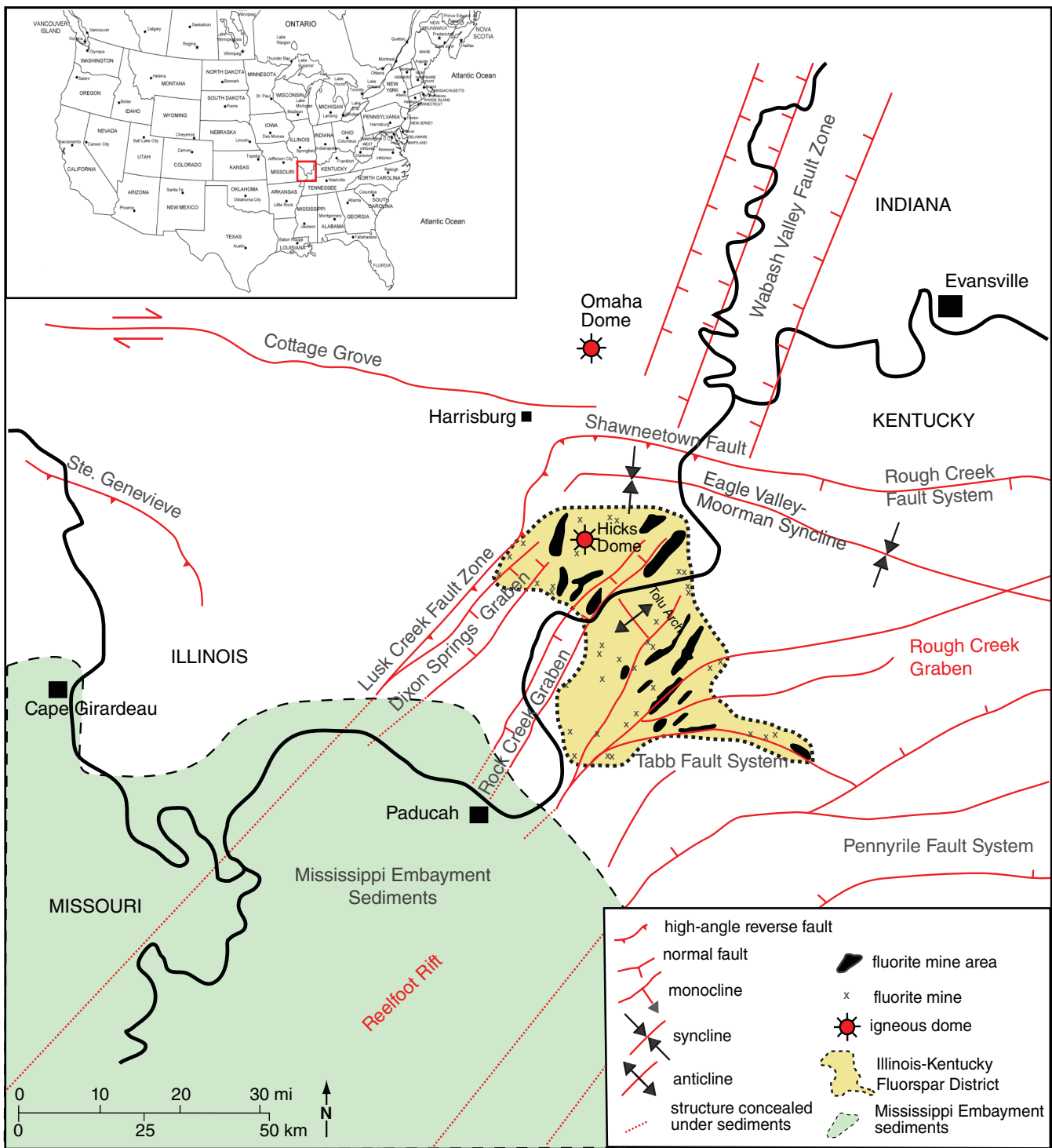


**Figure 1** Map showing the location of the Illinois-Kentucky Fluorspar District and the major tectonic relationships (adapted from Denny et al. 2008).

time (Nelson 1995; Nelson et al. 1999). Seismic surveys indicate that growth faults are present within the Cambrian sedimentary section in the Rough Creek Graben (Bertagne and Leising 1991),

indicating that a structural flexure was developing during the Cambrian. Post-Pennsylvanian compressional, and possibly strike-slip, movements are indicated along the Reelfoot Rift that

may be related to uplift of the Pascola Arch to the south (Howe and Thompson 1984). Igneous activity differentially uplifted the region along the Tolu Arch

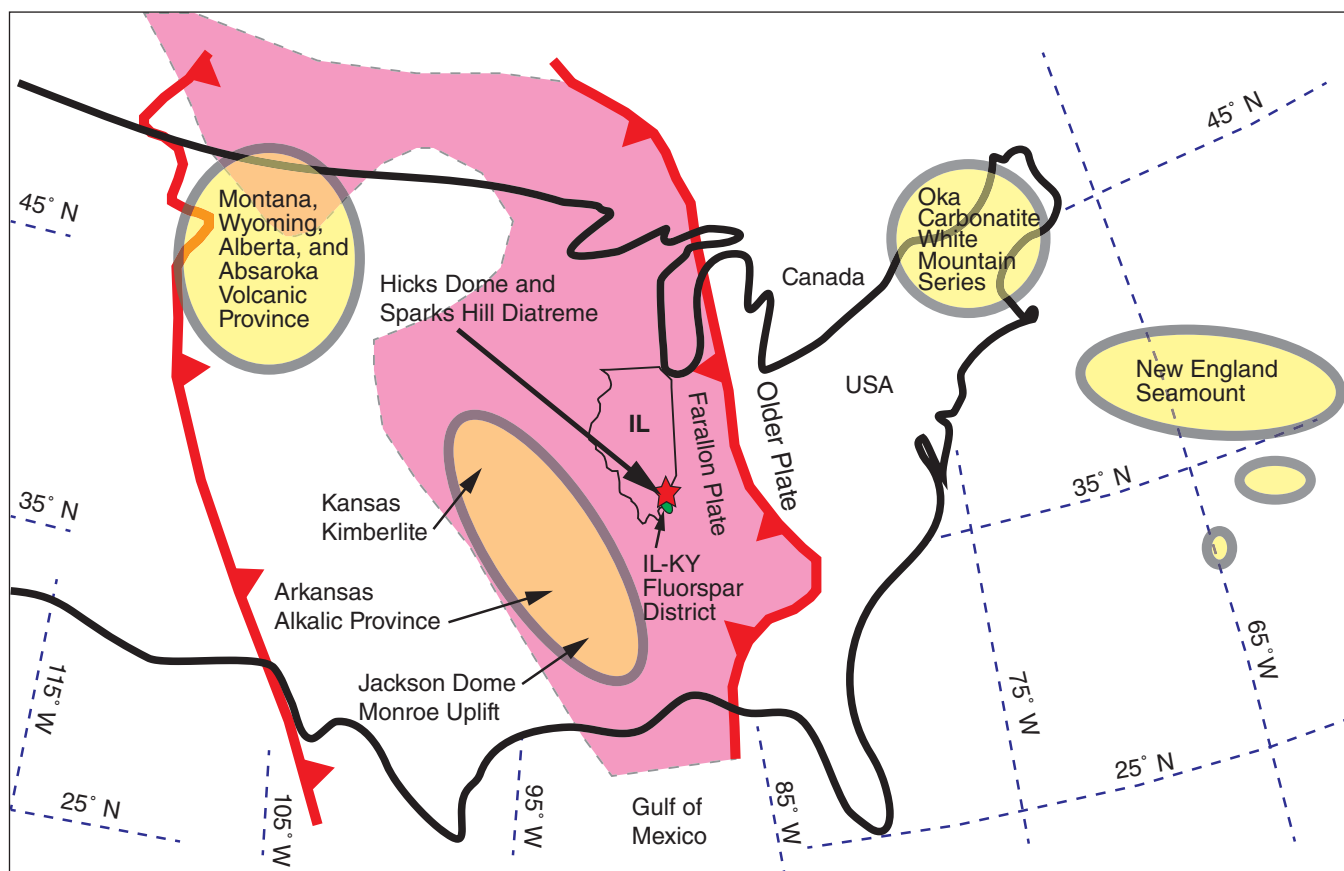


**Figure 2** Map showing the crustal plate boundaries and Cretaceous-Tertiary alkalic magmatism proposed by Duke et al. (2014).

and at Hicks Dome during the Permian. Finally, Cretaceous and Quaternary tectonic movements, predominantly strike-slip pull-apart structures, are documented by faults of the Fluorspar Area Fault Complex (Nelson et al. 1999). The overprinting of multiple tectonic events along with the igneous activity and subsequent subsidence have created extremely complex geologic relationships within this portion of the Midcontinent. Duke et al. (2014) suggested that Cretaceous through Tertiary kimberlite-carbonatite magmatism along a N 40° W linear zone 1,243 mi (2,000 km) to the west from Louisiana to Alberta reflects mantle upwelling through subducted slab windows associated with the convergent boundary system (Figure 2). Although the age of this alkalic magmatism is Cretaceous-Tertiary, the Permian-age dikes within the study area for this paper also trend in a north-northwest direction and more

or less parallel the Cretaceous-Tertiary alkalic trend.

Ultramafic igneous intrusions and diatremes have been discovered in the study area stretching in a north-northwest direction for more than 50 mi (80 km) from western Kentucky to the Omaha Dome in southeastern Illinois. Ultramafic lamprophyres have been documented in underground coal mines in southern Illinois, in several localities along the Tolu Arch, and at Hicks Dome. The Tolu Arch (Baxter et al. 1963) is a broad regional arch that trends north-northwest from northwestern Kentucky to southeastern Illinois. The presence of north-northwest-trending ultramafic dikes and the attitude of sedimentary beds in the area suggest that the Tolu Arch may be a result of magmatic intrusions (Nelson 1995). The ultramafic intrusions exhibit a strong magnetic contrast with the sedimentary host rocks of the region. An aeromagnetic

survey of the region identified several strong circular magnetic anomalies and several linear northerly-trending features that have been modeled as ultramafic dikes, sills, and pipes (Hildenbrand and Ravat 1997). The Coefield magnetic anomaly (also called the Lollipop magnetic anomaly) and the Cottage magnetic anomaly (Hildenbrand and Ravat 1997) exhibit the largest magnetic contrasts (Figure 3). Seismic investigations by Potter et al. (1995) suggest that the Permian igneous activity may intrude into the Paleozoic section in places, but in other places may reside only within the Precambrian section. Precise estimates of the size and extent of the Permian ultramafic intrusion are complicated by a lack of data, possibly attributable to the depth of emplacement.

The ultramafic rocks in this region have traditionally been classified as lamprophyre where the primary minerals are

**Table 1** Radiometric age determinations of ultramafic rock and breccia in southeastern Illinois and northwestern Kentucky (after Morehead 2013)

Age (Ma)	Analytical method	Location	Author(s)
258 ± 13	K-Ar on biotite	Grants Intrusive, SE of Hicks Dome	Zartman et al. (1967)
261 ± 9	K-Ar	Cottage Grove Dike peridotite, Illinois	Nelson and Lumm (1984)
267.8 ± 1.3	<sup>40</sup> Ar/ <sup>39</sup> Ar plateau date on phlogopite	Hutson Mine, Kentucky	Fifarek et al. (2001)
269.4 ± 0.4	<sup>40</sup> Ar/ <sup>39</sup> Ar plateau date on phlogopite	Hamp Mine intrusive breccia, Illinois	Fifarek et al. (2001)
269.61 ± 0.39	<sup>40</sup> Ar/ <sup>39</sup> Ar plateau date on phlogopite	Cottage Grove Dike, Cottage Grove, Illinois	Fifarek et al. (2001); Denny (2005)
271.0 ± 0.3	<sup>40</sup> Ar/ <sup>39</sup> Ar plateau date on phlogopite	Davenport Mine, Kentucky	Fifarek et al. (2001)
271.7 ± 0.7	<sup>40</sup> Ar/ <sup>39</sup> Ar plateau date on biotite	Grants Intrusive, SE of Hicks Dome	Snee and Hayes (1992)
272.1 ± 0.7	<sup>40</sup> Ar/ <sup>39</sup> Ar plateau date on amphibole	Grants Intrusive, SE of Hicks Dome	Reynolds et al. (1997)
272.7 ± 0.7	<sup>40</sup> Ar/ <sup>39</sup> Ar isochron on biotite	Grants Intrusive, SE of Hicks Dome	Snee and Hayes (1992)
272.7 ± 0.7	<sup>40</sup> Ar/ <sup>39</sup> Ar isochron on phlogopite	Grants Intrusive, SE of Hicks Dome	Reynolds et al. (1997)
275 ± 24	Rb-Sr on biotite	Downeys Bluff Sill, Hardin County, Illinois	Reynolds et al. (1997)
281 ± 14	K-Ar on hornblende	Grants Intrusive, SE of Hicks Dome	Zartman et al. (1967)

highly altered or as mica peridotites where olivine can be observed (Weller et al. 1952). Several attempts to classify the igneous rocks further have been undertaken. Lewis and Mitchell (1987) classified the ultramafic rocks of this province as alnöite, and Sparlin and Lewis (1994) suggested that some should be classified as monticellite-alnöite. Denny (2005) examined the Cottage Grove Dike in an underground coal mine in Saline County, Illinois, and agreed with Lewis and Mitchell (1987) and Sparlin and Lewis (1994) that the rocks should be classified as alnöite. Maria and King (2012) examined an ultramafic rock in a surface coal mine exposure in Illinois and suggested that the rock was a mela-aillikite. Morehead (2013) studied similar rocks around Hicks Dome and suggested that more than one igneous lithotype is present in this region. These highly altered rocks are certainly ultramafic lamprophyres, but a more detailed classification is difficult because of widespread alteration of the primary minerals. Morehead (2013) may be correct in assuming several ultramafic phases are present in the region, but radiometric age determinations by several authors (Table 1) concur that the ultramafic activity in southern Illinois and western Kentucky occurred during a relatively narrow time frame from Early to Middle Permian (Guadalupian Series). Other alkaline intrusions along the New Madrid Rift in Tennessee and

Missouri indicate a Mesozoic emplacement (Moody 1949; Kidwell 1951), and the Avon Diatreme in Missouri is thought to be Devonian intrusions (Shavers et al. 2016).

The explosive and ultramafic igneous activity in this region is proposed to be related to a northeast-southwest extension of the North American Plate along the Reelfoot Rift accompanied by partial melting of the mantle during the Permian (Fifarek et al. 2001). The geochemistry of these ultramafic intrusions is consistent with near primary melts from a metasomatized peridotite source containing phlogopite veins (Maria et al. 2016). Strontium (Sr)-neodymium (Nd) isotope compositions are consistent with a uniform mantle source, with no evidence of crustal contamination. Maria et al. (2016) suggested, based on samarium (Sm)-Nd-depleted mantle model ages (TDM), that source rocks of the Permian ultramafic rocks were from a lithospheric mantle that was metasomatized during the breakup of Rodinia approximately 540–624 million years ago (Ma).

Hicks Dome is a north-northwest-trending oval uplift, several kilometers in diameter, along the northern end of the Tolu Arch (Figure 3). The amount of stratigraphic uplift along this feature in southern Illinois is more than 4,000 ft (1,219 m; Nelson 1995). Sedimentary bedrock at Hicks Dome dips from a few

degrees to considerably more than 20°. Baxter et al. (1967) identified 25 separate dikes, sills, and breccia pipes at Hicks Dome. Bradbury and Baxter (1992) classified three types of igneous breccia near the apex of the dome based on clast geometry and composition: (1) vent breccias, (2) carbonatitic breccias, and (3) shatter breccias. The shatter breccias are dike-like intrusive bodies containing angular to subrounded clasts of country rock that were ripped up and incorporated during ascent. Carbonatitic breccias are composed of both igneous and sedimentary clasts set in a matrix of igneous carbonate. Bradbury and Baxter (1992) suggested that this style of breccia is a result of an explosive release of carbon dioxide (CO<sub>2</sub>)-rich gas exsolving from an alkaline ultramafic magma at depth. Vent breccias are described as bodies of indeterminate form, usually silicified, often containing sedimentary fragments originating from great depths. Brown et al. (1954) suggested that igneous intrusions at Hicks Dome interacted with near-surface groundwater to produce steam-fed (phreatomagmatic) explosive phases.

#### The Illinois-Kentucky Fluorspar District

Mississippian rocks that rise to the surface along the crest of the Tolu Arch and along the flanks of Hicks Dome in Hardin County, Illinois, are the host

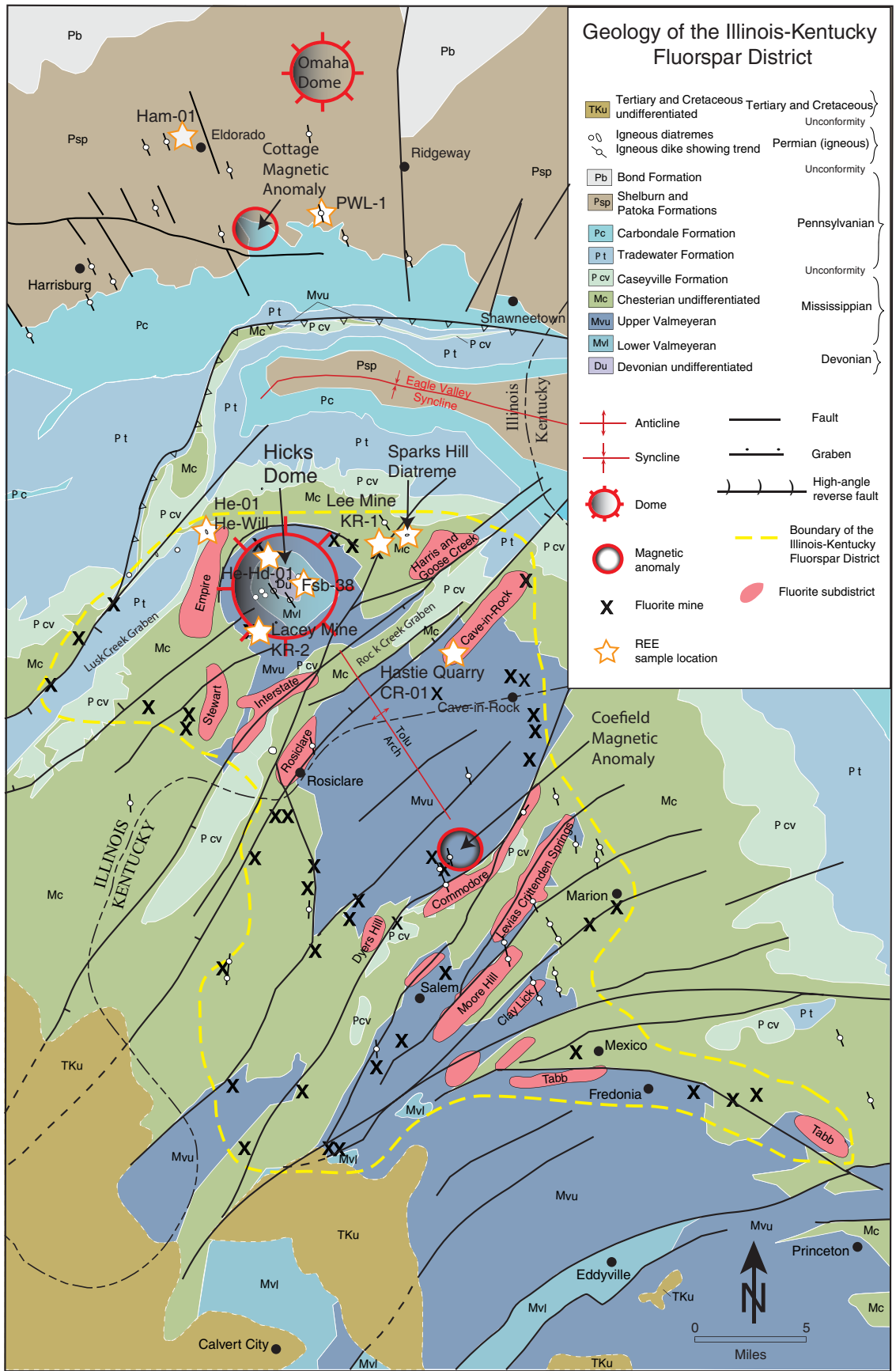


**Figure 3** Geologic map of the Illinois-Kentucky Fluorspar District (adapted from Denny et al. 2008) with locations of the Sparks Hill Diatreme and sample locations for the rare earth element (REE) analyses contained in this report.

rocks for the majority of the IKFD ore. Minerals commonly found in the ore bodies include fluorite, sphalerite, galena, calcite, dolomite, barite, pyrite, chalcopyrite, and quartz. Fluorite mineralization is dominant, occurring as bedding replacement deposits and vein deposits along vertical or nearly vertical faults. More than 7 million tons of fluorite have been produced from the IKFD, making it the largest fluorite district in the Western Hemisphere (Goldstein and Williams 2008).

Geologists working in early fluorite mines of the IKFD documented the presence of dikes and sills and assumed the igneous rocks had a direct genetic relationship with the fluorite mineralization (Bastin 1931; Weller et al. 1952). Studies of fluid inclusions in fluorite indicate that the fluid inclusions have salinities similar to present-day oil field brines and have homogenization temperatures between 70 and 160 °C (Freas 1961; Hall and Friedman 1963; Pinckney and Rye 1972; Richardson and Pinckney 1984). Because the fluid inclusion salinities and homogenization temperatures in the IKFD are similar to those in other MVT deposits, and because the IKFD fluorite ore contains lead and zinc minerals, some modern researchers consider the IKFD ore deposits to be MVT deposits (Ohle 1959). Spry et al. (1990) postulated, based on fluid inclusion data, the mixing of at least three ore solutions. Pinckney and Rye (1972) also argued for multiple hydrothermal episodes in the Cave-in-Rock subdistrict of the IKFD, based on oxygen and carbon isotope data. Using Sr isotope data, Ruiz et al. (1988) determined that at least two fluids were present and dated the mineralization to be approximately 200 Ma. Spry and Fuhrmann (1994) determined that at least three different fluids were responsible for the bedded replacement ore in the Cave-in-Rock subdistrict, based on fluid inclusion microthermometry. A possible genetic relationship to magmatism is supported by the helium-3 (<sup>3</sup>He) isotopic ratios of fluid inclusions from IKFD fluorite (Kendrick et al. 2002) and the age of fluorite mineralization as determined by Sm-Nd isotopic systematics (Chesley et al. 1994). Morehead (2013) characterized the carbon and oxygen isotopic ratios of car-

bonate in veins and the matrix of igneous rocks at Hicks Dome as transitional between primary magmatic values and reference values for unaltered Mississippian limestone. Hence, Morehead (2013) proposed that veins of carbonate at Hicks Dome are a product of primary magmatic carbonate “carbonatite” that was modified by magmatic-hydrothermal alteration and by low-temperature alteration from IKFD fluids.

#### **Carbonatite and Rare Earth Elements in the Study Area**

The presence of a carbonatite intrusion at depth beneath Hicks Dome was postulated by Wall and Mariano (1996) based on the presence of microcrystalline aggregates of xenotime in fluorite. This carbonatite affiliation was apparently detailed in a confidential report on Hicks Dome by Mariano (1987). The presence of carbonatite at Hicks Dome was also noted by Long et al. (2010) in their compilation of U.S. REE deposits, but no reference for the source of this information was given. Bradbury and Baxter (1992) described carbonatitic breccias at Hicks Dome and proposed the carbonate to be of magmatic origin. Morehead (2013) also suggested that a carbonatite is present in the Hicks Dome area.

Trace (1960) used X-ray diffraction to identify monazite and florencite collected from surface trenches at Hicks Dome and identified low levels of radioactivity. In hand-picked monazite samples, thorium was measured through quantitative spectrographic analysis to be 4.4 wt% and uranium to be 0.008 wt% (Trace 1960). Utilizing electron microprobe techniques, Denny (2005) determined the elemental compositions of several minerals in an ultramafic rock from Saline County, Illinois. The concentrations of cerium oxide and lanthanum oxide within 16 perovskite crystals in the Cottage Grove Dike range from 0.24 to 1.01 wt% and 0.13 to 0.39 wt%, respectively. Additionally, core-rim analyses of perovskite indicate concentrations in the cores of crystals to be twice as high as in the rims. Electron microprobe images show several perovskite crystals as having embayed borders as well as apparent replacement by a calcium (Ca)-aluminum (Al) sili-

cate mineral. A whole-rock analysis of the Cottage Grove Dike identifies the following REE concentrations (all values in parts per million, ppm): lanthanum (La) 103, cerium (Ce) 206, praseodymium (Pr) 23.9, Nd 93, Sm 15.7, europium (Eu) 4.66, gadolinium (Gd) 10.7, terbium (Tb) 1.4, dysprosium (Dy) 6.4, holmium (Ho) 0.9, erbium (Er) 2.1, thulium (Tm) 0.22, ytterbium (Yb) 1.2, and lutetium (Lu) 0.16. Unpublished semiquantitative data for the Philadelphia School Dike shows the following REE values: La 1,500, Ce 1,700, and Nd 370 ppm. Other reported REE values from igneous rocks and fluorite in the area are given by Denny et al. (2015), and REE analyses of fluorite from the Cave-in-Rock District were conducted by Chesley et al. (1994).

## **METHODS**

The core from the Sparks Hill Diatreme was cut lengthwise with a diamond saw and washed with water. Because the original wooden core boxes were in poor repair, the core was reboxed after splitting. The core from this borehole is nearly complete from 1,108 ft (338 m) through 1,346 ft (410 m), although some core loss (which probably occurred during drilling) is evident (Appendixes 1 and 2). Several standard thin sections of the core were produced at the ISGS core laboratory. The core and thin sections from Sparks Hill were examined through (1) standard optical methods, (2) energy-dispersive X-ray fluorescence spectrometry (ED-XRF), (3) electron microprobe backscattered images, (4) geochemical analysis, (5) cathodoluminescence (CL) microscopy, and (6) scanning electron microscopy-energy-dispersive X-ray (SEM-EDS) analysis.

Concentrations of Ba, Ce, and La were determined by ED-XRF at the ISGS. The X-ray activity was determined by counting the X-ray emissions of a sample with a lithium-drifted 30 mm<sup>2</sup> silicon crystal detector. A 2 cm<sup>2</sup> area of the core surface was selected and was bombarded with X-rays from a 300 mCi americium-241 (<sup>241</sup>Am) source using a Dy secondary target, which induces fluorescence and the emission of secondary X-rays. Concentrations of Ba, La, and Ce were determined relative to standard reference materials from the USGS and

National Institute of Standards and Technology (NIST). In addition, an REE standard graciously provided by the Great Western Minerals Group Limited was analyzed. The Great Western Minerals Group Limited obtained the standard from the Saskatchewan Research Council Geoanalytical Laboratories. The values determined from the standards are (all in ppm): Ba 106, 113 (accepted value 112); Ce 946, 910 (value 843); and La 506, 495 (value 529). Three intervals containing the highest REE concentrations observed from the ED-XRF were selected for electron microprobe analysis.

Standard polished thin sections from core USSH-3S at 1,120 ft (341 m), 1,165 ft (355 m), and 1,344 ft (410 m) were coated with carbon and analyzed with a Cameca electron microprobe at Texas A&M University. The electron beam current was 15 kV, and unknown minerals were compared with reference standards. The primary focus of the electron microprobe study was to determine the composition of the fine-grained matrix and to determine where the REEs reside in the samples.

Major oxide and trace element analytical results were obtained for several fluorite and igneous rock samples from southern Illinois. These analyses were performed at ALS Laboratories (Vancouver, Canada) by the lithium-borate fusion technique for inductively coupled plasma mass spectrometry (ICP-MS) analysis.

Small millimeter-wide veins of fluorite-pyrite-calcite-quartz were observed in the core at 1,083 ft (330 m). These veins were examined by CL microscopy and through SEM-EDS analysis to verify mineral compositions.

## RESULTS

The rock core from the Sparks Hill Diatreme was studied visually to characterize and classify the rock. The rock is composed of angular and rounded sedimentary clasts, largely sandstone, limestone, and shale, set in a fine-grained gray igneous matrix. Because of extensive alteration, formations from which the clasts originated are difficult to determine. Many of the clasts contain well-developed coronas or reaction rims with diameters ranging from several centimeters to less than a millimeter. The fine-grained matrix between the clasts could not be fully resolved optically but appear to be igneous, based on abundant visible laths of phlogopite. Very few of the “clasts” could be identified as igneous, but a few possible xenoliths of granite, probably from the Precambrian basement complex, were observed. Flow alignment of the matrix phlogopite laths is evident in some core intervals but absent in other sections. The core is crosscut in several places by thin veins of mainly calcite, but pyrite, chalcopyrite, and fluorite are also present. Vugs several millimeters in diameter lined with calcite, quartz, and small unidentified mafic crystals are also visible within the breccia matrix. Several intervals of dark green porphyritic “dike” material are present. Because of the fine texture, the only minerals readily identifiable in the dike phase are phlogopite and calcite. Further classification of the lamprophyre in this region may be possible if key minerals are identified (Table 2).

Through examination of the core, we observed several textural variations, which were designated as lamprophyre, diatreme, and breccia. Compositional information was added to this basic clas-

sification scheme by adding a modifier. For example, two compositional varieties observed in this core were quartz rich and carbonate rich. Care should be taken when applying modifiers because mineralization of these rocks may be due to secondary processes.

**Lamprophyre** The lamprophyre is an intrusive “dike or sill phase” that occurs throughout the diatreme intercept. It commonly appears porphyritic, with phlogopite phenocrysts in a fine groundmass of mafic micas, euhedral apatites, relict pyroxenes, and probably olivine, carbonate, clay, and iron oxide minerals (Figure 4). Phlogopite is generally the only mineral identifiable in a hand specimen. Abundant calcite and other carbonate minerals are usually present, and the rock may effervesce in dilute hydrochloric acid. The color ranges from light to dark green. Alteration progressively lightens the color of the rock to light gray as the primary minerals are altered to clays, serpentine, or chlorite or are replaced by carbonate minerals. The lamprophyre phase is similar to other ultramafic dikes observed in the region, which also range in color from dark green to dark gray where relatively unaltered to light gray where intensely altered. The borders of a few of these intrusions show phenocryst (usually phlogopite lath) alignment parallel to the contact with country rock, encircling xenoliths, or both.

**Diatreme** The diatreme is divided into four subtypes: clast-supported diatreme, matrix-supported diatreme, globular segregation diatreme, and pelletal diatreme.

1. *Clast-supported diatreme (>90% clasts)*. The clast-supported diatreme texture is composed of greater than

**Table 2** Generalized classification of lamprophyres with key mineral constituents

Common mineral	Key mineral constituents
Lamprophyre	Biotite, amphibole, or both with or without olivine, pyroxene, or feldspars. Feldspar, if present, is restricted to the groundmass.
Minette	Lamprophyre with biotite or phlogopite and <i>potassium feldspar</i> .
Aillikite	Ultramafic lamprophyre with olivine, biotite or phlogopite, calcite, dolomite, <i>magnesian spinel</i> , perovskite, clinopyroxene, amphibole, garnet, apatite, and <i>no feldspars</i> .
Alnöite	Ultramafic lamprophyre with biotite/phlogopite, melilite, carbonates, perovskite, garnet, olivine, augite, Fe-Ti oxides, apatite, and <i>no feldspars</i> .

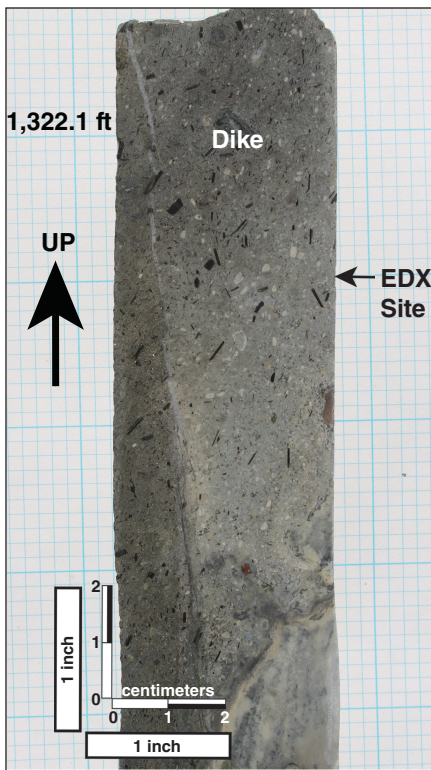


**Figure 4** Core photograph of lamprophyre with calcite veining. Laths are biotite crystals and the light gray portions show a higher degree of alteration. EDX, energy-dispersive X-ray fluorescence spectrometry.

90% clasts, which are predominantly rounded to subangular sedimentary clasts with a variable fraction of igneous xenoliths (Figure 5). Sedimentary clasts are typically altered limestone and sandstone, subangular in texture, and exhibit recrystallization rims extending 1 to 5 mm inward from the clast border. Sedimentary clast sizes range from several centimeters down to coarse sand, where they become indistinguishable from the matrix. The igneous matrix material is commonly fine- to medium-grained altered ultramafic material with a porphyritic texture of widely spaced phlogopite or biotite phenocrysts. Globular segregations and pelletal lapilli as well as rare altered granitic xenoliths are also present in this unit. The matrix of this unit is typically altered and contains small clasts, disaggregated sedimentary material, and secondary carbonate minerals. In thin sections, the effects of

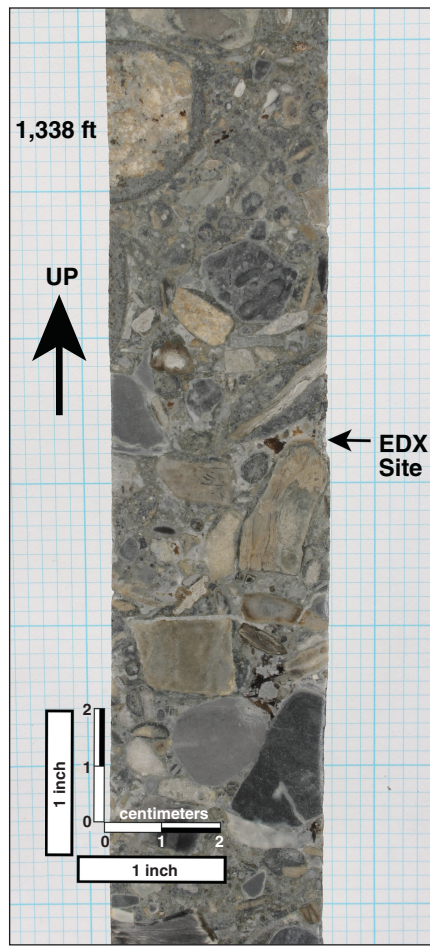


**Figure 5** Core photograph of clast-supported diatreme containing primarily brecciated sedimentary autoliths. EDX, energy-dispersive X-ray fluorescence spectrometry.

extensive carbonate and silica replacement are visible, leaving few primary textures. A clast-supported matrix and a few pelletal lapilli abutting angular sedimentary clasts are evidence of relocation and rapid transportation of the clasts.

2. *Matrix-supported diatreme (15%-50% matrix)*. This subtype consists of diatreme breccia with greater than 15% matrix material, which locally reaches 50% matrix. The clasts are subangular to rounded, highly altered, and recrystallized limestone and sandstone fragments. The matrix is a mixture of fine altered mafic minerals and small, highly altered sedimentary clasts. Pervasive serpentinization or chloritization gives this matrix a consistent

green color but with a mottled texture varying to lighter hues. Carbonate minerals are present throughout as secondary alteration, and patches of strong silicification can be found in the matrix and throughout the clasts.

3. *Globular segregation diatreme (rounded clasts without a nucleus) and nucleated globules (rounded clasts with a nucleus)*. Globular segregations are subrounded to well-rounded "clasts" of igneous origin devoid of a preferred crystal orientation (Figures 6 and 7). These rounded segregations, known as ocelli, range in size from a few millimeters to 2 cm in diameter and exhibit evidence of flow, such as flattening along the edges in contact with other globular segregations. Nucleated globular segregations typically show a random orientation of fine-grained igneous minerals. The nucleating clasts are commonly sedimentary, but igneous clasts are also present. Although this type of diatreme may contain pellets or xenoliths (sedimentary clasts in an igneous matrix), the igneous material surrounding the clasts does not show the encircling well-developed concentric fabric indicative of pelletal lapilli.

4. *Pelletal diatreme (round clasts with a nucleation grain)*. Pelletal lapilli are rounded to well-rounded spherical "clasts" of igneous origin with a core or pellet of a single clast surrounded by igneous material. The core pelletal clasts may also be angular to subangular limestone and sandstone fragments. The mantle can have a concentric, layered appearance with a preferred orientation of tabular crystals perpendicular to the radius. The aligned crystals are most often tabular phlogopite and euhedral apatite.

**Breccia and Autolithic Breccia** The breccia is clast supported with a stockwork of angular sedimentary rock clasts (>90% clasts) in a lamprophyre matrix. The angular nature of the clasts and less defined coronas and reaction rims distinguish this unit from the clast-supported diatreme texture. Sporadically present at the margins of the intrusive body as an intermediate unit between the country rock and the diatreme texture, the breccia subtype is thought to grade into the clast-supported diatreme material. Clasts of this breccia are

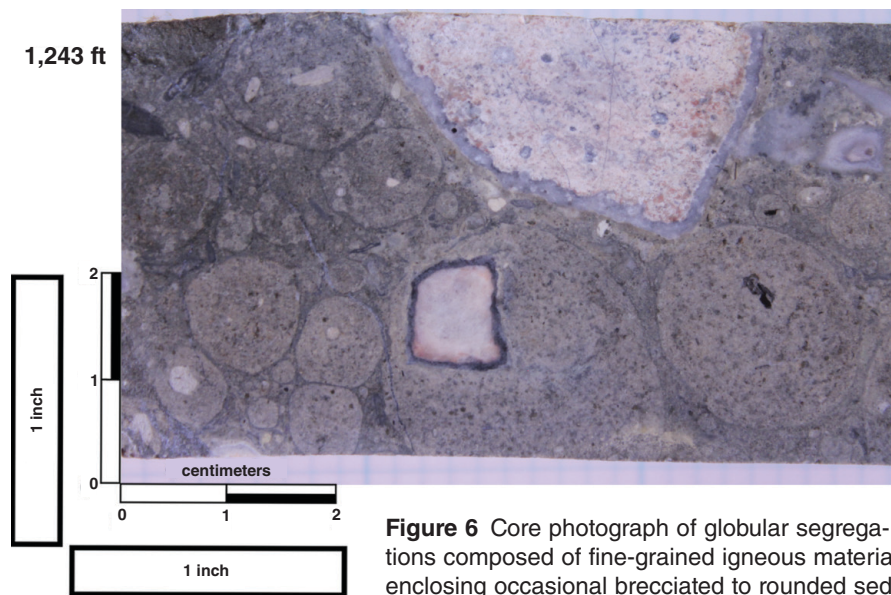


**Figure 6** Core photograph of globular segregations composed of fine-grained igneous material enclosing occasional brecciated to rounded sedimentary clasts. This texture is similar to pelletal lapilli but lacks the well-defined nucleated core present in pelletal lapilli.

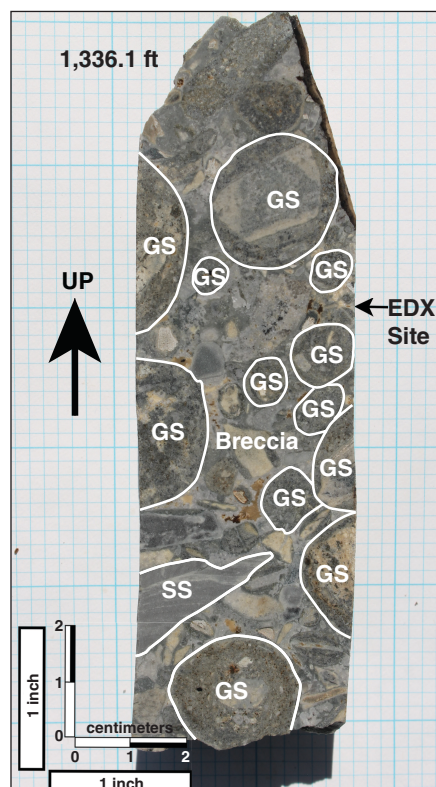


**Figure 7** Core photograph of diatreme showing a mixture of textures, including globular segregations. EDX, energy-dispersive X-ray fluorescence spectrometry; GS, globular segregation; SS, sandstone.

thought to have been transported relatively short distances from their sources. This unit would be analogous to the shatter breccia of Bradbury and Baxter (1992), which the authors attribute to rock bursting or explosive shattering of the rock in place.

### Energy-Dispersive X-ray Fluorescence Spectrometry

The core was scanned every 2 ft by ED-XRF for Ba, Ce, and La. The sample target for each ED-XRF analysis covers an area of 2 cm<sup>2</sup>. The resulting ED-XRF data (Table 3, Figure 8) represent an average of this entire 2 cm<sup>2</sup> area, reflecting mixtures of many minerals, rocks, veins, and other components. The general area of each ED-XRF analysis was photographed (Appendix 1) and examined macroscopically, and a description of the clasts and minerals present in each analyzed section was recorded. The column in Table 3 labeled “precise footage” shows the exact depth in feet at which the core was analyzed. This detail was deemed necessary to ascertain precisely which texture was associated with elevated values of Ba, Ce, and La. Earlier investigations of the Sparks Hill Diatreme (Denny et al. 2015) indicated that the REEs are concentrated within the matrix of the diatreme, suggesting that ED-XRF scans of samples that con-

tain fewer sedimentary clasts and more igneous matrix should contain higher concentrations of REEs. On the basis of the results of the ED-XRF analyses, samples from 1,120 ft (341 m), 1,164 ft (355 m), and 1,344 ft (410 m) were selected for further examination by electron SEM-EDS microscopy to determine the source of anomalous Ce and La.

### Cathodoluminescence and Scanning Electron Microscopy–Energy-Dispersive X-ray Analyses of a Fluorite Veinlet

Several small veinlets of fluorite-pyrite-calcite-quartz were observed in the core at 1,083 ft (330 m). One of the veinlets is a few millimeters wide and cuts the core at a very shallow angle along the length of the core, which was drilled at an angle of 66° from horizontal. The veinlets bisect a well-rounded dolostone clast that is approximately 3 cm wide. The rounding of the clast is probably due to transportation and impacts as the clast was mobilized by the volatile-rich diatreme intrusion. To characterize the fluorite vein and sequence of vein filling, we prepared a polished thin section to examine by CL microscopy.

The dolostone clast is surrounded by fine-grained igneous material, and a corona or reaction rim that appears to be a second generation of calcite is evident. The veins are composed of calcite, quartz, chalcopryrite, and pyrite on either side of the clast, but within the clast, the veinlet is composed primarily of fluorite with quartz and calcite along the veinlet margins (Figure 9). The CL and SEM-EDS analyses indicated an early quartz event consisting of prismatic quartz crystals up to 400 μm wide and 1.6 mm long that crystallized on the vein walls. Following the quartz growth event, minor chalcopryrite and pyrite crystallization occurred. Chalcopryrite and pyrite are more prevalent where the vein crosscuts igneous matrix, but they also occur as small crystals (chalcopryrite <300 μm; pyrite <150 μm) where the vein crosscuts the dolostone clast. Quartz, chalcopryrite, and pyrite are followed by a thin coating of calcite that lines the quartz, chalcopryrite, pyrite, and vein walls. Fluorite filling follows calcite. However, microfractures within

**Table 3** Energy-dispersive X-ray fluorescence spectrometry (ED-XRF) analyses of barium (Ba), lanthanum (La), and cerium (Ce) from the Sparks Hill Diatreme<sup>1</sup>

Precise footage	Ba	La	Ce	Precise footage	Ba	La	Ce
1,074	132	326	496	1,196.1	389	489	777
1,076.2	143	387	555	1,198	771	529	829
1,078	134	358	513	1,200	1,284	49	95
1,080.1	127	275	400	1,202	607	246	441
1,082	148	372	584	1,204	427	149	281
1,084	147	314	481	1,205.9	81	25	65
1,986.2	147	533	766	1,207.9	430	482	738
1,088	131	378	524	1,209.9	578	479	753
1,089.9	106	162	292	1,211.7	79	34	79
1,092	126	367	550	1,214	738	362	553
1,094	191	300	498	1,215.9	1,102	362	580
1,095.7	116	179	306	1,218.1	137	47	101
1,098.1	103	271	415	1,219.6	850	335	520
1,099.9	60	39	78	1,222	591	338	497
1,101.7	73	115	199	1,224	699	443	705
1,103.9	110	250	386	1,225.8	434	549	855
1,106.1	86	159	256	1,228	1,143	273	435
1,108.1	103	257	430	1,230	322	353	548
1,110.2	204	856	1,342	1,229.9	407	398	619
1,112.3	88	200	341	1,234	418	816	1,291
1,114	59	41	87	1,236.1	352	527	801
1,116	61	68	124	1,238	244	492	762
1,118.1	80	121	209	1,240.3	324	605	935
1,120	286	1,609	2,768	1,242.1	200	356	546
1,122	81	141	253	1,244	116	98	175
1,124.1	147	442	658	1,245.9	143	364	498
1,126	135	575	961	1,248.3	172	288	446
1,127.9	55	34	73	1,249	165	202	316
1,130	121	364	537	Missing samples			
1,132.2	74	114	199	1,284	470	346	565
1,133.8	91	179	306	1,286.1	142	380	576
1,136	199	837	1,194	1,288.1	161	259	448
1,138	175	151	257	1,290.2	136	434	619
1,140	98	151	229	1,292	229	1,046	1,610
1,142	138	323	509	1,294	144	591	817
1,144.1	137	184	303	1,296.3	162	639	887
1,146.2	148	506	700	1,298	128	305	452
1,147.8	83	118	199	1,300	126	408	614
1,150.2	67	55	111	1,302	145	639	905
1,152	90	147	240	1,304	126	386	598
1,154	150	598	1,046	1,306.1	90	93	164
1,156	80	117	196	1,307.9	144	400	596
1,158	103	167	283	1,310	164	884	1,085
1,160	93	107	187	1,312	114	380	564
1,162	150	561	890	1,314	96	167	263
1,164.5	213	1,244	1,670	1,315.9	76	83	153
1,166.1	213	947	1,367	1,318	78	61	131
1,168.0	101	201	312	1,320.2	153	488	714
1,170.0	77	66	122	1,322.1	397	360	610
1,172	106	178	270	1,324	544	293	509
1,173.9	167	543	816	1,326.1	821	314	544
1,176.1	398	132	230	1,328.1	1,128	280	496
1,178	162	387	604	1,330.1	61	66	105
1,180	216	847	1,245	1,333	127	194	349
1,181.9	384	253	412	1,334.1	123	486	579
1,184	1,980	993	1,636	1,336.1	484	278	474
1,186.1	675	179	282	1,338	125	376	552
1,188	535	286	451	1,340	117	467	667
1,190	772	557	888	1,342	127	409	621
1,192.1	695	328	553	1,344.2	276	1,472	2,406
1,194	715	312	500	1,346	115	302	478

<sup>1</sup>Sample footages are apparent depths (in feet) below the surface in borehole USSH-3S, and all elemental values are parts per million by weight (ppm). Photographs of the areas examined by ED-XRF are included in Appendix 1.

the fluorite are cemented by calcite, suggesting calcite and fluorite crystallization occurred nearly simultaneously. The vein clearly cuts across the igneous diatreme phase of the Sparks Hill Diatreme and contains the latest-forming minerals that have been identified.

### Electron Microprobe

The aforementioned ED-XRF analysis from 1,164.5 ft (355 m) in core USSH-3S yielded 1,244 ppm of La and 1,670 ppm of Ce. To determine the location of the Ce and La anomaly, the section was scanned for Ce, which is false-colored red on the backscattered electron image (Figure 10a). This false-colored backscattered electron map shows that the Ce is widely scattered throughout the unresolved fine-grained igneous matrix of the diatreme. A high concentration can be observed in a nearly circular pattern, which, on further examination by electron microprobe analyses (Table 4), proved to mark the presence of the mineral florencite (Figure 10b and 10c). Florencite [CeAl<sub>3</sub>(PO<sub>4</sub>)<sub>2</sub>(OH)<sub>6</sub>] was observed in aggregates along the boundaries of other minerals, including apatite, consistent with its being a late-stage mineral and possibly an alteration product. Some of the apatite grains are euhedral, whereas the edges of other apatite grains appear to be resorbed as a result of alteration or magmatic reactions (Figure 11). Minerals that were identified through the electron microprobe analysis are dolomite, apatite, niobium-rutile, magnesian spinel, and florencite (Table 2).

### Geochemical Analyses (Inductively Coupled Plasma Mass Spectrometry)

Major oxide and trace-element analyses of several fluorite veins and igneous rocks were analyzed by ICP-MS methods (Tables 5 and 6). The major-element chemistry of Sparks Hill (Denny et al. 2010) has been diluted by the effects of brecciation and possibly hydrothermal fluids, but it still retains the low SiO<sub>2</sub> (36.9%) and high CaO (15.2%) characteristics of these ultramafic intrusions. As a group, these rocks are marked by high concentrations of potassium oxide (K<sub>2</sub>O) and titanium dioxide (TiO<sub>2</sub>) and low concentrations of sodium oxide (Na<sub>2</sub>O).

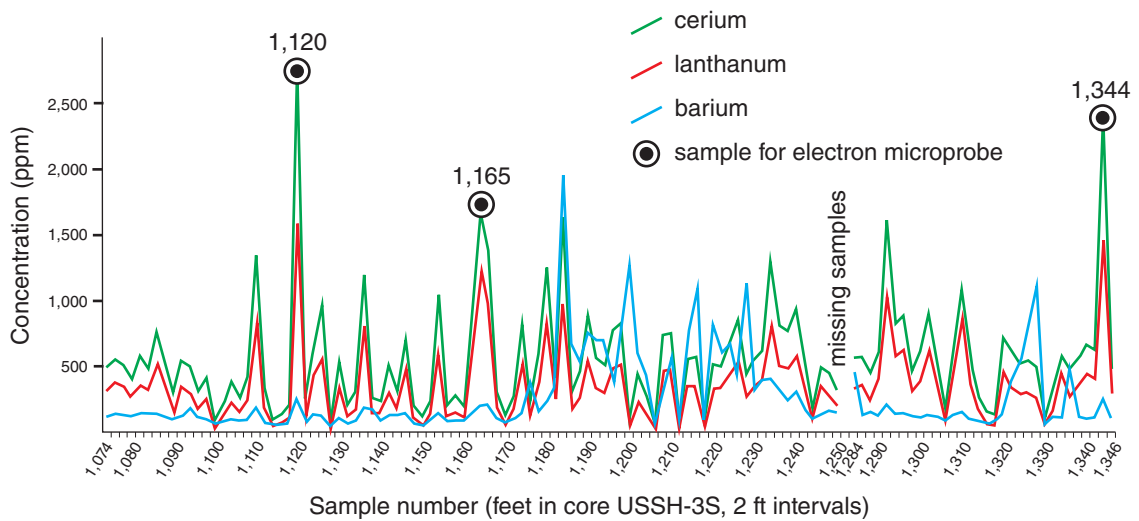


**Figure 8** Plot of barium, cerium, and lanthanum concentrations in 2 ft (0.6 m) intervals from the Sparks Hill Diatreme core (2 cm<sup>2</sup> spots).

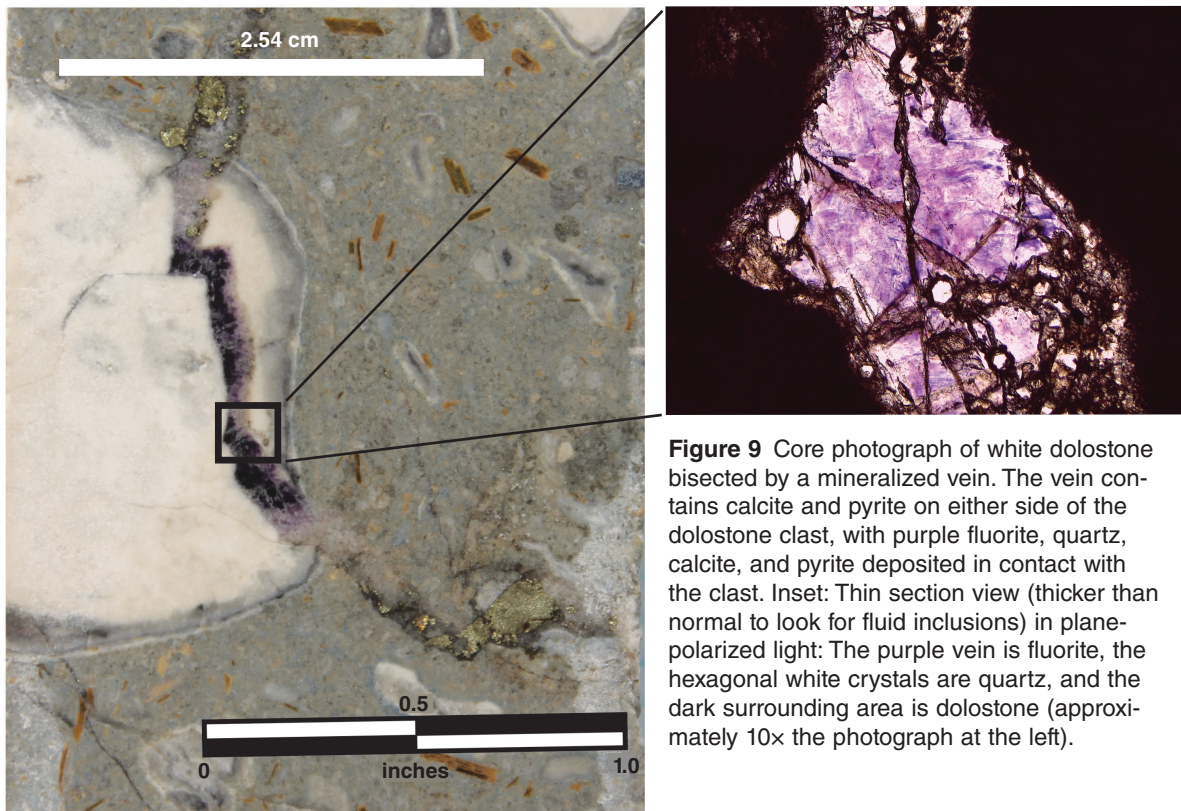


**Figure 9** Core photograph of white dolostone bisected by a mineralized vein. The vein contains calcite and pyrite on either side of the dolostone clast, with purple fluorite, quartz, calcite, and pyrite deposited in contact with the clast. Inset: Thin section view (thicker than normal to look for fluid inclusions) in plane-polarized light: The purple vein is fluorite, the hexagonal white crystals are quartz, and the dark surrounding area is dolostone (approximately 10x the photograph at the left).

The REE plots were normalized with the chondrite values from Taylor and McLennan (1985). Raw data from fluorite analyses in the Cave-in-Rock District (Chesley et al. 1994) were also normalized with the chondrite values and plotted as comparison data. The ultramafic lamprophyre samples from different parts of southern Illinois, although rep-

resentative of a variety of textures and degrees of alteration, exhibit relatively uniform patterns (Figure 12) marked by the enrichment of light REE (LREE) and strong REE fractionation. The REE pattern for Sparks Hill is a very close match with patterns of the nearby intrusions. The three samples (Figure 12) from more than 3,000 ft (914 m) depth below the

surface of Hicks Dome (Fsb-38) contain the highest overall REE concentrations.

Some mineral compositions were also characterized by electron microprobe techniques. The composition of phlogopite is especially useful for classification purposes. Although the micas are bronze colored, chemical analyses

**Table 4** Electron microprobe analyses of minerals within lamprophyres in the study area<sup>1</sup>

Material analyzed	Element or compound																Total (wt%)
	Al <sub>2</sub> O <sub>3</sub>	SiO <sub>2</sub>	P <sub>2</sub> O <sub>5</sub>	SrO	SO <sub>3</sub>	CaO	BaO	Y <sub>2</sub> O <sub>3</sub>	FeO	La <sub>2</sub> O <sub>3</sub>	Ce <sub>2</sub> O <sub>3</sub>	Pr <sub>2</sub> O <sub>3</sub>	Nd <sub>2</sub> O <sub>3</sub>	H <sub>2</sub> O			
Fluorite	0.09	0.110	0.24	0.52	0.01	0.01	0.02	0.02	0.01	0.04	0.04	0.03	0.05				
DL (2σ)																	
Sample no.																	
USSH1165_c_flo1	30.2	<0.110	24.8	7.42	4.55	0.37	0.036	<0.02	0.35	6.71	8.66	1.12	1.55	10.7	96.5		
USSH1165_c_flo2	30.5	<0.110	24.7	7.44	4.37	0.35	<0.02	<0.02	0.35	6.55	9.76	1.18	1.85	10.8	97.8		
USSH1165_c_flo3	31.3	<0.110	24.5	6.94	4.18	0.37	0.020	<0.02	0.19	6.47	10.52	1.48	2.47	10.9	99.3		
USSH1165_d_flo1	30.0	0.207	23.5	6.77	4.37	1.63	0.034	<0.02	0.21	6.46	10.51	1.54	2.15	10.7	98.1		
USSH1165_d_flo2	31.1	0.161	23.9	6.98	4.23	0.63	<0.02	<0.02	0.64	6.72	10.77	1.32	2.01	10.8	99.2		
Apatite	F	CaO	P <sub>2</sub> O <sub>5</sub>	Cl	SrO	Y <sub>2</sub> O <sub>3</sub>	FeO	MnO	La <sub>2</sub> O <sub>3</sub>	Ce <sub>2</sub> O <sub>3</sub>	Pr <sub>2</sub> O <sub>3</sub>	Nd <sub>2</sub> O <sub>3</sub>	H <sub>2</sub> O				
DL (2σ)	0.21	0.05	0.08	0.002	0.01	0.009	0.006	0.006	0.019	0.019	0.016	0.016					
Sample no.																	
USSH1120_apat01L	3.28	55.0	39.8	0.078	0.301	0.037	0.207	0.022	0.099	0.081	<0.016	0.072	0.146	99.1			
USSH1344_a_apat1R	3.26	54.1	41.3	0.009	1.207	0.011	0.097	0.132	0.098	0.294	0.044	0.154	0.211	100.9			
USSH1344_a_apat1C	3.13	54.3	41.5	0.008	1.046	0.023	0.075	0.120	0.127	0.269	0.050	0.202	0.279	101.0			
USSH1344_b_apat1R	5.96	54.4	38.9	<0.002	0.066	0.087	0.047	<0.006	<0.019	<0.019	<0.016	0.041	0.000	99.4			
USSH1344_b_apat1C	3.83	49.4	40.2	0.007	4.230	0.024	0.081	0.169	0.734	1.519	0.219	0.593	0.000	101.1			
USSH1344_c_apat1	5.54	53.6	38.1	<0.002	0.212	0.066	0.108	0.011	<0.019	0.048	0.027	0.082	0.000	97.8			
USSH1344_c_apat2	3.76	51.9	40.8	<0.002	2.744	0.049	0.134	0.068	0.474	1.030	0.187	0.517	0.000	101.6			
USSH1344_c_apat3	4.92	53.8	38.6	<0.002	0.073	0.049	0.206	<0.006	<0.019	<0.019	<0.016	<0.016	0.000	97.6			
USSH1344_c_apat4	4.97	53.4	37.5	<0.002	0.083	0.044	0.210	<0.006	0.042	<0.019	<0.016	0.020	0.000	96.2			
USSH1344_d_apat1R	1.64	54.8	40.3	0.080	0.394	0.024	0.207	0.044	0.096	0.127	0.034	0.102	0.937	98.9			
USSH1344_d_apat1C	2.12	54.9	41.6	0.075	0.422	<0.009	0.132	0.032	0.044	0.137	0.027	0.087	0.745	100.3			
Mica	F	Na <sub>2</sub> O	Al <sub>2</sub> O <sub>3</sub>	MgO	SiO <sub>2</sub>	Cl	K <sub>2</sub> O	CaO	Cr <sub>2</sub> O <sub>3</sub>	FeO	MnO	TiO <sub>2</sub>	H <sub>2</sub> O				
DL (2σ)	0.24	0.05	0.08	0.07	0.12	0.05	0.07	0.07	0.10	0.18	0.14	0.25					
Sample no.																	
WH20101j_1_phl_1R	1.35	0.30	13.9	21.7	38.6	<0.05	9.90	<0.07	<0.10	7.03	<0.14	4.01	3.52	100.5			
WH20101j_1_phl_1C	1.33	0.34	14.4	21.3	37.6	<0.05	9.77	<0.07	<0.10	6.77	<0.14	3.89	3.47	99.1			
WH20101j_1_phl_2R	0.93	0.31	12.0	24.0	40.1	<0.05	8.53	0.13	<0.10	6.77	<0.14	2.92	3.74	99.6			
WH20101j_1_phl_2C	1.39	0.32	14.2	22.1	38.1	<0.05	9.91	<0.07	<0.10	6.47	<0.14	4.05	3.49	100.1			
WH20101j_2_phl_1R	1.19	0.31	12.5	22.6	39.8	<0.05	10.14	<0.07	<0.10	7.10	<0.14	3.48	3.62	100.8			
WH20101j_2_phl_1C	1.51	0.30	13.4	22.3	39.1	<0.05	9.98	<0.07	<0.10	6.79	<0.14	3.71	3.46	100.7			
WH20101j_2_phl_2R	1.16	0.28	13.2	22.0	38.8	<0.05	9.88	<0.07	<0.10	7.17	<0.14	3.73	3.60	100.0			
WH20101j_2_phl_2C	1.48	0.37	13.2	22.3	39.2	<0.05	10.16	<0.07	<0.10	6.71	<0.14	3.99	3.48	100.9			
WH20101j_2_phl_3R	1.23	0.33	12.1	22.4	39.4	<0.05	10.09	0.08	<0.10	7.06	<0.14	3.65	3.55	99.9			
WH20101j_2_phl_3C	1.28	0.28	13.0	22.1	39.4	<0.05	10.20	<0.07	<0.10	6.63	<0.14	3.94	3.56	100.4			
WH20101j_2_phl_4R	1.69	0.27	13.9	21.9	38.3	<0.05	9.84	<0.07	<0.10	6.57	<0.14	3.96	3.34	99.9			
WH20101j_2_phl_4C	1.31	0.24	13.4	21.7	38.9	<0.05	10.01	<0.07	<0.10	7.16	<0.14	4.01	3.53	100.4			

<sup>1</sup>DL, detection limit.

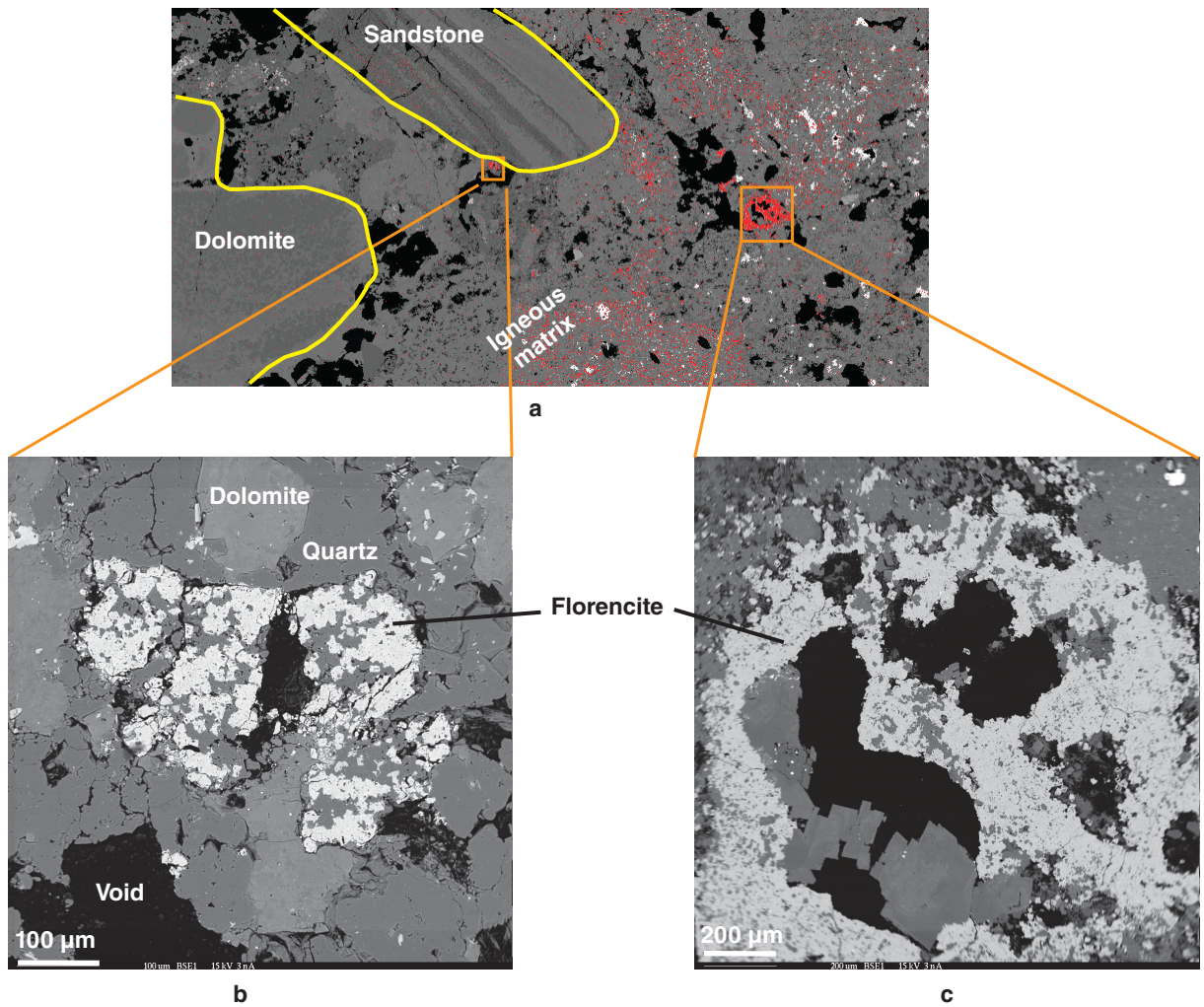
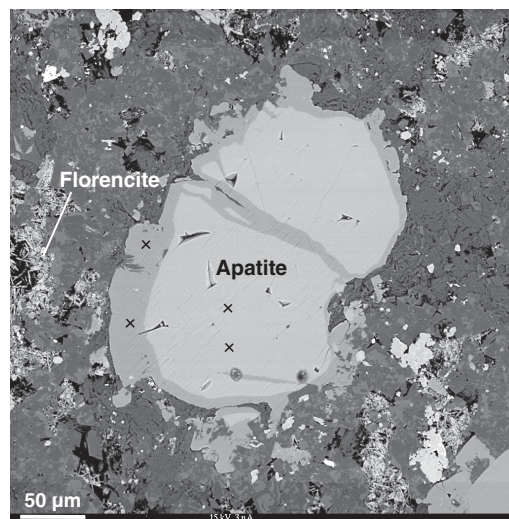


**Figure 10** (a) False-colored backscattered electron image from the sample at 1,344 ft (410 m). Red color is false-colored to show concentrations of cerium. (b, c) Florencite with dolomite and quartz associated with open spaces or voids.



x Energy-dispersive X-ray analysis location

**Figure 11** Backscattered electron image showing apatite from 1,344 ft (410 m) in the Sparks Hill Diatreme with zonation along the edges.

**Table 5** Geochemical analyses of lamprophyres in the study area<sup>1</sup>

Element	Unit	CH-01	CH-02	SH-1179	SH-1190	SH-1326	PWL-1	KR-3	He-01	He-Will	Ham-01	Fsb-38 (3,148 ft)	Fsb-38 (3,172 ft)	Fsb-38 (3,174 ft)
F	%	0.18	0.17	0.43	0.17	0.32	0.15	0.1	0.15	0.14	0.39	0.76	0.47	0.61
Ag	ppm	*	*	*	*	*	2	3	10	<1	<1	<1	0.76	<0.01
Ba	ppm	852	785	210	968	913	592	597	806	944	1,075	1,420	1,250	1,850
Ce	ppm	154.5	166.5	1,135	801	509	157.5	467	123	128	173.5	531	1,155	548
Co	ppm	*	*	*	*	*	58.9	15.3	4.4	3.9	73.4	40.5	41.2	38.8
Cr	ppm	690	760	10	90	160	860	30	30	20	770	160	86	74
Cs	ppm	1.92	1.67	0.3	17.75	6.03	1.1	0.77	1.45	1.58	1.02	5.92	4.18	5.44
Cu	ppm	*	*	*	*	*	37	9	<5	59	100	70	877	65.3
Dy	ppm	4.42	4.6	23.8	9.28	12.95	4.35	6.7	3.87	4.14	5.37	15.7	178	16.5
Er	ppm	1.52	1.57	10.2	3.88	5.09	1.87	3.59	2.14	1.99	1.83	7.2	13.3	7.2
Eu	ppm	3	3.22	15.7	7.26	8.3	3.12	4.27	2.01	2.02	3.64	12.2	20.5	10.1
Ga	ppm	13.6	13.5	16.2	19	23.5	13.2	13.5	31.7	34.9	15.2	19	20.2	20.8
Gd	ppm	7.78	8.17	39.8	17.15	8.82	9.82	17.15	6.69	4.43	8.5	22.9	35.7	32.2
Hf	ppm	5.8	5.4	23	16.8	13.1	6.2	7	21.2	22.7	5.7	15.9	12.9	9.3
Ho	ppm	0.69	0.71	4.09	1.56	2.2	0.75	1.3	0.8	0.78	0.87	3	5.4	2.8
La	ppm	77.2	83	561	500	293	84	293	74.3	70.7	88.5	290	276	303
Lu	ppm	0.12	0.12	1.11	0.51	0.44	0.11	0.33	0.25	0.3	0.16	0.52	0.6	0.8
Mo	ppm	*	*	*	*	*	2	3	5	4	7	<2	46.5	1
Nb	ppm	122.5	126	245	395	313	118.5	155	603	573	133	231	152.5	50.7
Nd	ppm	63	68.3	494	245	186	64.2	143	44.9	42.9	75.4	228	234	228
Ni	ppm	*	*	*	*	*	384	16	14	12	401	60	65.1	58.7
Pb	ppm	*	*	*	*	*	52	59	21	18	12	19	42	28
Pr	ppm	17.65	19.1	139	84.2	54.8	17.55	45.5	13.35	13.2	19.7	61	62.5	134.5
Rb	ppm	57.7	54.6	18.5	56.8	76.9	45.8	35.4	106.5	140.5	78.8	134	116	61.9
Rb	ppm	11.1	11.75	66.5	30.2	30.1	10.75	17.55	7.07	7.43	13.35	37.6	40.3	128
Sm	ppm	2	2	1	3	4	2	2	2	3	2	4	2.7	<1
Sn	ppm	881	760	1,530	1,985	2,350	482	1,315	848	765	470	3,040	1,750	3,250
Sr	ppm	7.7	8.3	7	15.5	17.5	6.8	5.8	21.8	22.3	7.7	14.4	3.88	1.42
Ta	ppm	0.95	0.99	4.78	2.01	2.7	1.08	1.7	0.78	0.76	1.17	3.11	4.3	3.9
Tb	ppm	9.22	9.97	26.4	29.5	20.9	9.58	13.8	38	43.4	11.35	20.6	39	51
Th	ppm	<0.5	<0.5	<0.5	<0.5	<0.5	<0.5	<0.5	<0.5	<0.5	0.9	<0.5	<0.5	<0.5
Ti	ppm	0.2	0.17	1.35	0.53	0.61	0.15	0.38	0.25	0.3	0.24	0.78	0.8	0.9
Tm	ppm	2.46	2.34	9.16	3.87	12.1	2.46	5.55	17.95	21.3	2.94	7.95	8.4	6.5
U	ppm	303	297	157	245	369	315	135	57	55	280	237	232	199
V	ppm	1	1	45	11	8	1	3	2	3	2	12	8.5	3
W	ppm	17.2	16.8	99.8	40.5	54.1	17.3	29.9	19.1	19.8	20.8	67.9	119	64
Y	ppm	0.99	0.96	8.2	3.46	3.44	1.09	2.47	1.84	2.03	1.19	4.21	4.7	5.3
Yb	ppm	*	*	*	*	*	45	107	135	127	345	203	124	185
Zn	ppm	250	226	2,050	629	585	244	310	1,340	1,490	257	972	>500	457
Zr	ppm	30.4	29.8	13.3	30.1	29.5	17.5	36.9	53.1	53.8	32.3	24.7	*	*
Al <sub>2</sub> O <sub>3</sub>	wt%	5.45	5.03	2.68	6.95	7.91	6.16	7.32	18.35	19	6.45	5.4	*	*
Fe <sub>2</sub> O <sub>3</sub>	wt%	12.4	12.6	10.5	12.6	15.1	7.28	7.01	3.65	3.88	13.45	13.8	*	*
CaO	wt%	12.35	11.55	28.2	14.85	19.45	29	15.2	2.67	2.63	13.6	20	*	*
MgO	wt%	16.65	16.9	7.5	6.51	7.42	5.3	5.8	1.04	1.09	15.45	7.84	*	*
Na <sub>2</sub> O	wt%	0.59	0.41	0.2	2.54	1.74	0.28	2.13	8.58	8.08	0.22	1.48	*	*
K <sub>2</sub> O	wt%	1.18	1.11	0.74	2.64	2.25	0.98	1.42	4.11	4.7	2.07	3.79	*	*
Cr <sub>2</sub> O <sub>3</sub>	wt%	0.09	0.09	<0.01	0.01	0.02	0.13	0.01	<0.01	<0.01	0.11	0.02	*	*
TiO <sub>2</sub>	wt%	3.8	3.9	0.63	3.57	4.15	3.64	1.19	0.44	0.47	3.93	3.25	*	*
MnO	wt%	0.19	0.18	0.38	0.33	0.3	0.26	0.2	0.19	0.19	0.2	0.35	*	*
P <sub>2</sub> O <sub>5</sub>	wt%	0.75	0.7	6.16	1.73	2.46	0.81	0.79	0.22	0.23	0.86	2.79	*	*
SrO	wt%	0.1	0.09	0.18	0.24	0.28	0.06	0.17	0.11	0.09	0.06	0.39	*	*
BaO	wt%	0.09	0.08	0.02	0.11	0.1	0.07	0.07	0.09	0.1	0.12	0.17	*	*
LOI	wt%	16	16.2	29.5	15.85	10.8	17.4	21.4	6.49	4.99	9.77	14.95	*	*
Total	wt%	100.04	98.64	99.99	98.03	101.48	98.9	99.6	99	99.3	98.6	98.9	*	*

<sup>1</sup>Samples were analyzed by the inductively coupled plasma mass spectrometry (ICP-MS) method with a lithium-borate fusion. Trace elements were analyzed by ICP-MS (values in ppm). A less than sign (<) indicates lower than the detection limit. An asterisk (\*) indicates elements were not analyzed. Major oxide values are in weight percent (wt%), LOI, loss on ignition.

**Table 6** Geochemical analyses of calcite and fluorite in the study area

Element	Unit	Mixed calcite and fluorite			Fluorite only			
		KR-1	KR-2	LCS-01	He-Hd-01	CR-01	MCS-01	Beard-01
F	%	7.47	1.33	*	*	*	*	*
Ag	ppm	8	<1	*	<1	<1	*	*
Ba	ppm	18	19.8	205	3.1	319	1,270	30.9
Ce	ppm	11	79.6	5.9	2	1.5	2.3	0.7
Co	ppm	1.9	1.1	*	0.8	0.9	*	*
Cr	ppm	20	10	10	<10	10	10	<10
Cs	ppm	0.03	0.11	<0.01	0.03	1.5	0.05	0.02
Cu	ppm	269	1,170	*	<5	<5	*	*
Dy	ppm	2.09	11.05	0.8	0.71	0.97	0.4	0.21
Er	ppm	0.9	7.16	0.32	0.26	0.4	0.19	0.07
Eu	ppm	1.2	5.62	0.35	0.31	0.2	0.13	0.12
Ga	ppm	0.5	1.4	0.9	0.2	0.5	0.2	0.1
Gd	ppm	2.72	11.5	1	0.94	1.11	0.56	0.34
Hf	ppm	0.04	0.6	<0.2	0.8	<0.2	<0.2	<0.2
Ho	ppm	0.39	2.56	0.15	0.13	0.18	0.08	0.04
La	ppm	3.9	30.2	2.4	1.2	1.1	1.4	<0.5
Lu	ppm	0.04	1	0.04	0.01	0.02	0.01	<0.01
Mo	ppm	<2	<2	*	<2	<2	*	*
Nb	ppm	3.3	2.7	0.3	1.4	2.8	0.6	0.2
Nd	ppm	9.2	48	4.1	1.9	1	1.2	0.6
Ni	ppm	17	9	*	<5	<5	*	*
Pb	ppm	>10,000	238	*	<5	<5	*	*
Pr	ppm	1.87	10.95	1.01	0.32	0.2	0.29	0.11
Rb	ppm	1.5	4.1	0.7	0.6	3.3	0.6	0.9
Sm	ppm	2.56	11.95	1.02	0.61	0.47	0.39	0.2
Sn	ppm	<1	4	<1	<1	<1	<1	<1
Sr	ppm	161	203	187.5	32.2	98.1	87.2	32.2
Ta	ppm	0.2	<0.1	<0.1	<0.1	0.1	<0.1	<0.1
Tb	ppm	0.36	1.94	0.15	0.13	0.17	0.08	0.04
Th	ppm	0.31	1.06	0.13	0.2	0.66	0.18	0.05
Tl	ppm	<0.5	<0.5	<0.5	<0.5	<0.5	<0.5	<0.5
Tm	ppm	0.07	1.09	0.05	0.01	0.03	0.02	0.01
U	ppm	0.07	0.24	0.07	0.07	0.47	0.05	<0.05
V	ppm	10	9	5	<5	8	<5	<5
W	ppm	1	1	<1	1	1	<1	<1
Y	ppm	16	94.2	6.1	14.8	17.5	7.4	4
Yb	ppm	0.51	7.31	0.25	0.12	0.17	0.11	<0.03
Zn	ppm	<5	<5	*	<5	12	*	*
Zr	ppm	21	28	2	42	10	<2	<2
SiO <sub>2</sub>	wt%	6.87	12.75	*	0.52	3.91	*	*
Al <sub>2</sub> O <sub>3</sub>	wt%	0.09	0.53	*	0.15	0.52	*	*
Fe <sub>2</sub> O <sub>3</sub>	wt%	0.31	0.57	*	0.06	0.32	*	*
CaO	wt%	52.9	50	*	66.6	65.3	*	*
MgO	wt%	0.21	0.31	*	0.01	1.21	*	*
Na <sub>2</sub> O	wt%	0.02	0.02	*	0.04	0.07	*	*
K <sub>2</sub> O	wt%	0.01	0.14	*	0.03	0.08	*	*
Cr <sub>2</sub> O <sub>3</sub>	wt%	<0.01	<0.01	*	<0.01	<0.01	*	*
TiO <sub>2</sub>	wt%	0.02	0.04	*	<0.01	0.02	*	*
MnO	wt%	0.04	0.07	*	<0.01	0.01	*	*
P <sub>2</sub> O <sub>5</sub>	wt%	0.04	0.01	*	0.03	0.05	*	*
SrO	wt%	0.02	0.03	*	<0.01	0.01	*	*
BaO	wt%	<0.01	<0.01	*	0.04	*	*	*
LOI	wt%	32.2	0.7	*	4.56	*	*	*
Total	wt%	92.7	68.1	*	76.1	*	*	*

<sup>1</sup>Samples were analyzed by the inductively coupled plasma mass spectrometry (ICP-MS) method with a lithium-borate fusion. Trace elements were analyzed by ICP-MS (values in ppm). A less than sign (<) indicates lower than the detection limit. An asterisk (\*) indicates elements were not analyzed. Major oxide values are in weight percent (wt%). Totals are low because of poor F analysis results. LOI, loss on ignition.

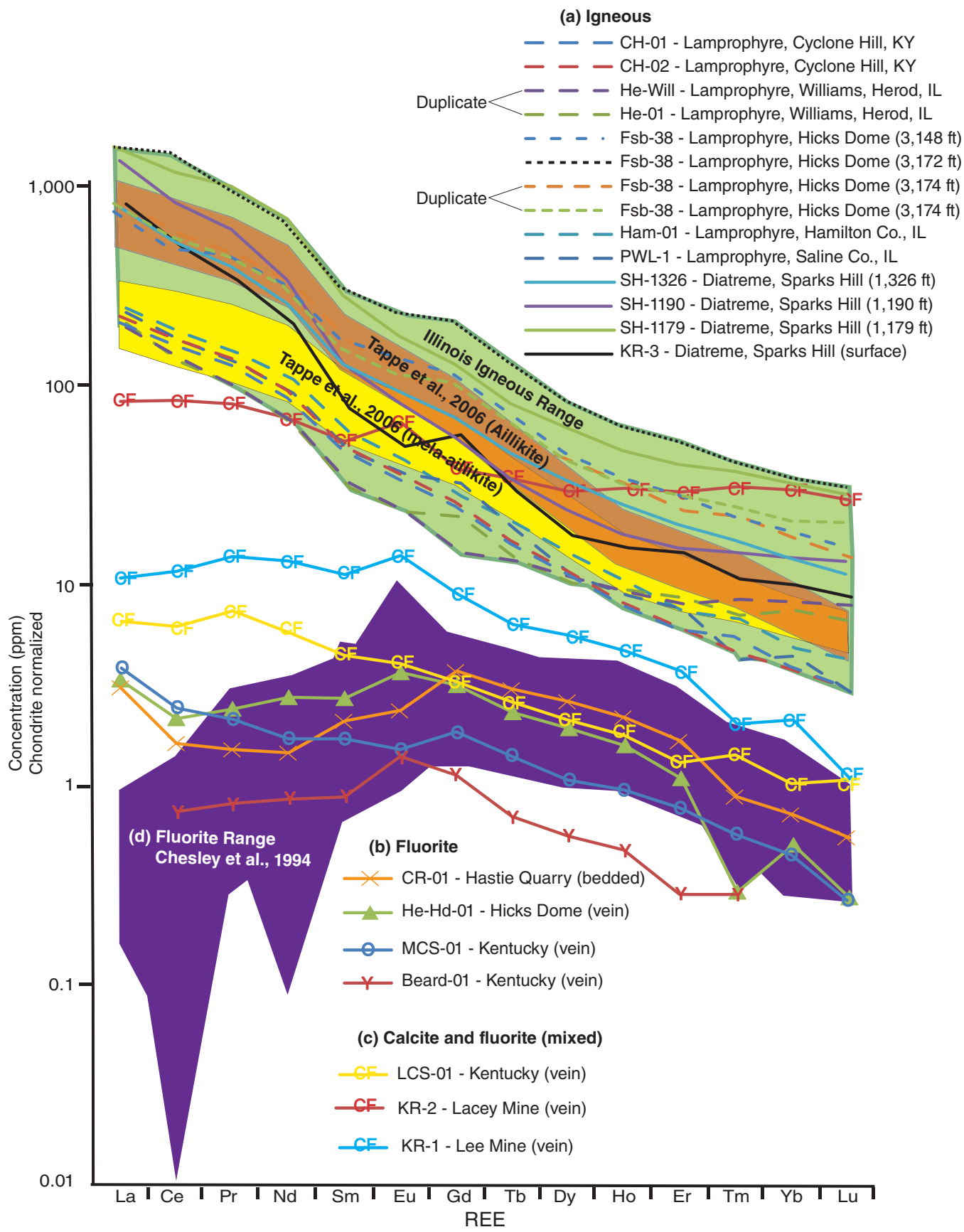


**Figure 12** Plot of rare earth element (REE) concentrations from (a) igneous rock, (b) fluorite, (c) mixed fluorite and calcite, and (d) fluorite from the Cave-in-Rock subdistrict-bedded replacement ore. The aillikite and mela-aillikite fields in the igneous rock plot are from Tappe et al. (2006), the Illinois igneous range is from this work, and the Cave-in-Rock fluorite range is from Chesley et al. (1994).

indicate the magnesium (Mg)/iron (Fe) ratio of mica at Hicks Dome is near the threshold between biotite and phlogopite (Morehead 2013). The phlogopite in the Sparks Hill Diatreme, like the phlogopite in nearby lamprophyres, is rich in Al and titanium (Ti; Figure 13), consistent with their designation as ultramafic lamprophyres. The Sparks Hill phlogopite forms a small field just beyond the Ti-rich end of Mitchell's Wauboukigou field and just beyond the Ti-rich, Al-poor corner of the type alnöite field. With the phlogopite from other nearby lamprophyre localities (e.g., Cottage Grove, Wildcat Hills), a relatively broad field is delineated, extending from approximately 6% TiO<sub>2</sub> and 15% aluminum oxide (Al<sub>2</sub>O<sub>3</sub>) down to 1% TiO<sub>2</sub> and 11% Al<sub>2</sub>O<sub>3</sub>. Although documented core-to-rim compositional trends are still relatively few, a pattern of evolution toward lower Al and Ti is apparent, in contrast to the documented pattern for alnöite. The micas in the globular segregations plot at higher Al levels (Figure 13) and are not phlogopite but low-Mg, high-Fe biotite. This composition is not characteristic of ultramafic lamprophyres. At this point, it is unclear whether these micas might represent xenocrysts or, alternatively, might have been chemically altered.

## DISCUSSION

### Lamprophyre and Diatremes

The Sparks Hill Diatreme is geochemically similar to ultramafic intrusions nearby in Illinois (Wildcat Hills, Will Scarlet, Cottage Grove) and Kentucky (Clay Lick). In particular, the REE pattern from the Sparks Hill Diatreme is marked by enrichment of LREE, and the strong REE fractionation closely matches the pattern exhibited by other lamprophyres in southern Illinois. These rocks appear to represent well the chemistry of the source rocks, with no trends easily attributable to fractional crystallization. Strontium- and Nd-isotope data also give no indication of crustal contamination (Maria et al. 2016). Low values of heavy REEs (HREEs) suggest melting deep within the garnet stability zone of the mantle. Enrichment in both compatible and incompatible elements is consistent with the small percentage

melting of an enriched mantle source. Maria et al. (2016) suggested that the lamprophyres in this region originated from a lithospheric peridotite source enriched in incompatible elements by a prior metasomatic event and contain phlogopite-rich veins. Samarium-Nd model ages are consistent with enrichment, perhaps linked to an underplating of magma, during the breakup of Rodinia.

The suite of minerals identified for this study in the Sparks Hill Diatreme includes calcite, apatite, phlogopite, rutile, serpentine, chalcopyrite, pyrite, magnetite, dolomite, fluorite, quartz, and REE-bearing florencite and synchysite. The electron microprobe analysis of the Sparks Hill core (USSH-3S) shows that some of the REEs are contained in very fine grained zones within the matrix between sedimentary clasts. Florencite [CeAl<sub>3</sub>(PO<sub>4</sub>)<sub>2</sub>(OH)<sub>6</sub>] was identified in all three intervals analyzed. The identification of florencite and fluorite in the Sparks Hill Diatreme and at Hicks Dome (Trace 1960) suggests similar igneous origins. Carbonatites are rich in REEs, and Wall and Mariano (1996) proposed that a typical intrusive carbonatite sequence would be an "early calcite carbonatite with apatite hosting much of the REE at low levels, accessory pyrochlore, then sometimes a dolomite carbonatite with slightly higher levels of REE, and finally subordinate veins of a rare earth (RE)-rich carbonatite, often ferrocarbonatite containing RE minerals such as ferrocarbonates and monazite" (p. 196–197). Ultramafic lamprophyres are commonly associated with carbonatites, and carbonatite may well be present beneath Hicks Dome, as hypothesized by Wall and Mariano (1996) and Morehead (2013). When associated with carbonatites, the accompanying REE mineralization is usually associated with fluid phases that were expelled from the carbonatite magmas (Verplank and Van Gosen 2011). However, REE mineralization associated with carbonatites has been linked to both magmatic and hydrothermal processes (Trofanenko et al. 2016), indicating that hydrothermal processes must be considered. Doroshkevich et al. (2009) have documented a mineral assemblage at Amba Dongar much like those present at Sparks Hill and Hicks Dome, which they

attribute to hydrothermal overprinting of a carbonatite complex, ending with late-stage fluorite mineralization.

Several authors studying lamprophyres and carbonatites have recognized that F, Ba, Sr, and REEs in particular are partitioned into a fluid phase rather than a carbonatitic magmatic phase (e.g., Bühn 2008), with preferential incorporation of REEs into fluids rich in CO<sub>2</sub> (Cooper and Patterson 2008). In other words, hydrothermal processes driven by CO<sub>2</sub>-rich fluids from the ultramafic lamprophyre might be the source of the REE mineralization. Diatremes are associated with volatile-rich conditions, typically linked to degassing of volatile-rich, silica-undersaturated, alkaline ultramafic magmas (Lloyd and Stoppa 2003) and sometimes to phreatomagmatic processes (e.g., Lorenz 2003). An abundance of phlogopite and carbonate and the absence of feldspars point to a volatile-rich magma. Also consistent with the degassing model, globular segregations, or ocelli, and pelletal lapilli have been observed in the Sparks Hill Diatreme and beneath Hicks Dome (Morehead 2013). Cooper (1979) suggested that ocelli associated with lamprophyres are the result of a two-stage process in which advanced magma crystallization results in the boiling of a residual liquid, culminating in two separate fractions: (1) a silicate fraction saturated in H<sub>2</sub>O and CO<sub>2</sub>, and (2) a gaseous phase with dissolved solids also rich in CO<sub>2</sub> (Williams et al. 1982). Pelletal lapilli may represent the interface between the erupting magma and the separating volatile-rich component (Lloyd and Stoppa 2003).

Separation of a CO<sub>2</sub>-rich fluid from the magma is indicated by the metasomatized sedimentary clasts, clay alteration, carbonate recrystallization, silicification, and serpentinization commonly observed in thin sections. The separated fluids would inherit, to some extent, the trace element characteristics of the parental ultramafic magma, and minerals such as calcite and fluorite can preserve the REE pattern of the hydrothermal fluids from which they precipitate (Bau and Dulski, 1995; Möller et al. 1998). Fluorite samples CR-01, He-Hd-01, MCS-01, LCS-01, and Beard-01 exhibit REE patterns with slopes from

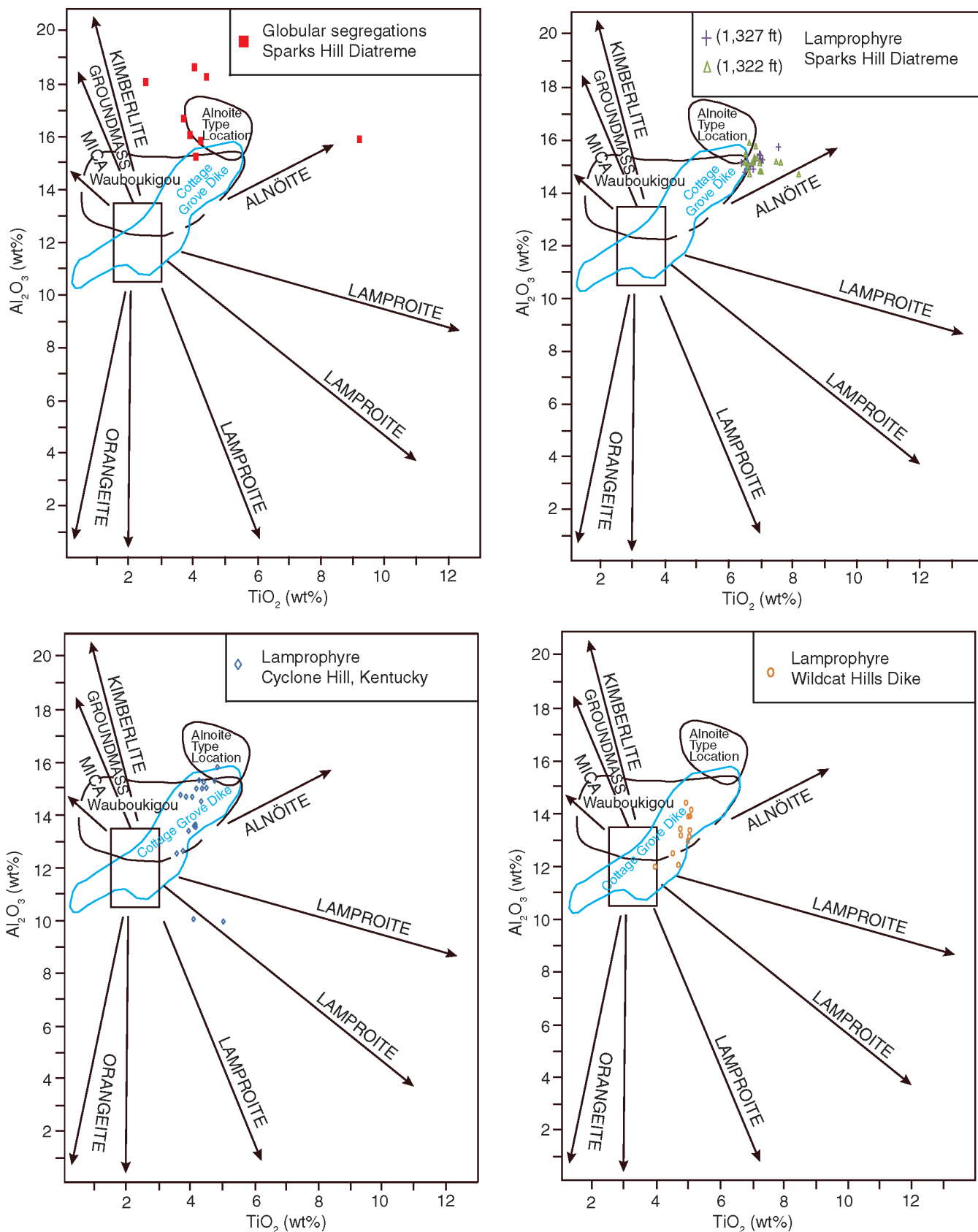


**Figure 13** Binary plots of phlogopite titanium dioxide ( $\text{TiO}_2$ ) and aluminum oxide ( $\text{Al}_2\text{O}_3$ ) contents from ultramafic lamprophyres from the region and ultramafic lamprophyres within the Sparks Hill Diatreme (compositional fields and trends from Mitchell 1995).

Gd to Lu that are similar to those of the ultramafic lamprophyres, possibly indicating an igneous source for the fluorite (Figure 12). One would expect the LREE to be enriched relative to the HREE in the CO<sub>2</sub>-rich fluid because of the greater incompatibility of the LREE. However, the relative depletion in LREE within the fluorite could reflect earlier crystallization of florencite and synchysite. The small positive Eu anomaly might reflect the influence of a felsic crystalline basement (Schwinn and Markl 2005). The mixed calcite-fluorite sample KR-1 exhibits very nearly the same pattern, although at higher concentrations approaching those of the lamprophyres. The mixed calcite-fluorite sample KR-2 exhibits the highest concentrations of REEs, actually crossing the field of lamprophyres. The LREEs for this sample are still relatively depleted, but not to the same extent as in the other fluorite and calcite-fluorite samples. Perhaps the progressive depletion of LREEs and overall drop in REEs from KR-2 to Beard is indicative of timing (Huang et al. 2007), with KR-2 representing early-stage mineralization. Sample KR-2 also exhibits the small positive Eu anomaly but differs from the others in that the slope from Gd to Lu reflects enrichment of HREEs relative to the trend exhibited by the lamprophyres.

Recent modeling (Migdisov and Williams-Jones 2014) suggests that fluorine-bearing hydrothermal fluids transport REEs as complexes with chloride ions at low pH or as sulfate ions at higher pH. Interaction with carbonate country rock would neutralize acidity and promote precipitation of rare earth-bearing minerals. Fluoride ions, although not playing an important transport role, act as an REE binding ligand to promote the precipitation of REE-bearing minerals such as fluorite and synchysite (Migdisov and Williams-Jones 2014; Trofanenko et al. 2016). Phosphate can also play the role of binding ligand, and the presence of florencite in association with the Sparks Hill Diatreme suggests that the dolomite country rock may contain phosphate.

## Fluorite and the Illinois-Kentucky Fluorspar District

Ore deposits of the IKFD have been considered MVT deposits primarily because of their overall geologic characteristics and analytical data for primary fluid inclusions in fluorite. Freas (1961) reported homogenization temperatures in fluorite as low as 70 °C in the area of Cave-in-Rock, Illinois. It should be noted that the ore deposits are horizontal bedding replacement or mantos type in the Cave-in-Rock district, but the majority of the ore deposits occur along nearly vertical veins in the IKFD. Cunningham and Heyl (1980) reported homogenization temperatures of approximately 175 °C in fluorite- and barite-hosted fluid inclusions from near the top of Hicks Dome, and approximately 220 to 270 °C in barite at a depth of 2,339 ft (713 m). The present-day brines of the Illinois Basin contain only 2.6 ppm of fluorine (Hall and Friedman 1963), whereas other present-day heated fluids that are depositing fluorite range between 14 and 20 ppm of fluorine (Cunningham and Heyl 1980), indicating that an additional source of fluorine (other than a basinal brine) is necessary to produce the fluorite-rich ore of the IKFD.

Rare earth element patterns for the IKFD fluorite samples, although overlapping those of the fluorite samples from this study, are made distinct by a humplike shape driven by greater depletion of LREEs, a marked negative Ce anomaly, and a larger positive Eu anomaly. The greater degree of LREE depletion might indicate that the IKFD fluids represent later-stage mineralization (Huang et al. 2007). The positive Eu anomaly could reflect interaction with feldspar-bearing bedrock, but might alternatively indicate low fluid temperatures. Positive Eu anomalies have been observed in hydrothermal fluorite with crystallization temperatures below 200 °C because of the thermochemical reduction of Eu<sup>3+</sup> to Eu<sup>2+</sup> (Schwinn and Markl 2005). In fluids above 200 °C, the large size of the Eu<sup>2+</sup> ion inhibits its incorporation into the fluorite crystal lattice. The strong negative Ce anomaly is consistent with a

meteoric signature (Schwinn and Markl 2005). In fact, the similarity of REE patterns for the IKFD fluorite and the type A fluorite of Schwinn and Markl (2005) suggest that the origins of the IKFD fluorite might be tied to meteoric waters flowing through crystalline bedrock.

## CONCLUSIONS

We propose that the Sparks Hill Diatreme represents a volatile-rich phase of an ultramafic lamprophyre intrusion associated with rifting and melting of a metasomatically enriched lithospheric mantle. The volatile-rich nature of the magma resulted in explosive intrusion and brecciation of the overlying country rock, with suspension of sedimentary clasts and igneous material within a nearly vertical pipe. Fluid-rock exchange during late-stage magmatic activity hydrothermally altered the clasts and deposited fluorite in thin veins (Figure 7). The various textures of the diatreme probably correlate with different parts of the diatreme structure. The clast-supported diatreme and breccia textures should be more abundant near the edge of the diatreme, whereas the lamprophyre and diatreme textures should be more common in the center of the diatreme. A few crosscutting lamprophyric intrusions complicate the geometry of this intrusive. These crosscutting dikes may indicate the core was drilled into the lower or root portion of the diatreme, where mixed diatreme and hypabyssal lamprophyre phases would be spatially associated (Mitchell 1986). However, the composition of the micas in the globular segregations are characterized by low Mg and high Al and Fe and appear to be distinct from the other micas in other phases of this igneous intrusion, suggesting the intrusion might be multiphase. It is not clear whether the globular segregations characterize a disparate igneous phase or a hydrothermally altered phase.

A comparison of the REE patterns for fluorite with those of the ultramafic igneous rocks of the region shows good correspondence among the HREEs but a

significant separation of the LREEs. It is possible that the more incompatible LREEs fractionated away to an as-yet-undiscovered location. It is also possible that crystallization of florencite and synchysite, which preferentially incorporate the LREEs, was responsible for the relative LREE depletion of the fluid. The fact that Eu is preferentially incorporated into the fluorite structure at temperatures below 200 °C may explain the positive Eu anomaly in fluorite in the Cave-in-Rock District. The spatial coincidence of the HREE-enriched calcite-fluorite (KR-2) and the igneous rock sample from the Sparks Hill Diatreme (Figure 11) implies the HREEs may have been mobilized by CO<sub>2</sub>-rich fluids that later precipitated calcite. The presence of rare earth minerals such as xenotime, synchysite, and florencite along with abundant carbonate in the intrusives suggests a possible carbonatite fractionation of the ultramafic intrusion. The identification of REE-carbonate and REE-phosphate minerals along with the convex pattern of REE plots for IKFD fluorite is similar to other carbonatite-related fluorite deposits, such as the fluorite at Maoniping, Sichuan Province, China (Huang et al. 2007). Bradbury and Baxter (1992) classified some of the intrusions near Hicks Dome as carbonatitic. The formation of a carbonatite complex associated with the igneous activity agrees with the findings of Mariano (1987) and Reynolds et al. (1997), who argued for a genetic link between the Permian igneous activity at Hicks Dome and fluorite mineralization.

The fluorite in a crosscutting vein crystallized only within the confines of a dolostone clast (Figure 9), which suggests that the dolostone altered the chemistry of the fluid to allow fluorite precipitation. Likewise, most fluorite mineralization in the IKFD is associated with a carbonate host rock. Although the carbonate acts as a source of Ca for fluorite, it may also buffer the pH of an acidic ore fluid, promoting the precipitation of fluorite and other REE-bearing minerals. Fluid inclusion data strongly support a mineralization model that includes fluid mixing, and  $\delta^{13}\text{C}$  and  $\delta^{18}\text{O}$  data of ore-stage calcite associated with fluorite beneath Hicks Dome are intermediate between primary magmatic carbonatite

and sedimentary limestone host rock values (Morehead 2013). The available data seem to fit a model in which the fluorine-rich IKFD ore fluids were likely formed through the mixing of several sources, including groundwater, NaCl-rich "MVT brine," and hydrothermal and magmatic fluids associated with the ultramafic intrusions.

## ACKNOWLEDGMENTS

Funding for this work was obtained from the ISGS. This manuscript was also supported by the USGS, National Cooperative Geologic Mapping Program, under assistance award number G10AC00418. The ISGS is within the Prairie Research Institute at the University of Illinois at Urbana-Champaign, and the USGS is within the U.S. Department of the Interior. The authors acknowledge Texas A&M University for the electron microprobe analyses. We also thank the Great Western Minerals Group Ltd. for supplying rare earth standards for the ED-XRF analyses. Credit is also given to Adam Kittler for performing the ED-XRF analyses and April Halley for editorial and cartographic services. The authors appreciate the constructive and informative reviews of this manuscript by Steve Bergman and Martin Appold. The views and conclusions contained in this document are those of the authors and should not be interpreted as necessarily representing the official policies, either expressed or implied, of the State of Illinois or the U.S. Government.

## REFERENCES

Bastin, E.S., 1931, The fluorspar deposits of Hardin and Pope Counties, Illinois: Illinois State Geological Survey, Bulletin 58, 116 p.

Bau, M., and P. Dulski, 1995, Comparative study of yttrium and rare-earth element behaviors in fluorine-rich hydrothermal fluids: Contributions to Mineralogy and Petrology, v. 119, p. 213–223.

Baxter, J.W., G.A. Desborough, and C.W. Shaw, 1967, Areal geology of the Illinois fluorspar district. Part 3—Herod and Shetlerville Quadrangles: Illinois State Geological Survey, Circular 413, 41 p.

Baxter, J.W., P.E. Potter, and F.L. Doyle, 1963, Areal geology of the Illinois fluorspar district. Part 1—Saline Mines, Cave in Rock, Dekoven, and Repton Quadrangles: Illinois State Geological Survey, Circular 342, 43 p.; map, 1:24,000.

Bertagne, A.J., and T.C. Leising, 1991, Interpretation of seismic data from the Rough Creek Graben, western Kentucky and southern Illinois, in M.W. Leighton, D.R. Kolata, D.F. Oltz, and J.J. Eidel, eds., Interior cratonic basins: American Association of Petroleum Geologists, Memoir 51, p. 199–208.

Bradbury, J.C., and J.W. Baxter, 1992, Intrusive breccias at Hicks Dome: Illinois State Geological Survey, Circular 550, 23 p.

Brown, J.S., J.A. Emery, and P.A. Meyer Jr., 1954, Explosion pipe in test well on Hicks Dome, Hardin County, Illinois: Economic Geology, v. 49, no. 8, p. 891–902.

Bühn, B., 2008, The role of the volatile phase for REE and Y fractionation in low-silica carbonate magmas: Implications from natural carbonatites, Namibia: Mineralogy and Petrology, v. 92, p. 453–470.

Chesley, J.T., A.N. Halliday, T.K. Kyser, and P.G. Spry, 1994, Direct dating of Mississippi Valley-type mineralization: Use of Sm/Nd in fluorite: Economic Geology, v. 89, p. 1192–1199.

Cooper, A.F., 1979, Petrology of ocellar lamprophyres from western Otago, New Zealand: Journal of Petrology, v. 20, p. 139–163.

Cooper, A.F., and L.A. Patterson, 2008, Carbonatites from a lamprophyric dyke-swarm, South Westland, New Zealand: The Canadian Mineralogist, v. 46, p. 753–777.

Cunningham, C.G., and A.V. Heyl, 1980, Fluid inclusion homogenization temperatures throughout the sequence of mineral deposition in the Cave-in-Rock area, southern Illinois: Economic Geology, v. 75, no. 8, p. 1226–1231.

- Denny, F.B., 2005, The Cottage Grove Dike and mafic igneous intrusions in southeastern Illinois and their relation to regional tectonics and economic resources: Southern Illinois University at Carbondale, M.S. thesis, 83 p.
- Denny, F.B., A. Goldstein, J.A. Devera, D.A. Williams, Z. Lasemi, and W.J. Nelson, 2008, The Illinois-Kentucky Fluorite District, Hicks Dome, and Garden of the Gods in southeastern Illinois and northwestern Kentucky, *in* A.H. Maria and R.C. Counts, eds., From the Cincinnati Arch to the Illinois Basin: Geological field excursions along the Ohio River valley: Geological Society of America, Field Guide 12, p. 11–24.
- Denny, F.B., R.N. Guillemette, and L. Lefticariu, 2015, Rare earth mineral concentrations in ultramafic alkaline rocks and fluorite within the Illinois-Kentucky Fluorite District: Hicks Dome cryptoexplosive complex, southeast Illinois and northwest Kentucky (USA), *in* Z. Lasemi, ed., Proceedings of the 47th Forum on the Geology of Industrial Minerals: Illinois State Geological Survey, Circular 587, p. 77–92.
- Denny, F.B., B. King, J. Mulvaney-Norris, and D.H. Malone, 2010, Bedrock geology of Karbers Ridge Quadrangle, Hardin, Gallatin, and Saline Counties, Illinois: Illinois State Geological Survey, Illinois Geologic Quadrangle Map, IGQ Karbers Ridge-BG, report, 7 p.; 2 sheets, 1:24,000.
- Doroshkevich, A.G., S.G. Viladkar, G.S., Ripp, and M.V. Burtseva, 2009, Hydrothermal REE mineralization in the Amba Dongar carbonatite complex, Gujarat, India: *The Canadian Mineralogist*, v. 47, p. 1105–1116.
- Duke, G.I., R.W. Carlson, C.D. Frost, B.C. Hearn Jr., and G.N. Eby, 2014, Continent-scale linearity of kimberlite-carbonatite magmatism, mid-continent North America: *Earth and Planetary Science Letters*, v. 403, p. 1–14.
- Fifarek, R.H., F.B. Denny, L.W. Snee, and D.P. Miggins, 2001, Permian igneous activity in southeastern Illinois and western Kentucky: Implications for tectonism and economic resources: Geological Society of America, Abstracts with Programs, v. 33, no. 6, p. A-420.
- Freas, D.H., 1961, Temperatures of mineralization by liquid inclusions, Cave-in-Rock fluorspar district, Illinois: *Economic Geology*, v. 56, p. 542–556.
- Goldstein, A., and D.A. Williams, 2008, The history of the Illinois Kentucky Fluorite District, *in* F.B. Denny, A. Goldstein, J.A. Devera, D.A. Williams, Z. Lasemi, and W.J. Nelson, The Illinois-Kentucky Fluorite District, Hicks Dome, and Garden of the Gods in southeastern Illinois and northwestern Kentucky, *in* A.H. Maria and R.C. Counts, eds., From the Cincinnati Arch to the Illinois Basin: Geological field excursions along the Ohio River valley: Geological Society of America, Field Guide 12, p. 18–20.
- Hall, W.E., and I. Friedman, 1963, Distribution of minor elements in ore and host rock, Illinois-Kentucky fluorite district and Upper Mississippi Valley zinc-lead district: *Economic Geology*, v. 63, p. 655–670.
- Hildenbrand, T.G., and D. Ravat, 1997, Geophysical setting of the Wabash Valley Fault System: *Seismological Research Letters*, v. 68, p. 567–585.
- Howe, J.R., and T.L. Thompson, 1984, Tectonics, sedimentation, and hydrocarbon potential of Reelfoot Rift: *Oil and Gas Journal*, v. 82, p. 179–190.
- Huang, Z., C. Xu, A. McCaig, C. Liu, J. Wu, D. Xu, W. Li, T. Guan, and H. Xiao, 2007, REE geochemistry of fluorite from the Maoniuping REE deposit, Sichuan Province, China: Implications for the source of ore-forming fluids: *Acta Geologica Sinica*, v. 81, no. 4, p. 622–636.
- Kendrick, M.A., R. Burgess, D. Leach, and R.A.D. Patrick, 2002, Hydrothermal fluid origins in Mississippi Valley-type ore deposits: Combined noble gas (He, Ar, Kr) and halogen (Cl, Br, I) analysis of fluid inclusions from the Illinois-Kentucky fluorspar district, Viburnum Trend, and Tri-State districts, Midcontinent United States: *Economic Geology*, v. 97, p. 453–469.
- Kidwell, A.L., 1951, Mesozoic igneous activity in the northern Gulf Coastal Plain: *Transactions of the Gulf Coast Association of Geological Societies*, v. 1, p. 182–199.
- Leach, D.L., R.D. Taylor, D.L. Fey, S.F. Diehl, and R.W. Saltus, 2010, A deposit model for Mississippi Valley-Type lead-zinc ores, Chapter A of Mineral deposit models for resource assessment: U.S. Geological Survey, Scientific Investigations Report 2010-5070-A, 52 p.
- Lewis, R.D., and R.H. Mitchell, 1987, Alnöite intrusions associated with rifting in the New Madrid Seismic Zone: Geological Society of America, Abstracts with Programs, v. 19, no. 7, p. 745.
- Lloyd, F.E., and F. Stoppa, 2003, Pelletal lapilli in diatremes—Some inspiration from the old masters: *GeoLines*, v. 15, p. 65–67.
- Long, K.R., B.S. Van Gosen, N.K. Foley, and D. Cordier, 2010, The principal rare earth elements deposits of the United States—A summary of domestic deposits and a global perspective: U.S. Geological Survey, Scientific Investigations Report 2010-5220, 96 p.
- Lorenz, V., 2003, Maar-diatreme volcanoes, their formation, and their setting in hard-rock or soft-rock environments: *GeoLines*, v. 15, p. 72–83.
- Maria, A.H., J.A. Dipietro, and K.F. Howard, 2016, Geochemistry and Sr-Nd isotopic compositions of Permian ultramafic lamprophyres in southern Illinois: Geological Society of America, Abstracts with Programs, v. 48, no. 7.
- Maria, A.H., and M.D. King, 2012, Petrology and geochemistry of an ultramafic dike in southern Illinois: Geological Society of America, Abstracts with Programs, v. 44, no. 7, p. 541.
- Mariano, A.N., 1987, Analytical report on 4 regolith samples and 4 pieces of drill core from Hicks Dome, Hardin County, Illinois: Confidential report to John Lee Carroll, 24 p.
- Migdisov, A.A., and A.E. Williams-Jones, 2014, Hydrothermal transport and

- deposition of the rare earth elements by fluorine-bearing aqueous liquids: *Mineralium Deposita*, v. 49, p. 987–997.
- Mitchell, R.H., 1986, *Kimberlites: Mineralogy, geochemistry, and petrology*: New York, Plenum Press, 442 p.
- Mitchell, R.H., 1995, *Kimberlites, orangeites, and related rocks*: New York, Plenum Press, 410 p.
- Möller, P., M. Bau, P. Dulski, and V. Luders, 1998, REE and Y fractionation in fluorite and their bearing on fluorite formation: Proceedings of the Ninth Quadrennial IAGOD Symposium: Stuttgart, Schweizerbart, p. 575–592.
- Moody, C.L., 1949, Mesozoic igneous rocks of northern Gulf Coastal Plain: *Bulletin of the American Association of Petroleum Geologists*, v. 33, p. 1410–1428.
- Morehead, A.H., 2013, *Igneous intrusions at Hicks Dome, southern Illinois, and their relationship to fluorine-base metal-rare earth element mineralization*: Southern Illinois University at Carbondale, M.S. thesis, 226 p.
- Nelson, W.J., 1995, Structural features in Illinois: *Illinois State Geological Survey, Bulletin 100*, 144 p.
- Nelson, W.J., F.B. Denny, L.R. Follmer, and J.M. Masters, 1999, Quaternary grabens in southernmost Illinois: Deformation near an active intraplate seismic zone: *Tectonophysics*, v. 305, p. 381–397.
- Nelson, W.J., and D.K. Lumm, 1984, Structural geology of southeastern Illinois and vicinity: *Illinois State Geological Survey, ISGS Contract Grant Report 1984-2*, 127 p.
- Ohle, E.L., 1959, Some considerations in determining the origin of ore deposits of the Mississippi Valley type: *Economic Geology*, v. 54, p. 769–789.
- Pinckney, D.M., and R.O. Rye, 1972, Variation of  $O^{18}/O^{16}$ ,  $C^{13}/C^{12}$ , texture, and mineralogy in altered limestone in the Hill Mine, Cave-in-Rock District, Illinois: *Economic Geology*, v. 67, p. 1–18.
- Potter, C.J., M.B. Goldhaber, P.C. Heigold, and J.A. Drahoval, 1995, Structure of the Reelfoot-Rough Creek rift system, Fluorspar area fault complex, and Hicks Dome, southern Illinois and western Kentucky—New constraints from regional seismic reflection data: U.S. Geological Survey, Professional Paper 1538-Q, 19 p.
- Reynolds, R.L., M.B. Goldhaber, and L.W. Snee, 1997, Paleomagnetic and  $^{40}\text{Ar}/^{39}\text{Ar}$  results from the Grant intrusive breccia and comparison to the Permian Downeys Bluff Sill—Evidence for Permian igneous activity at Hicks Dome, southern Illinois Basin: U.S. Geological Survey, Bulletin 2094-G, 16 p.
- Richardson, C.K., and D.M. Pinckney, 1984, The chemical and thermal evolution of fluids in the Cave-in-Rock fluorspar district, Illinois: *Mineralogy, paragenesis, and fluid inclusions*: *Economic Geology*, v. 79, p. 1833–1856.
- Ruiz, J., C.K. Richardson, and P.J. Patchett, 1988, Strontium isotope geochemistry of fluorite, calcite, and barite of the Cave-in-Rock fluorite district, Illinois: *Economic Geology*, v. 83, p. 203–210.
- Schwinn, G., and G. Markyl, 2005, REE systematics in hydrothermal fluorite: *Chemical Geology*, v. 216, p. 225–248.
- Shavers, E.T., A. Ghulam, J. Encarnacion, D.L. Bridges, and P.B. Luetkemeyer, 2016, Carbonatite associated with ultramafic diatremes in the Avon Volcanic District, Missouri, USA: Field, petrographic, and geochemical constraints: *Lithos*, v. 248–251, p. 506–516.
- Snee, L.W., and T.S. Hayes, 1992,  $^{40}\text{Ar}/^{39}\text{Ar}$  geochronology of intrusive rocks and Mississippi Valley-type mineralization and alteration from the Illinois-Kentucky fluorspar district, in M.B. Goldhaber and J.J. Eidel, eds., *Mineral resources of the Illinois Basin in the context of basin evolution*: U.S. Geological Survey, Open-File Report 92-1, p. 59–60.
- Sparlin, M.A., and R.D. Lewis, 1994, Interpretation of the magnetic anomaly over the Omaha Oil Field, Gallatin County, Illinois: *Geophysics*, v. 59, p. 1092–1099.
- Spry, P.G., and G.D. Fuhrmann, 1994, Additional fluid inclusion data for the Illinois-Kentucky fluorspar district: Evidence for the lack of a regional thermal gradient: *Economic Geology*, v. 89, p. 288–306.
- Spry, P.G., M.S. Koellner, C.K. Richardson, and H.D. Jones, 1990, Thermochemical changes in the ore fluid during deposition at the Denton Mine, Cave-in-Rock fluorspar district, Illinois: *Economic Geology*, v. 85, p. 172–181.
- Tappe, S., S.F. Foley, G.A. Jenner, L.M. Heaman, B.A. Kjarsgaard, R.L. Romer, A. Stracke, N. Joyce, and J. Hoefs, 2006, Genesis of ultramafic lamprophyres and carbonatites at Aillik Bay, Labrador: A consequence of incipient lithospheric thinning beneath the North Atlantic craton: *Journal of Petrology*, v. 47, p. 1261–1315.
- Taylor, S.R., and S.M. McLennan, 1985, *The continental crust: Its composition and evolution*: Oxford, UK, Blackwell Science, 312 p.
- Trace, R.D., 1960, Significance of unusual mineral occurrence at Hicks Dome, Hardin County, Illinois, in *Short papers in the geological sciences*, Geological Survey research, 1960: U.S. Geological Survey, Professional Paper 400-B, p. B63–B64.
- Trofanenko, J., A.E. Williams-Jones, G.J. Simandl, and A.A. Migdisov, 2016, The nature and origin of the REE mineralization in the Wicheeda Carbonatite, British Columbia, Canada: *Economic Geology*, v. 111, p. 199–223.
- Verplank, P.L., and B.S. Van Gosen, 2011, Carbonatite and alkaline intrusion-related rare earth element deposits—A deposit model: U.S. Geological Survey, Open File Report 2011-1256, 6 p.
- Wall, F., and A.N. Mariano, 1996, Rare earth minerals in carbonatites: A discussion centered on the Kangankunde Carbonatite, Malawi, in A.P. Jones, F. Wall, and C.T. Williams, eds., *Rare earth minerals*: London, Chapman and Hall, p. 193–225.

Weller, J.M., R.M. Grogan, and F.E. Tippie, 1952, Geology of the fluorspar deposits of Illinois: Illinois State Geological Survey, Bulletin 76, 150 p., 4 plates.

Williams, H., F.J. Turner, and C.M. Gilbert, 1982, Petrography—An introduction to the study of rocks in thin section: New York, W.H. Freeman and Company, 626 p.

Zartman, R.E., M.R. Brock, A.V. Heyl, and H.H. Thomas, 1967, K-Ar and Rb-Sr ages of some alkalic intrusive rocks from central and eastern United States: American Journal of Science, v. 265, p. 848–870.



## APPENDIX 1

**Table A1** Legend

Abbreviation	Descriptor
SS	Sandstone
CL	Clay
LS	Limestone
AL	Autolith
DS	Dolostone
Gr	Granite
Cal	Calcite
Sil	Silicified
Ig	Igneous
Ap	Apatite
bx	Breccia
Cpy	Chalcopyrite
Cal V.	Calcite vein
Ch	Chert
Py	Pyrite
Sh	Shale
Fl	Fluorite
Qtz	Quartz
PL	Pelletal lapilli
GS	Globular segregation

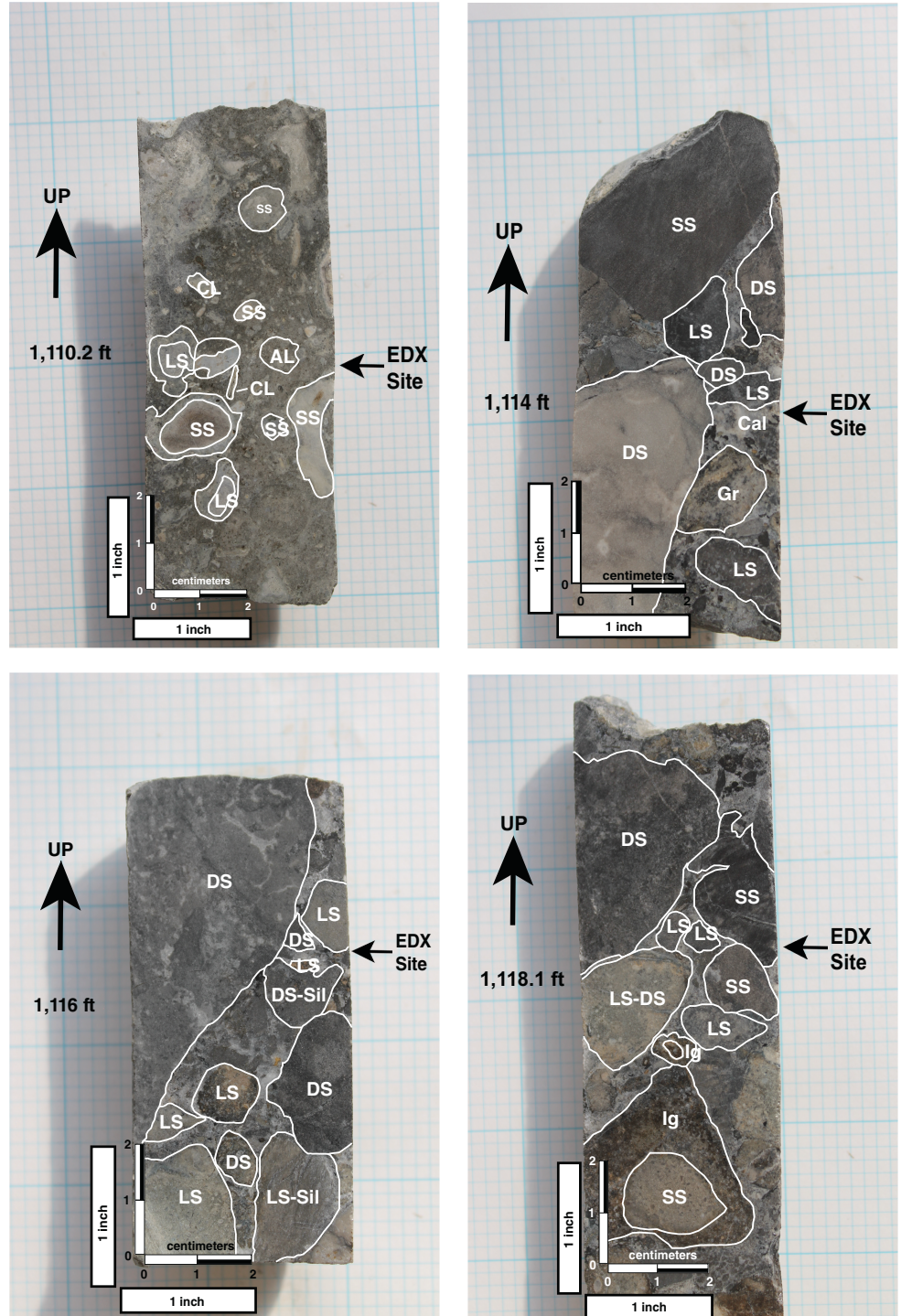


**Figure A1** Photographs of the areas scanned for each energy-dispersive X-ray fluorescence spectrometry (EDX) analysis. Number indicates the depth of core in feet.

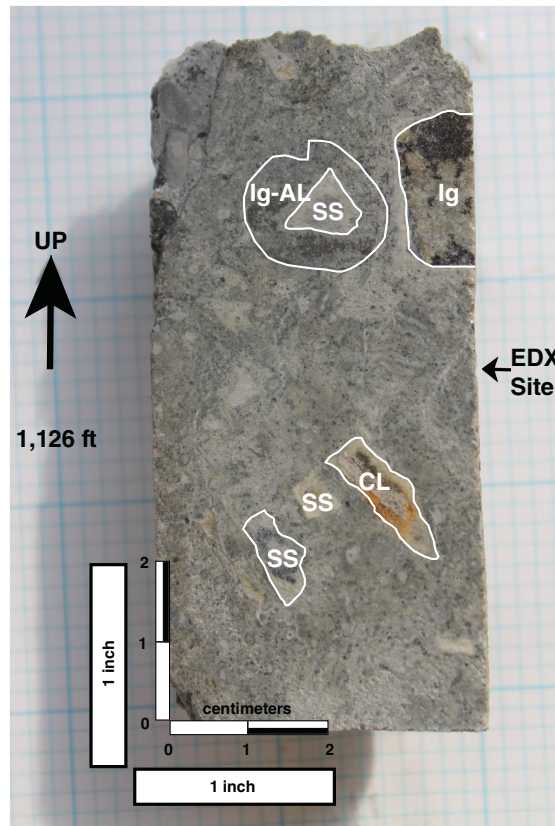
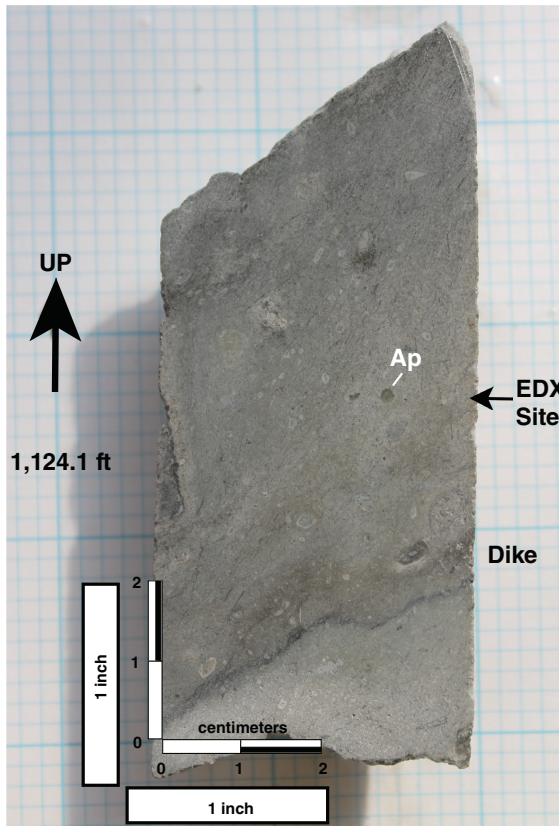
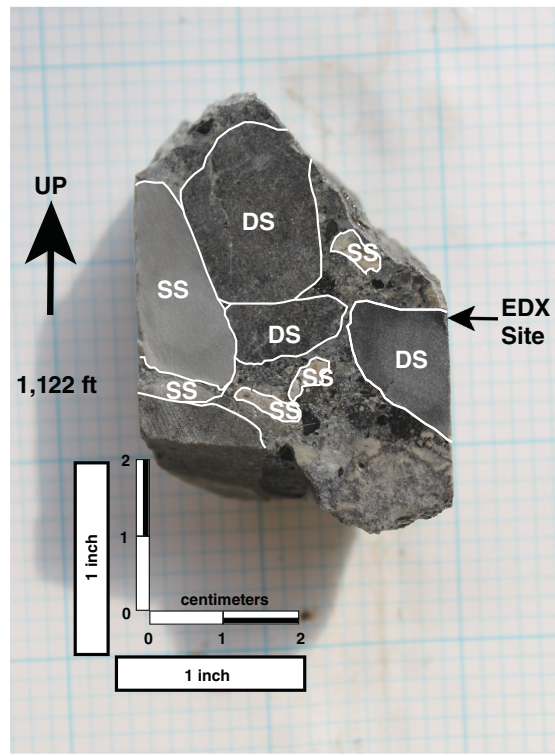
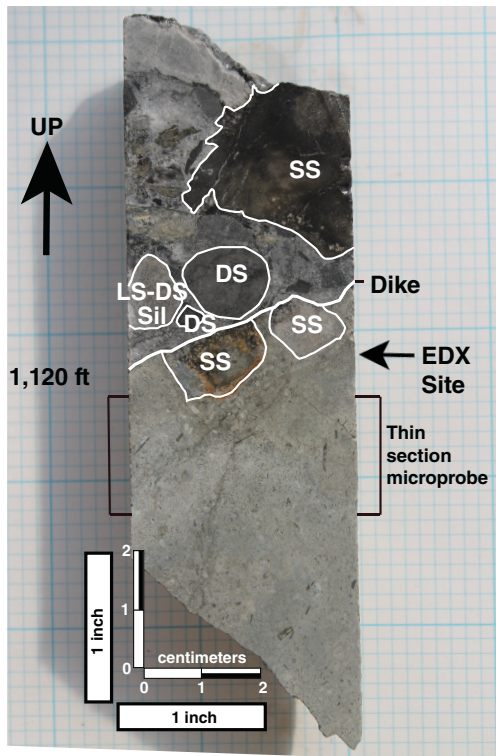


Figure A1 (Continued)

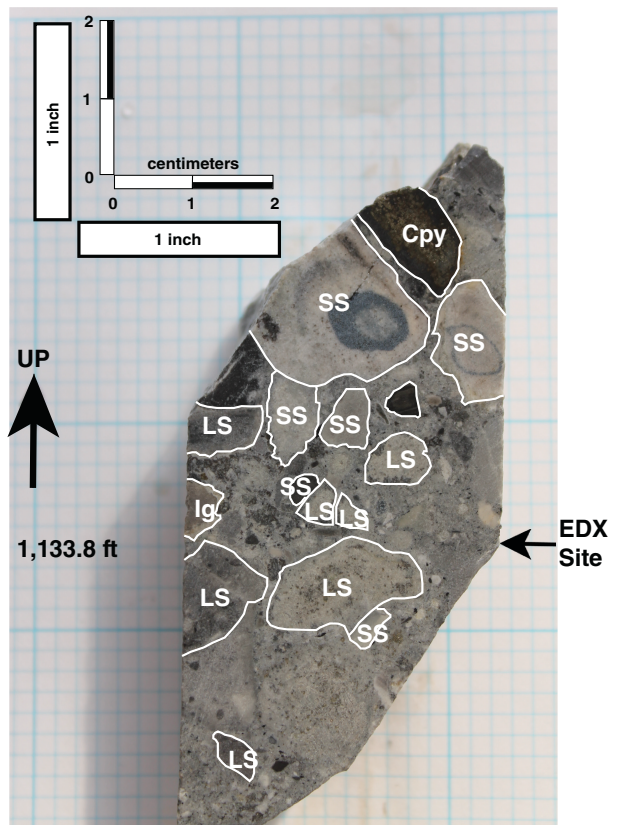
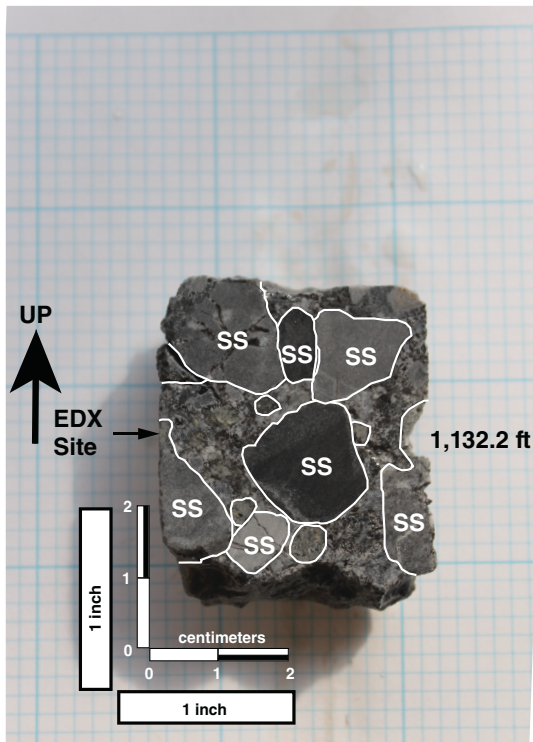
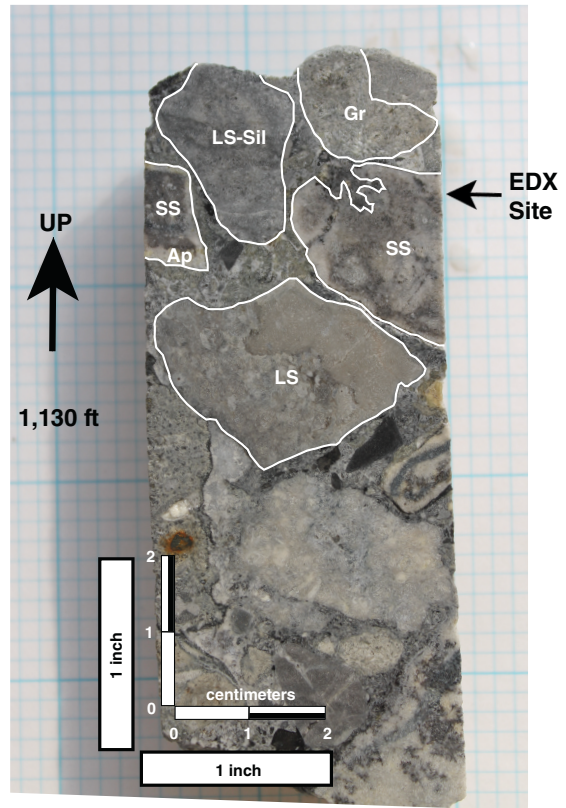
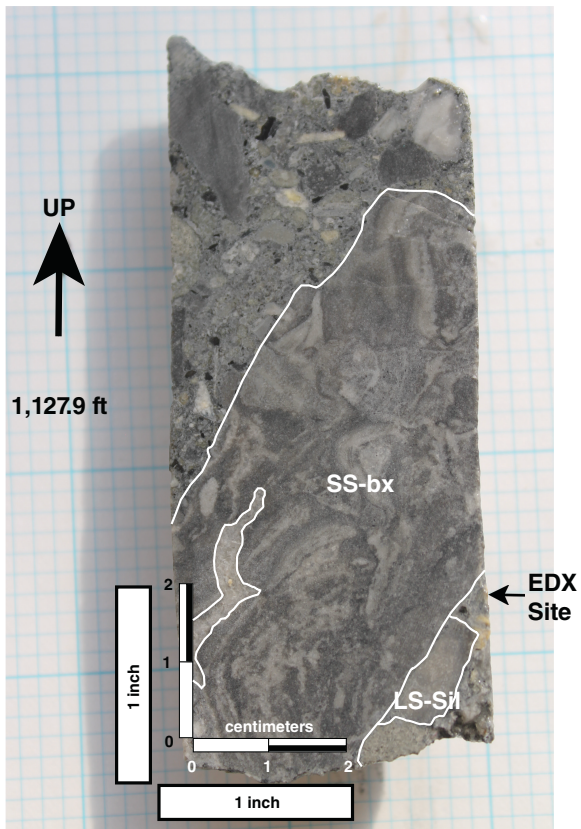


Figure A1 (Continued)

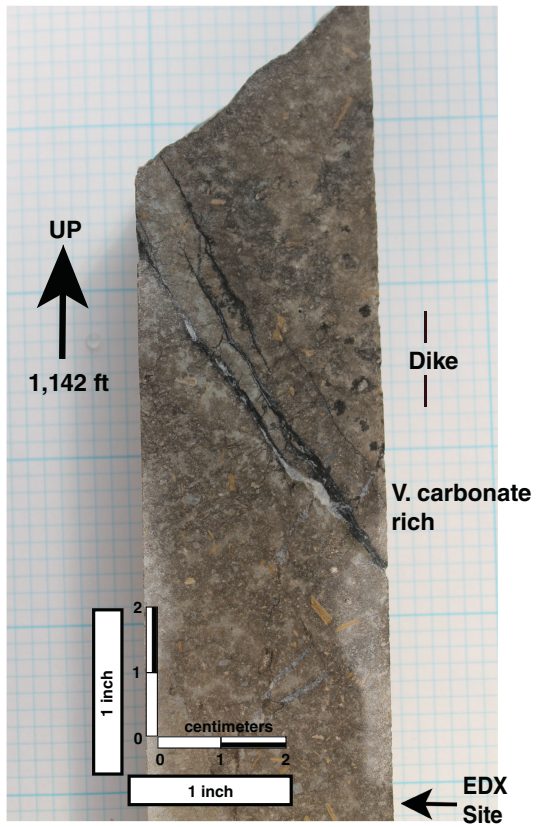
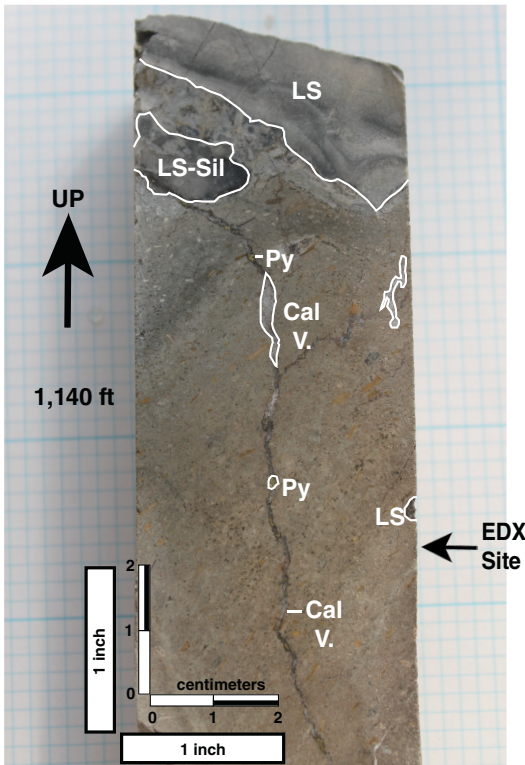
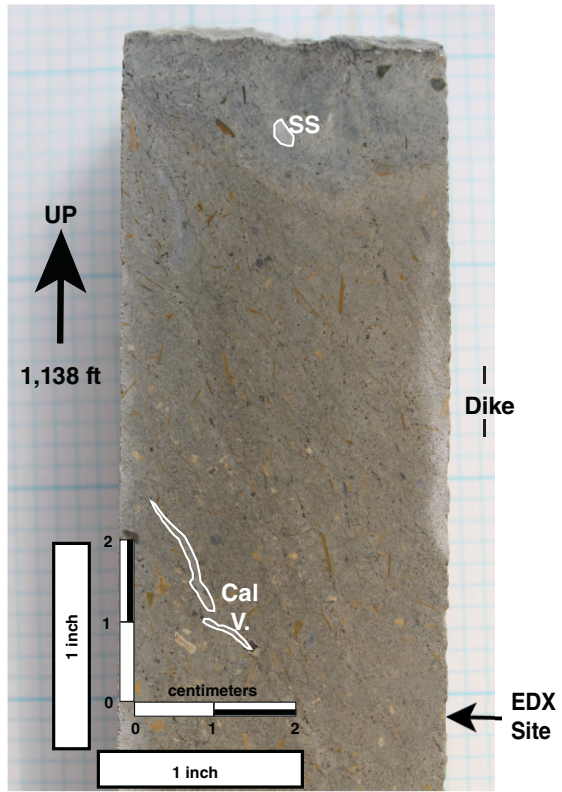
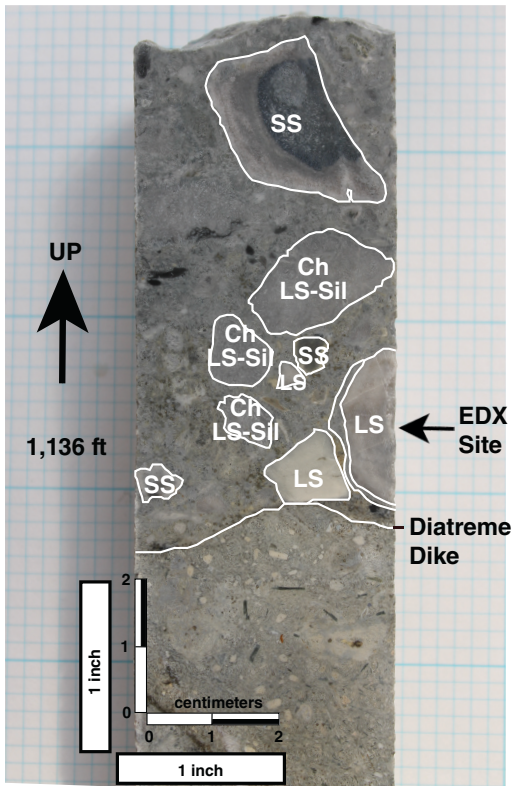


Figure A1 (Continued)

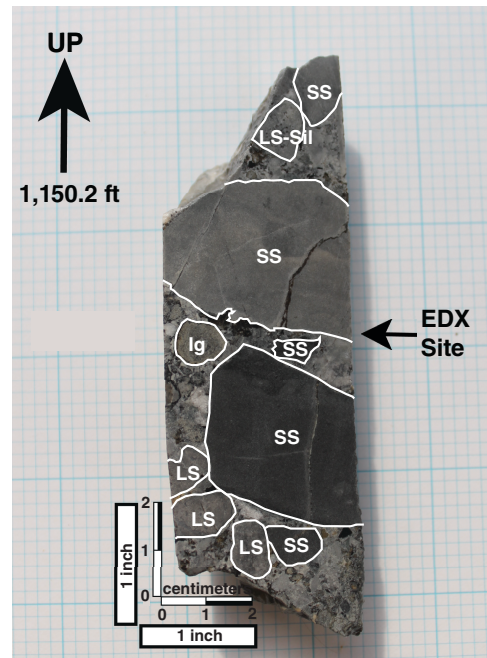
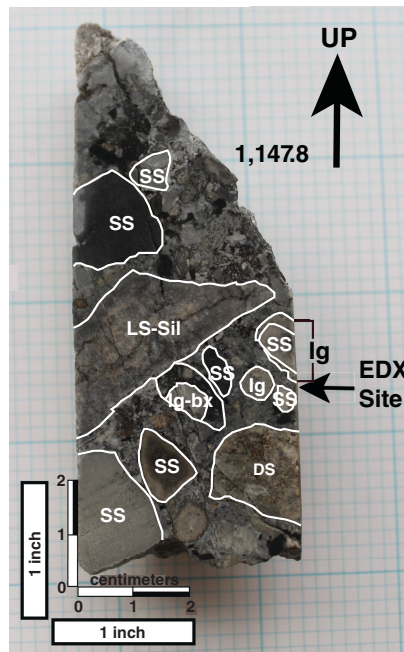
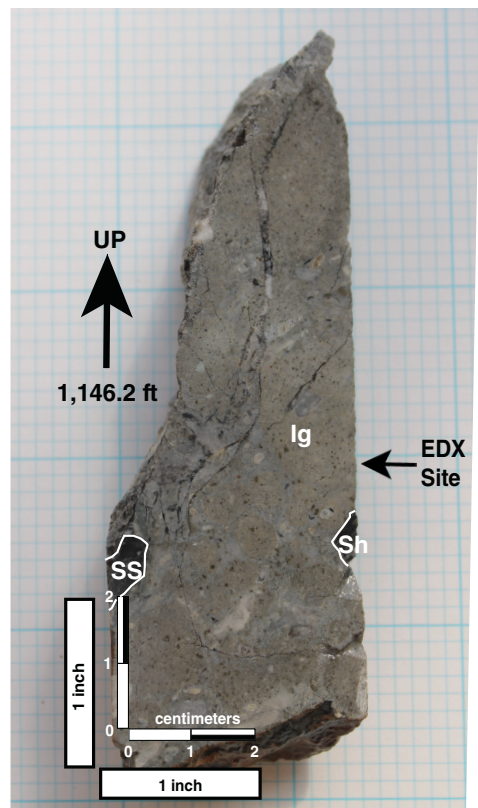
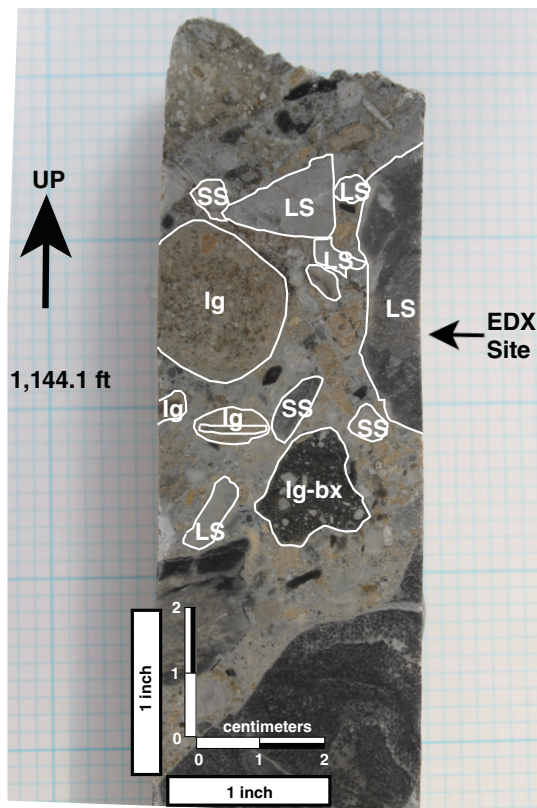


Figure A1 (Continued)



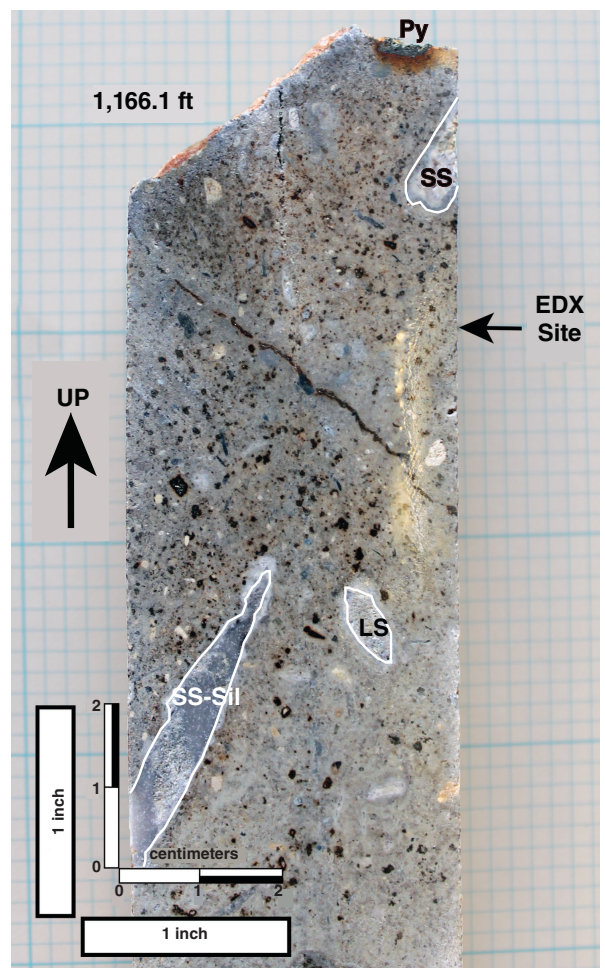
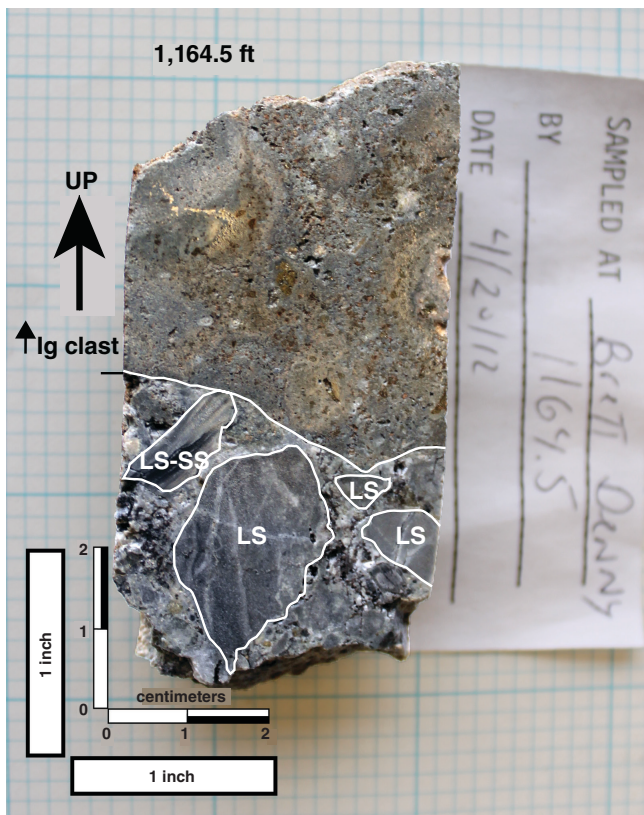
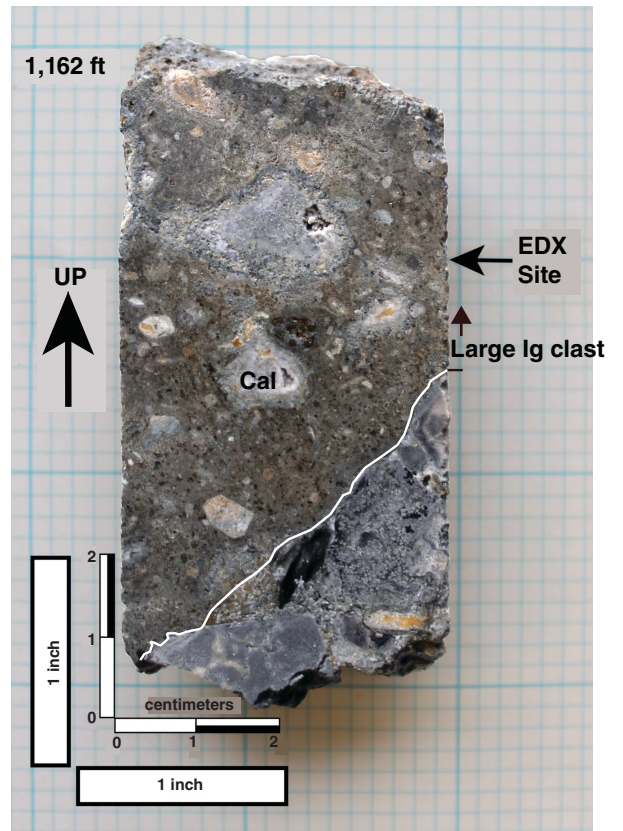
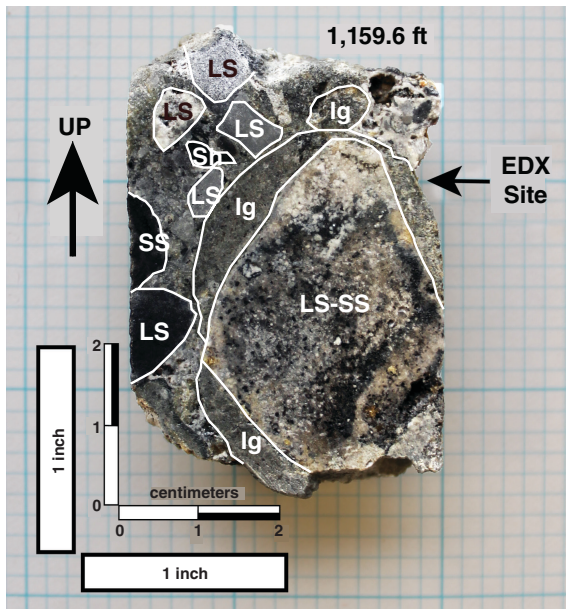
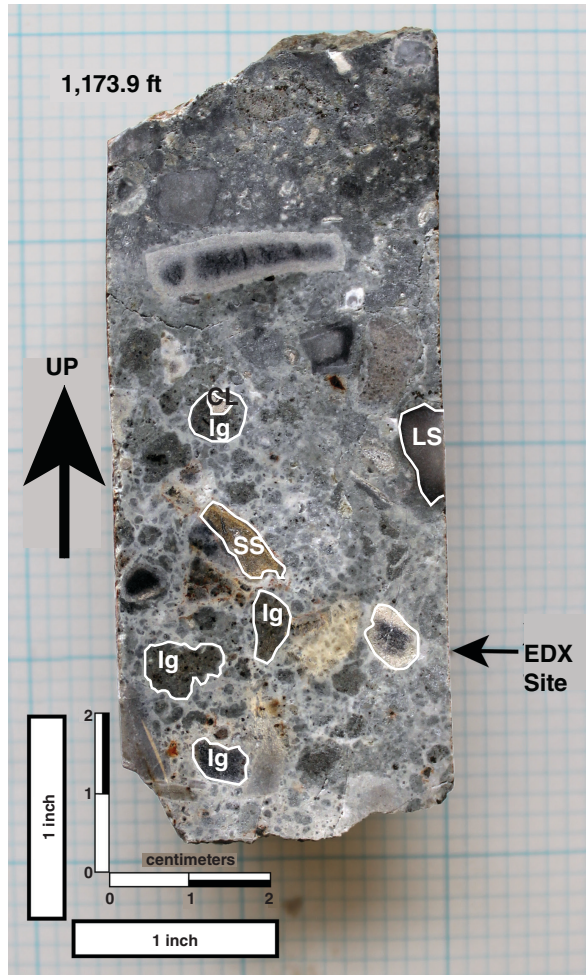
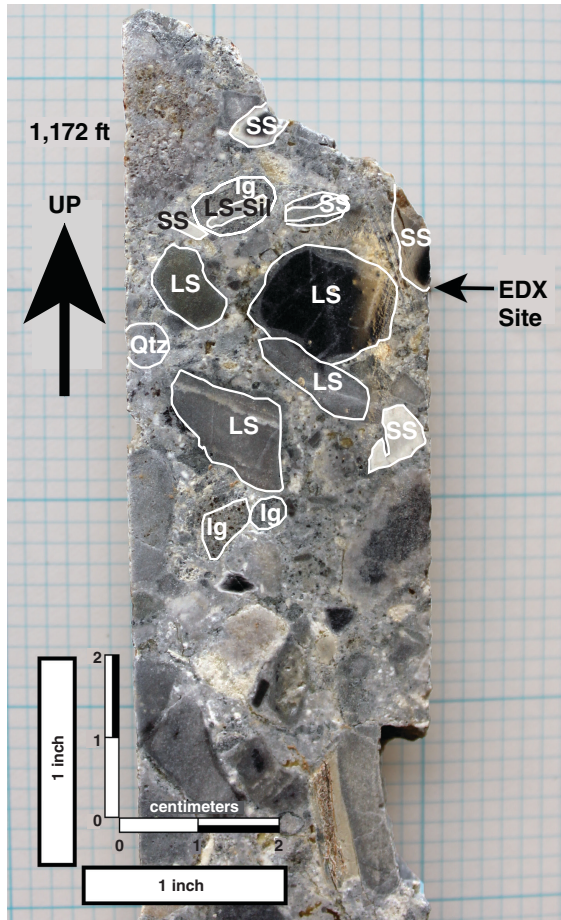
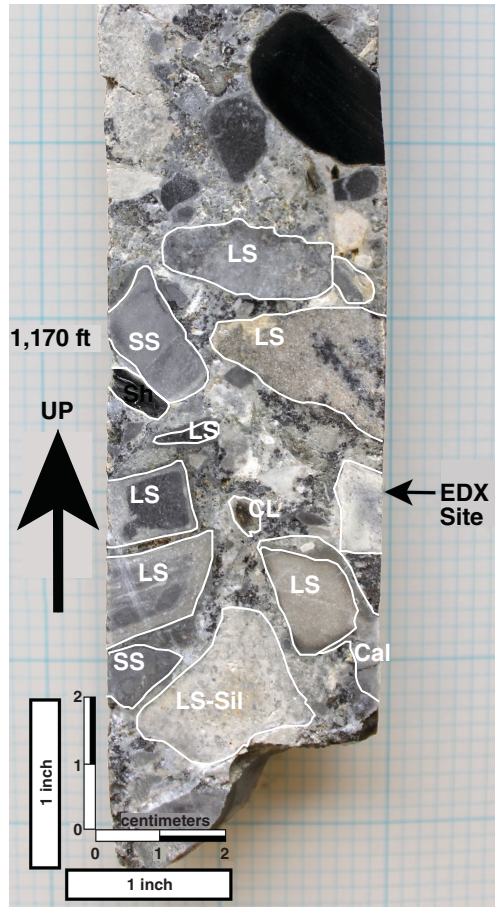
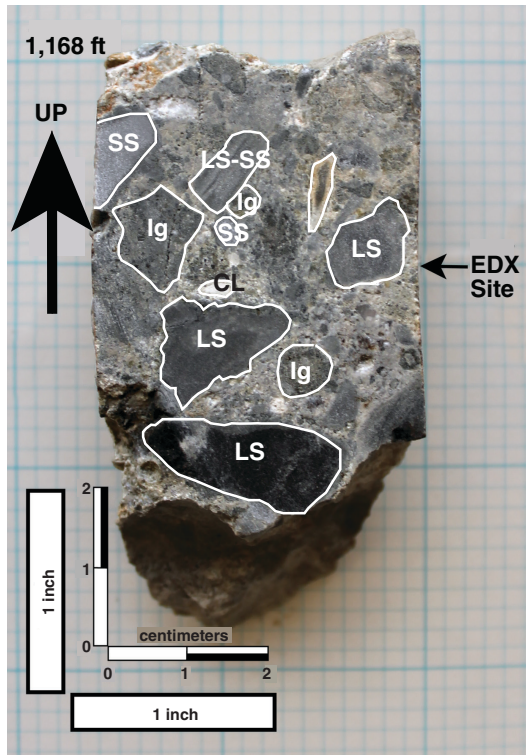


Figure A1 (Continued)



32 Figure A1 (Continued)

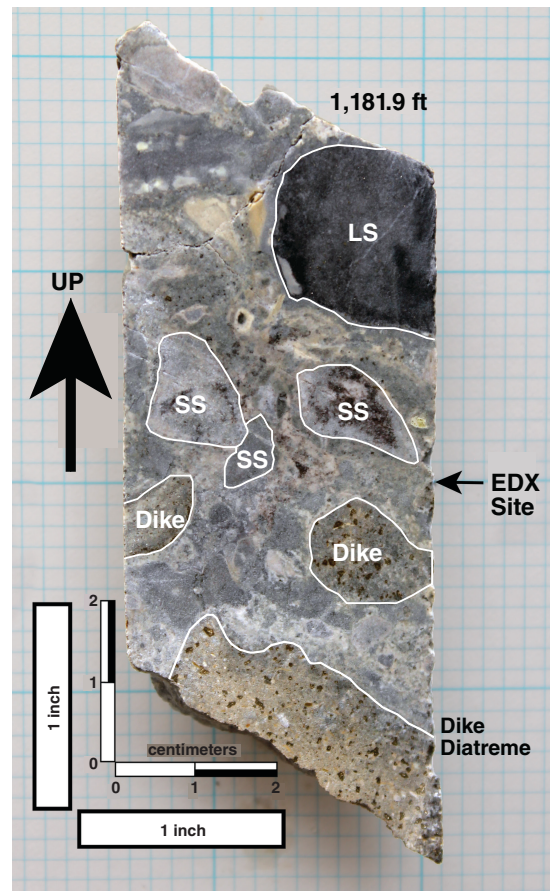
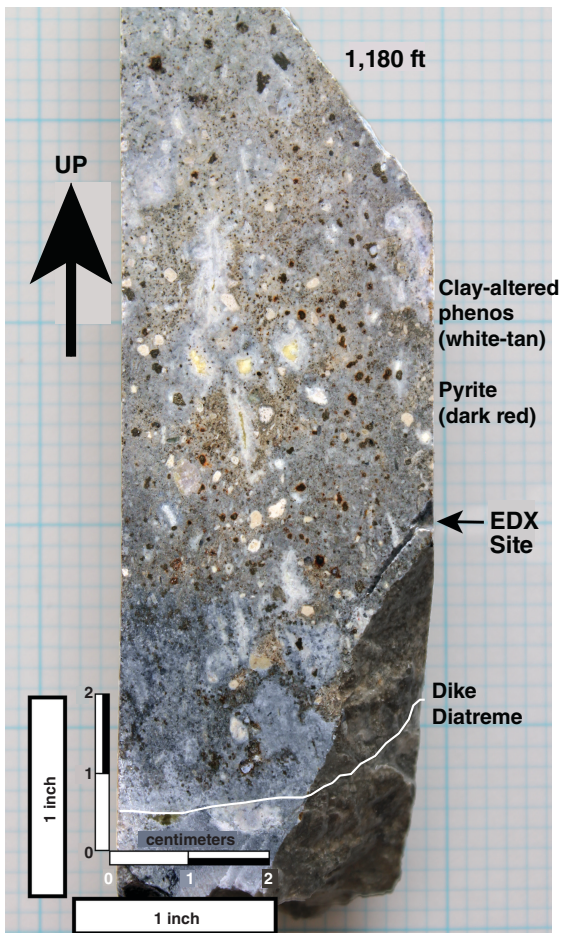
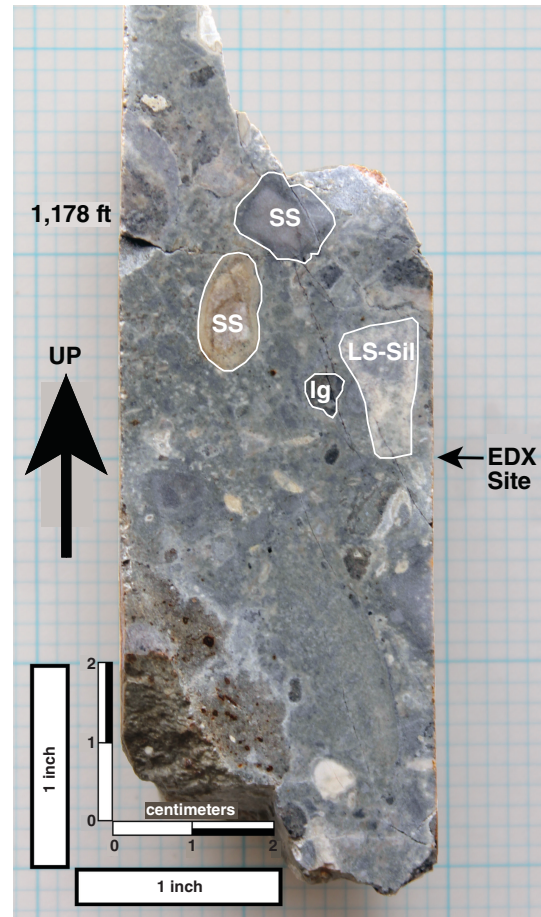
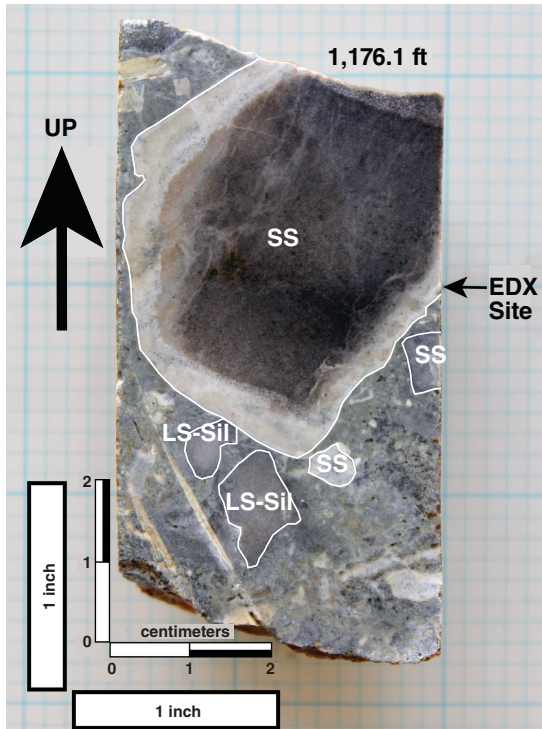
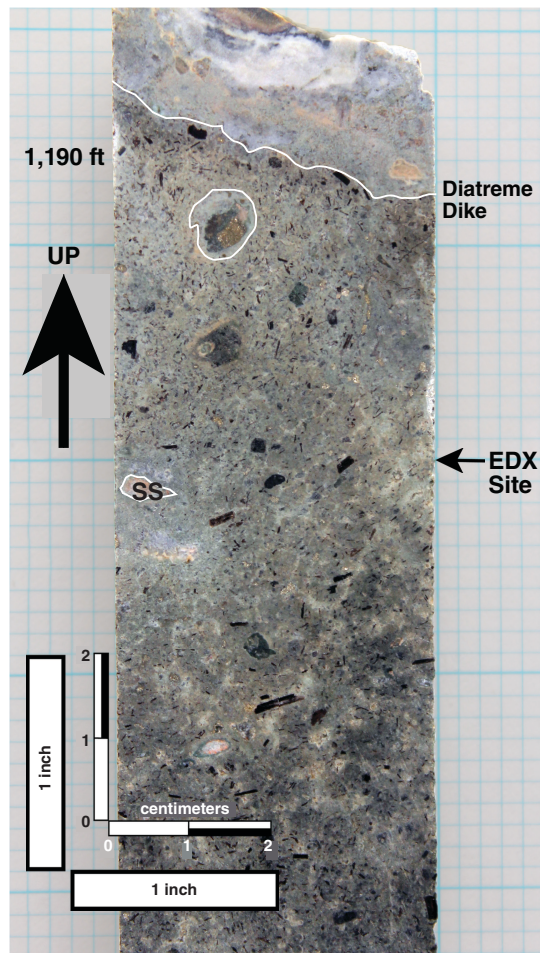
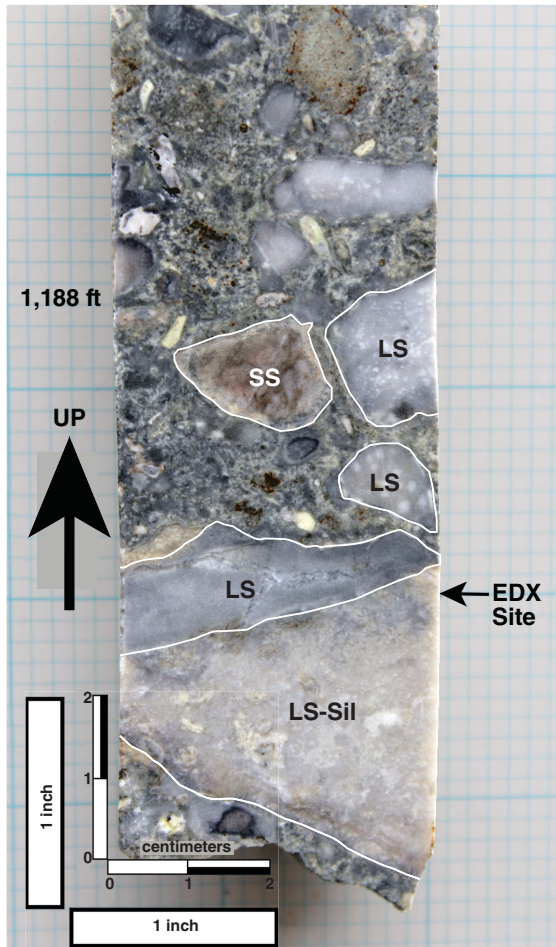
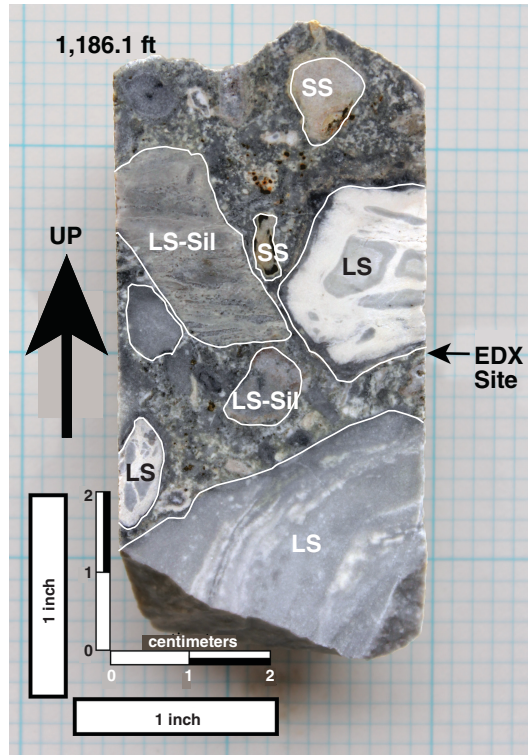
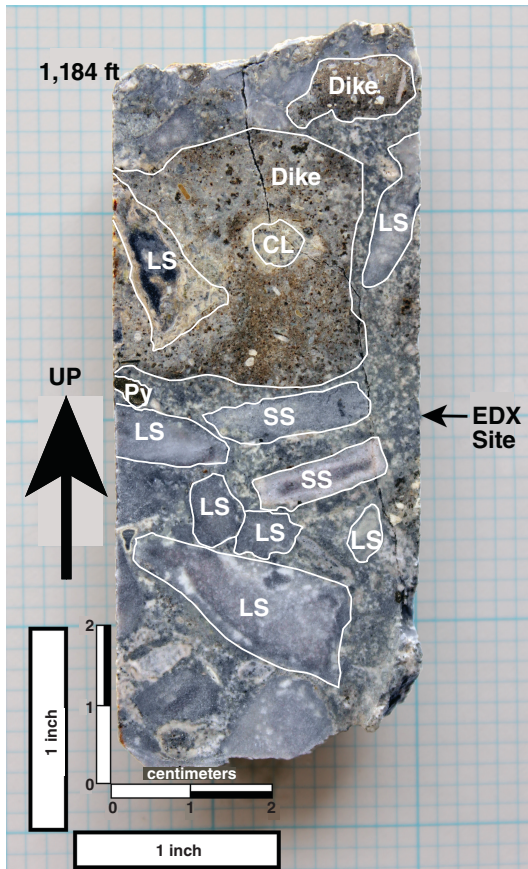


Figure A1 (Continued)



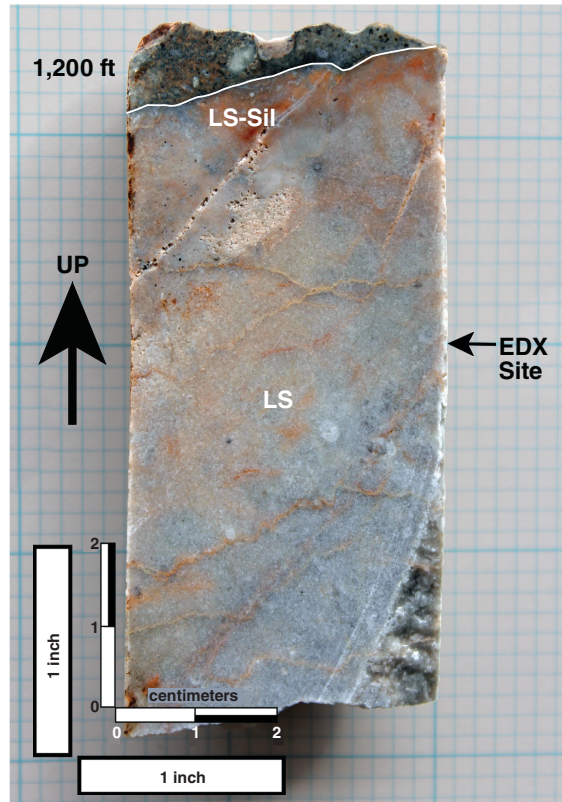
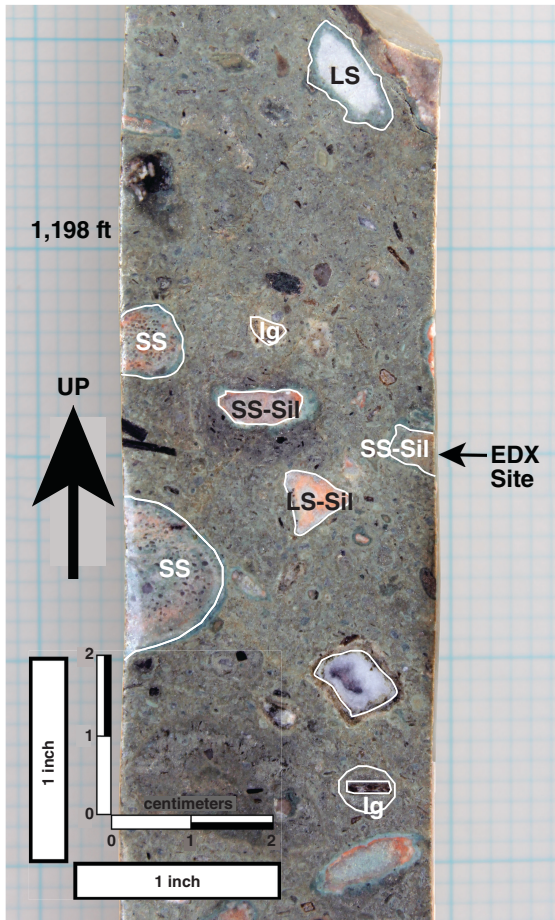
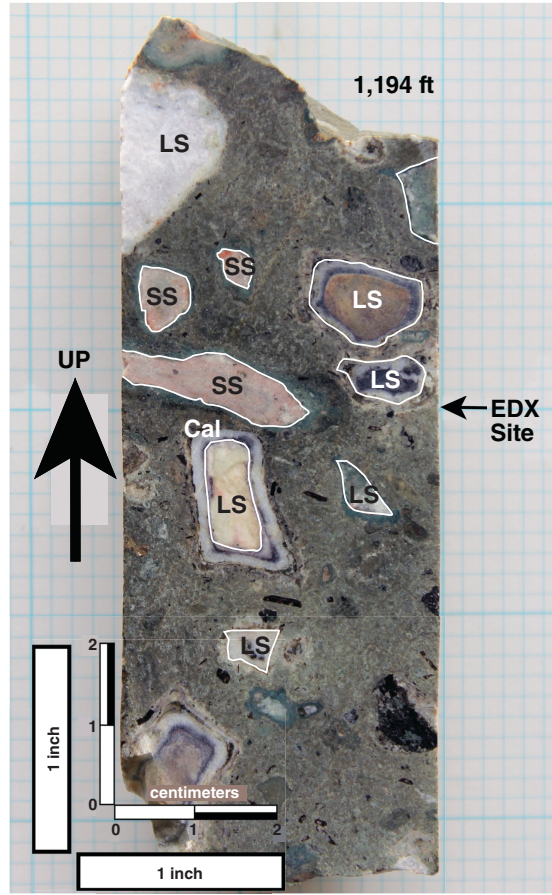
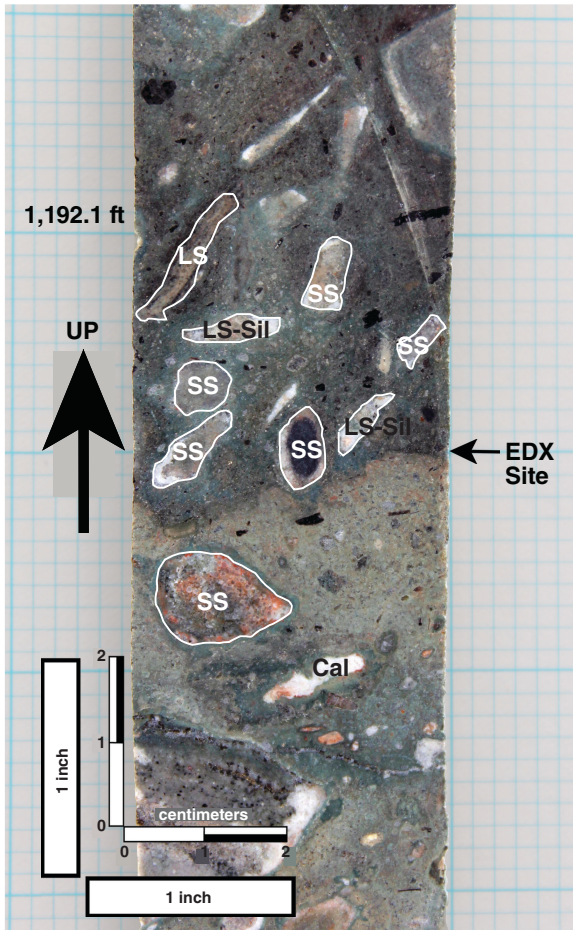


Figure A1 (Continued)

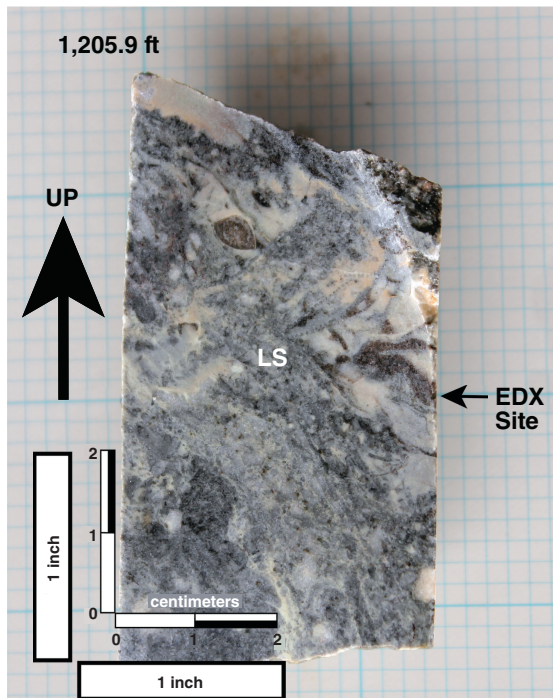
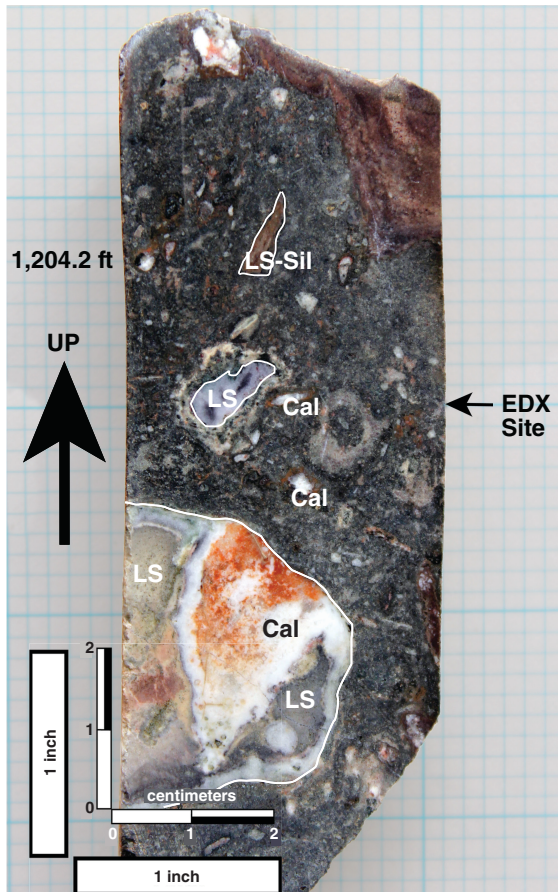
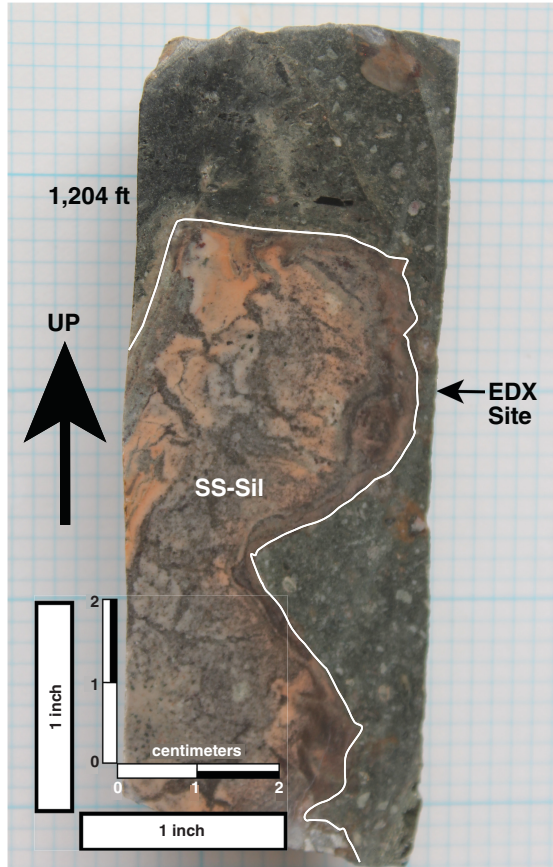
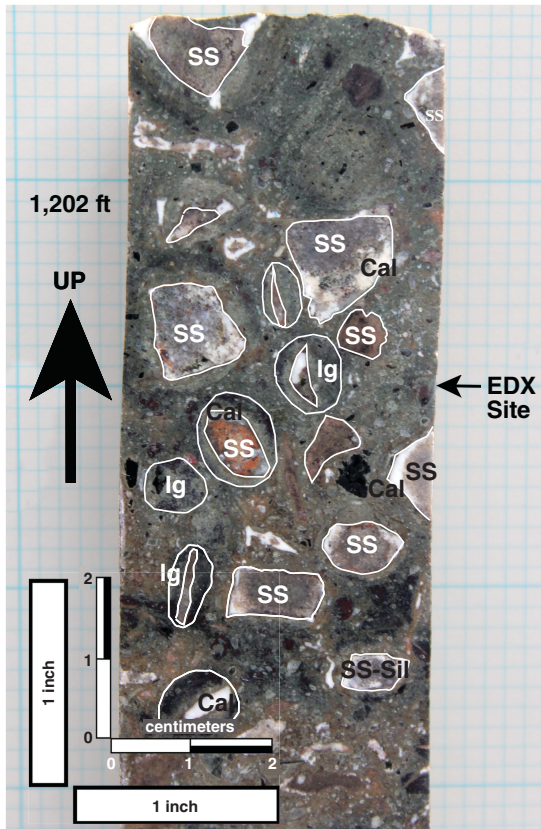


Figure A1 (Continued)

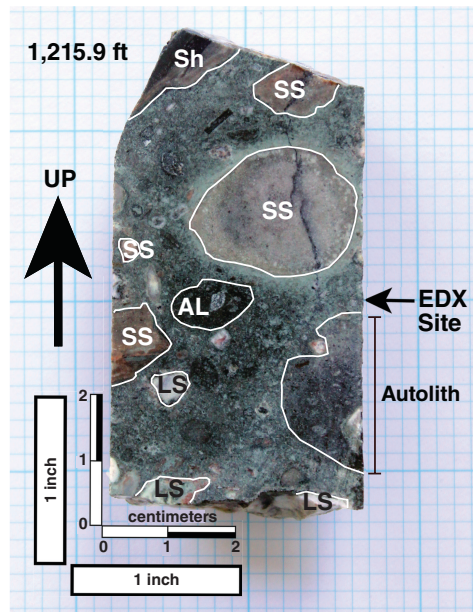
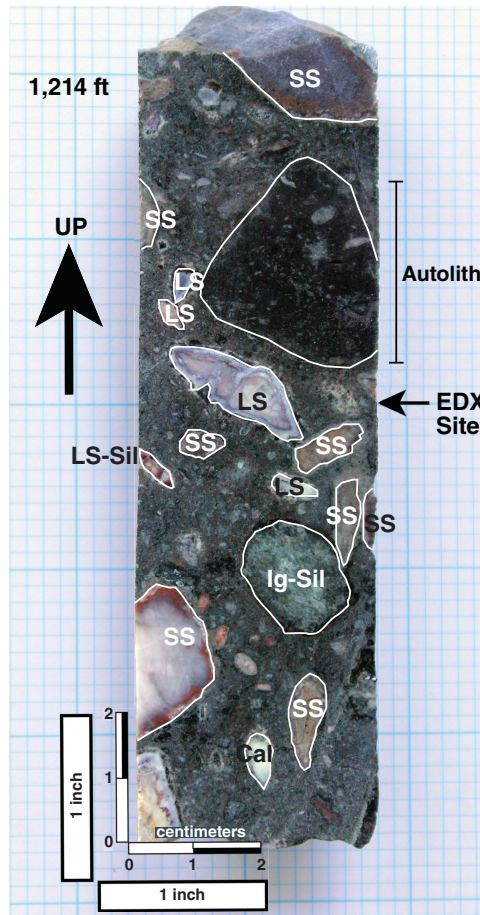
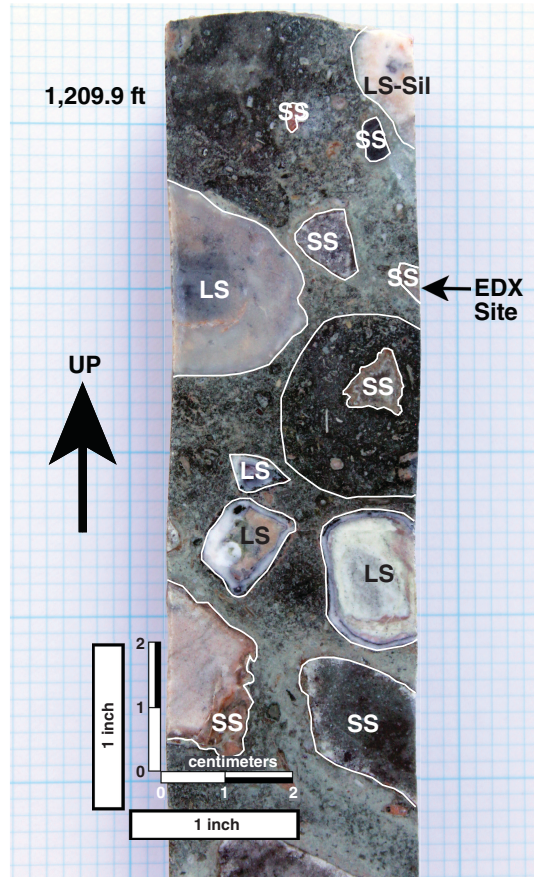
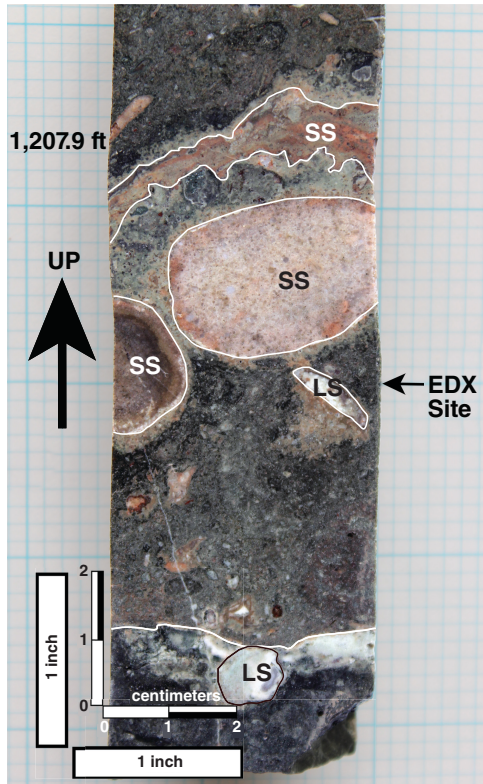


Figure A1 (Continued)

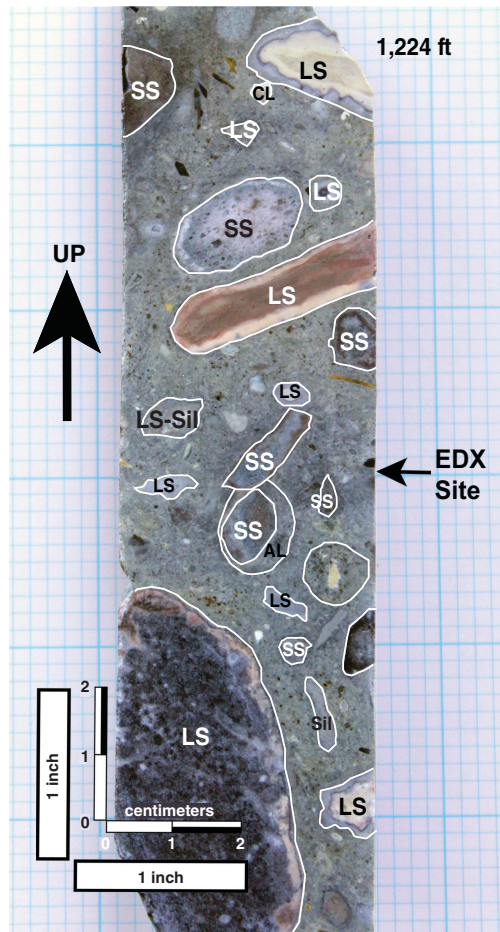
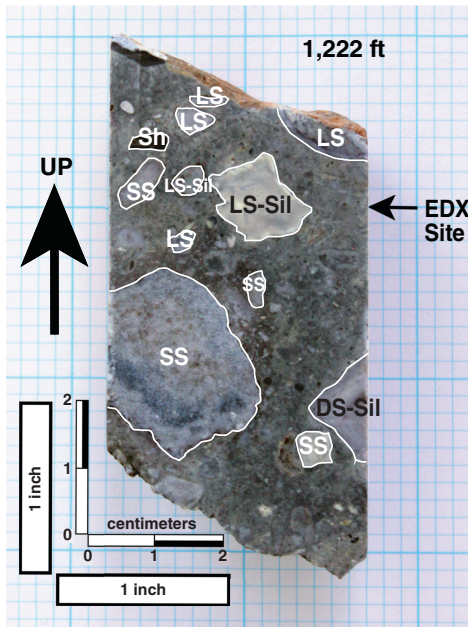
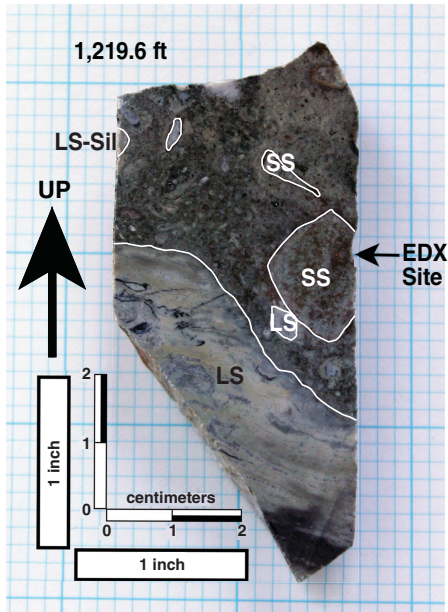
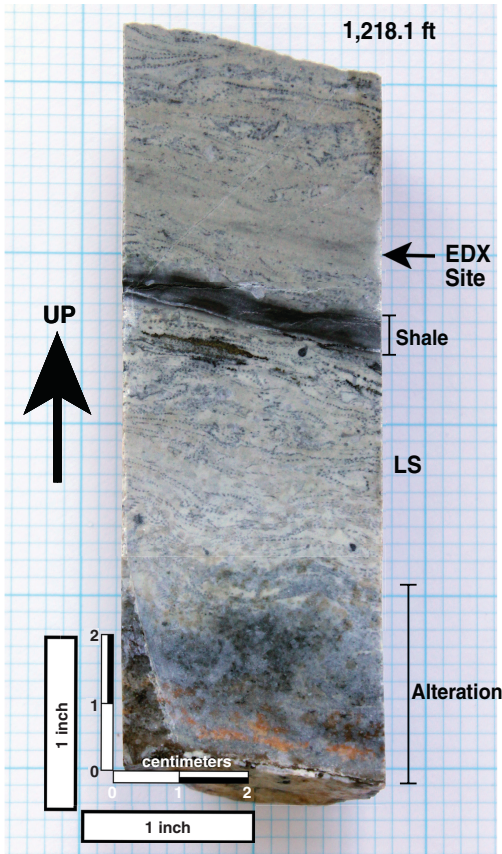


Figure A1 (Continued)





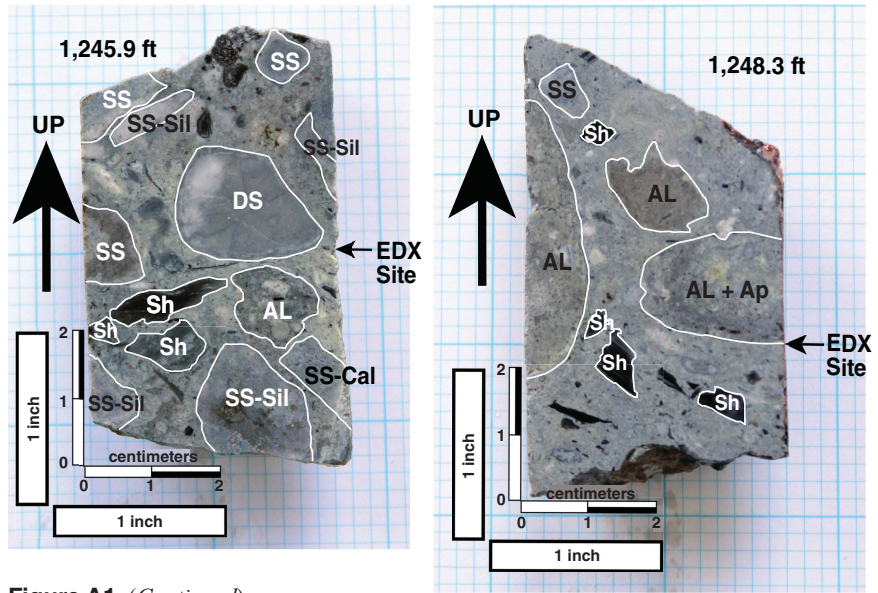
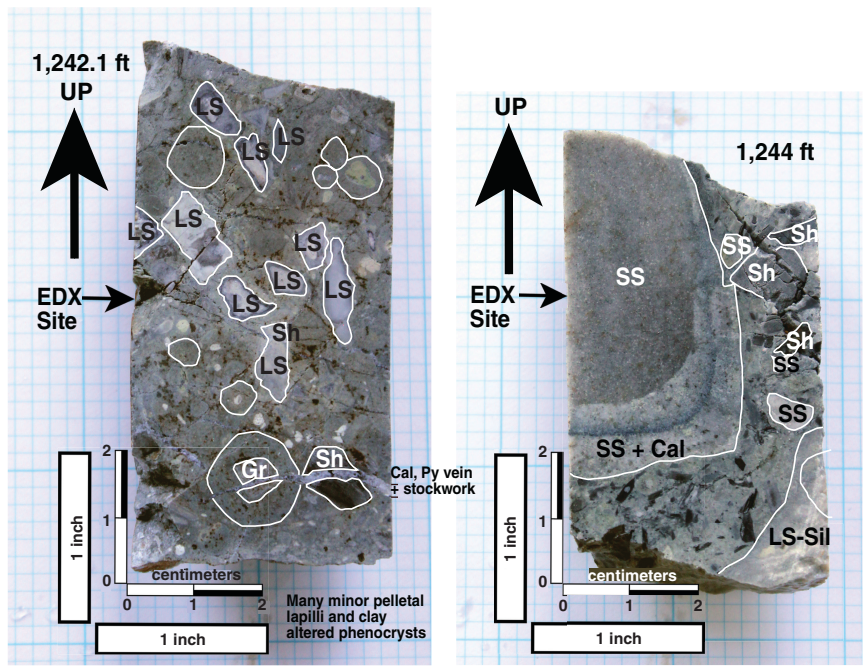


Figure A1 (Continued)

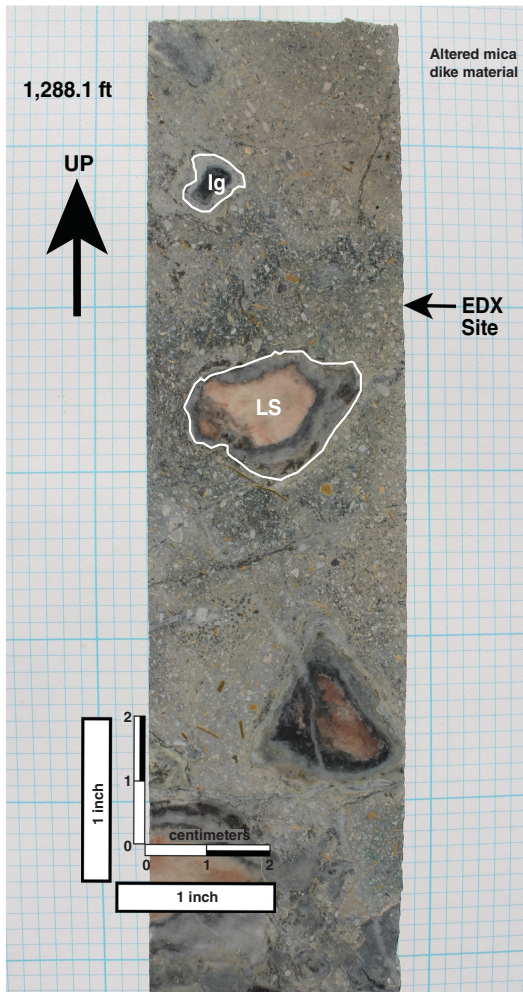
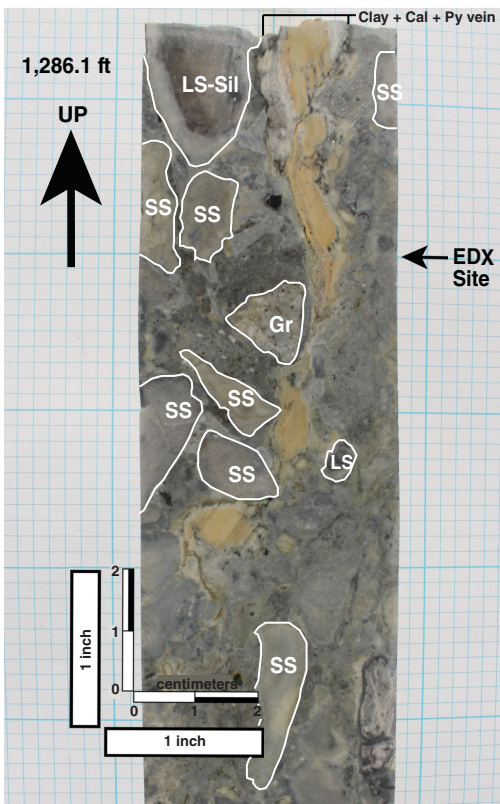
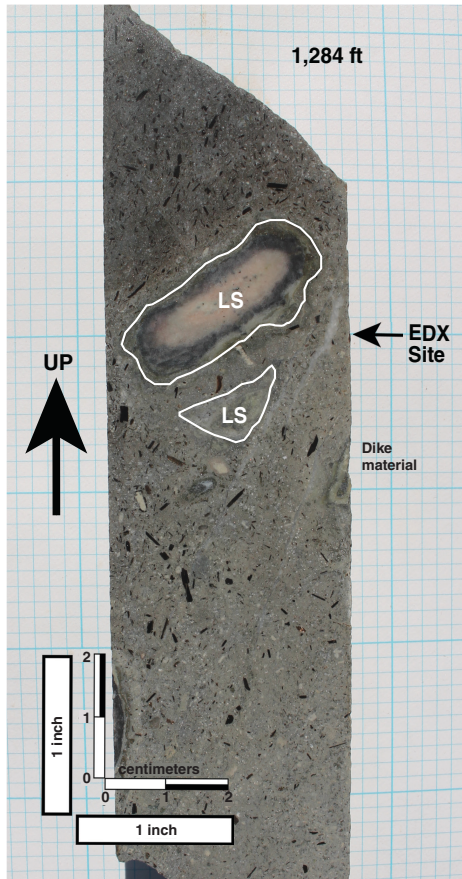
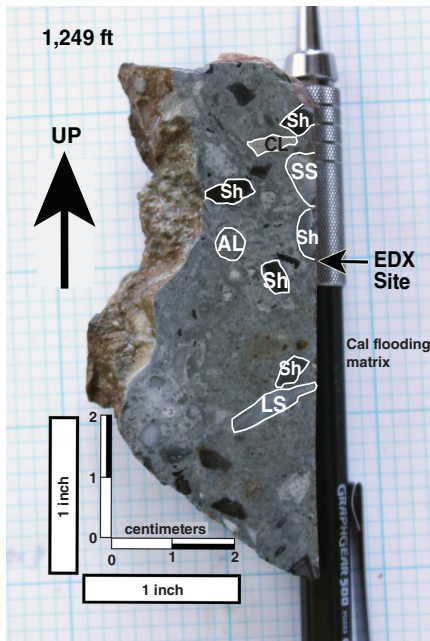


Figure A1 (Continued)

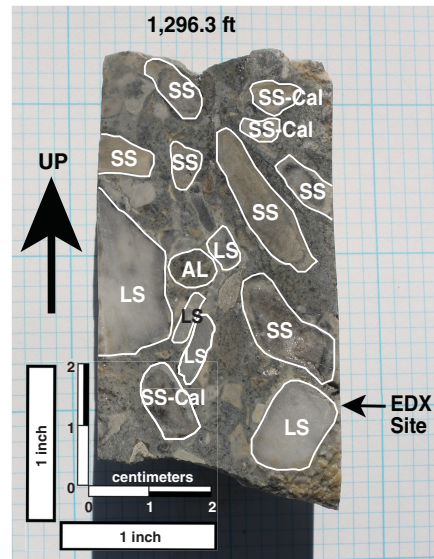
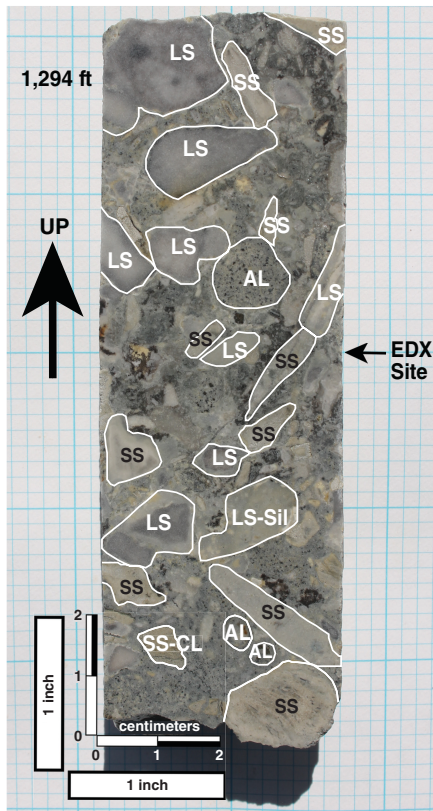
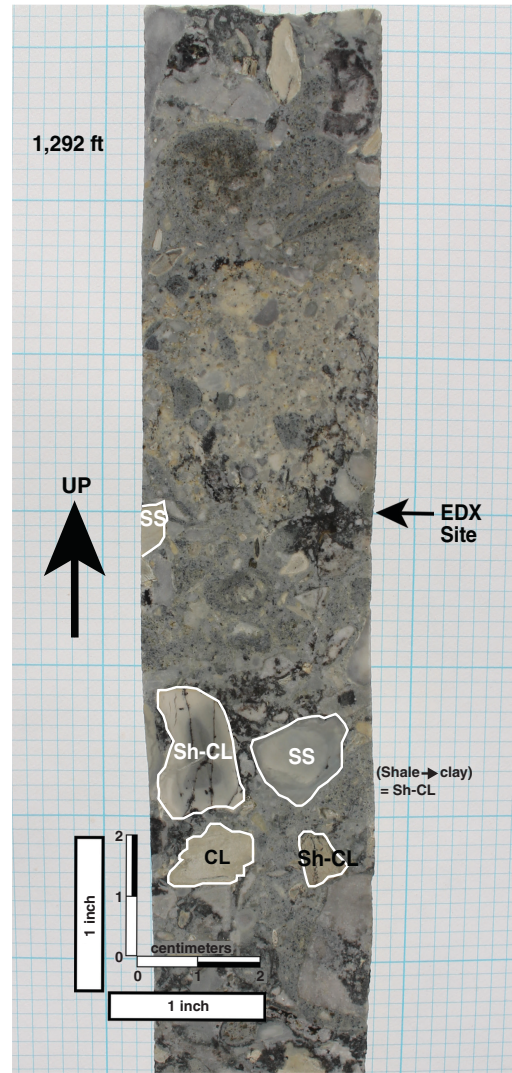
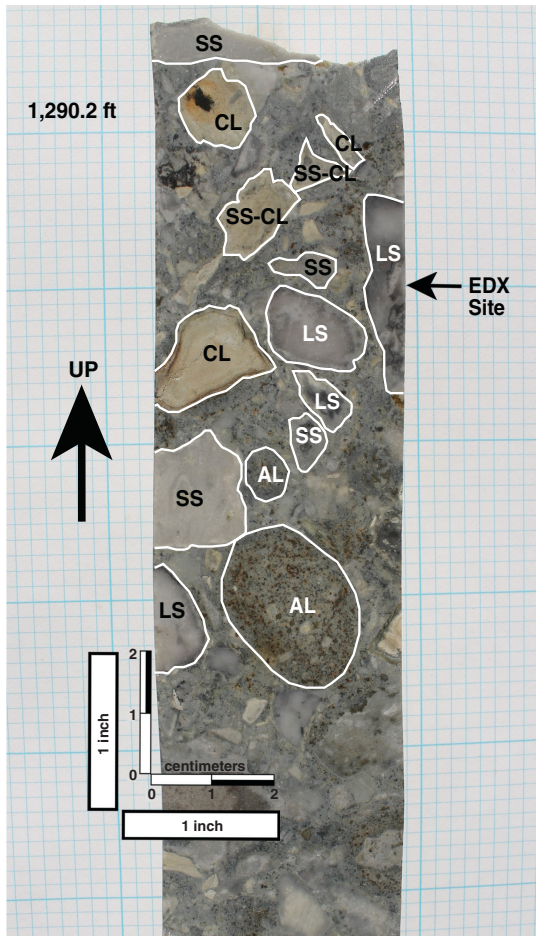


Figure A1 (Continued)

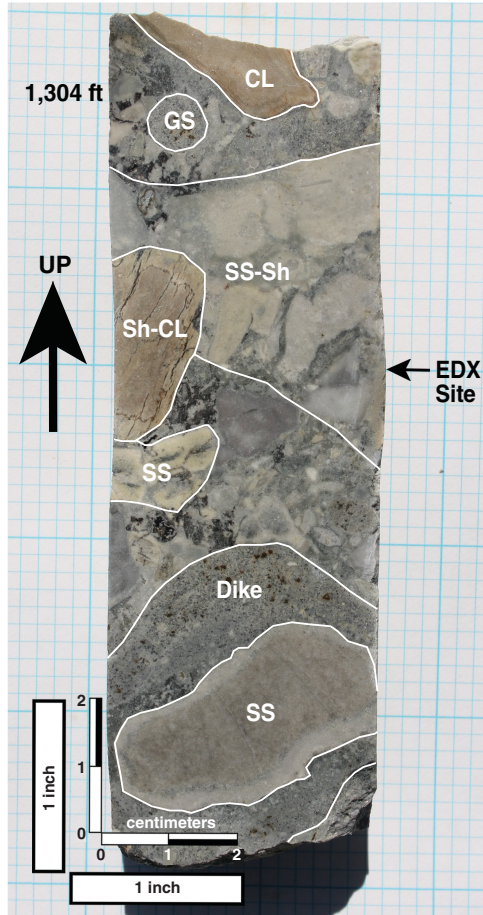
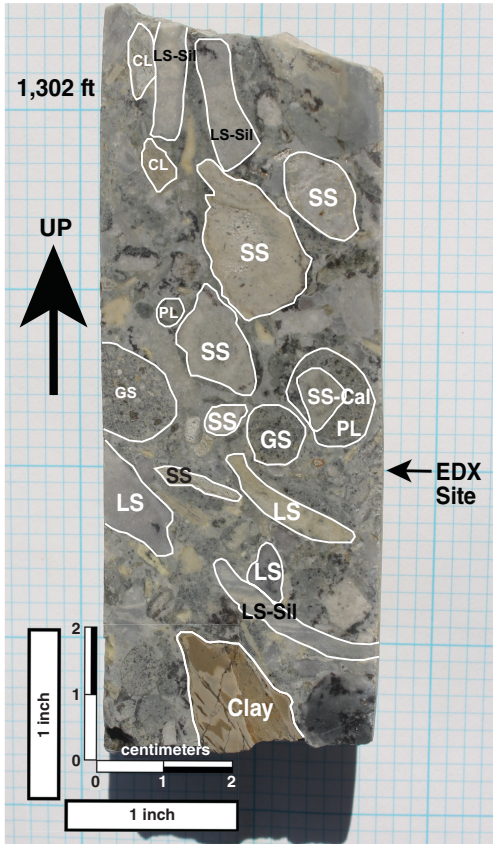
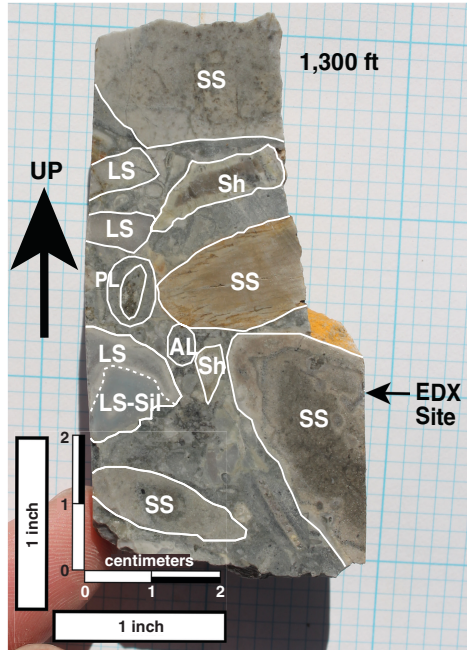
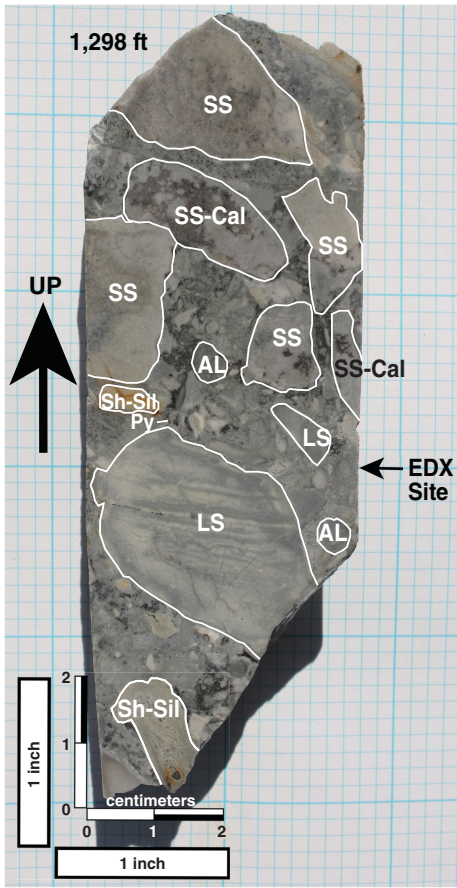


Figure A1 (Continued)

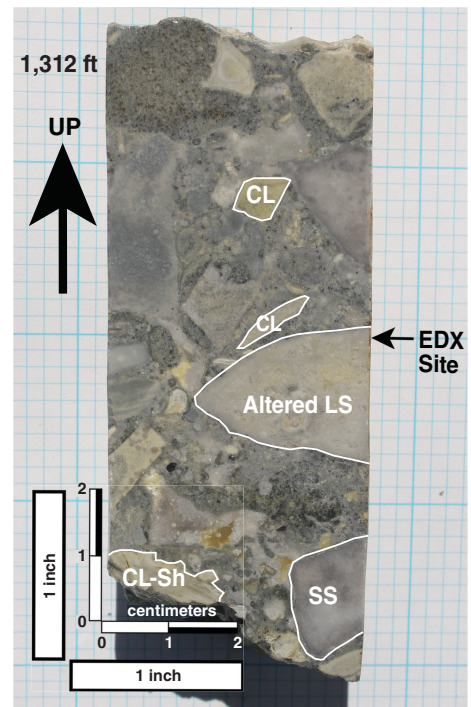
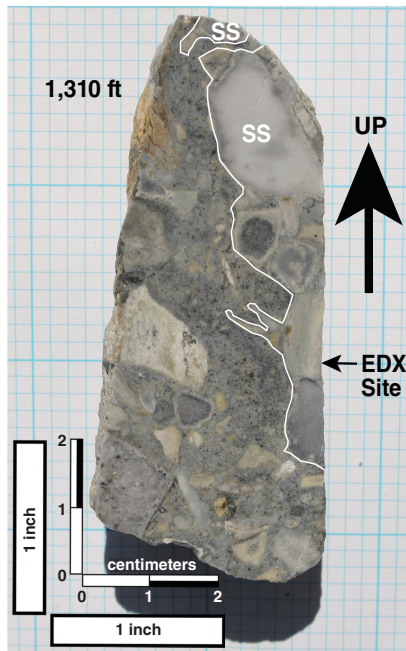
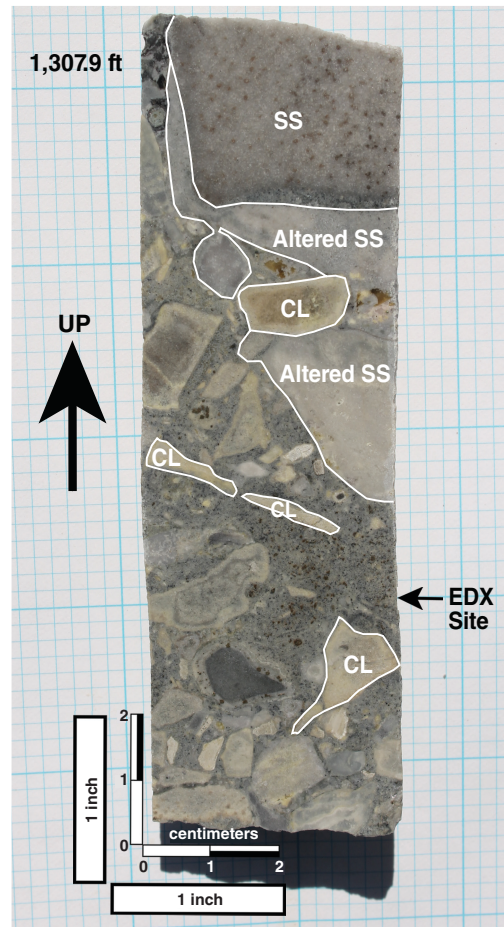
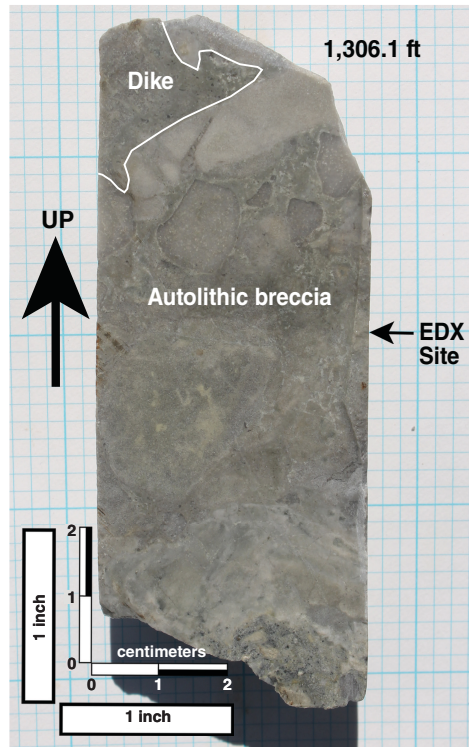


Figure A1 (Continued)

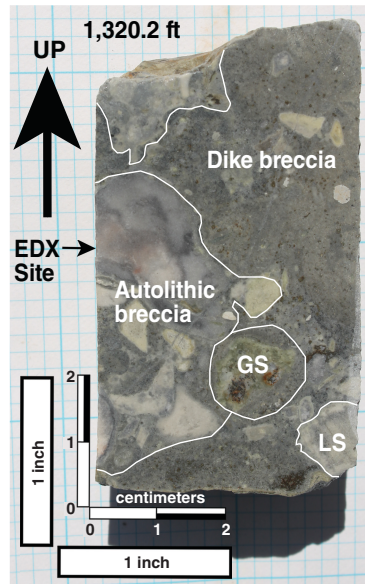
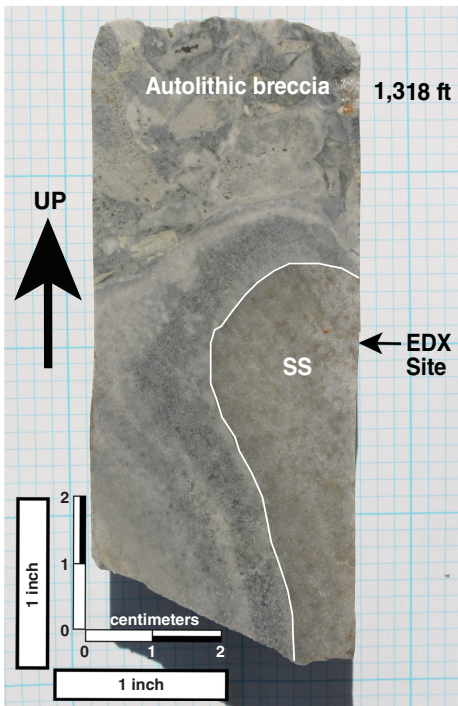
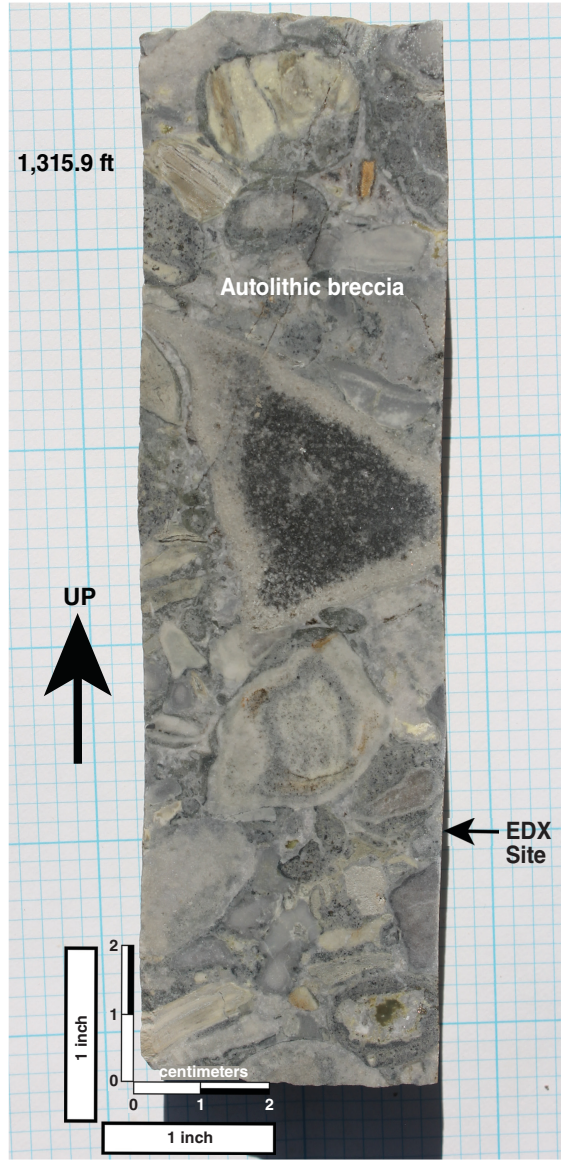
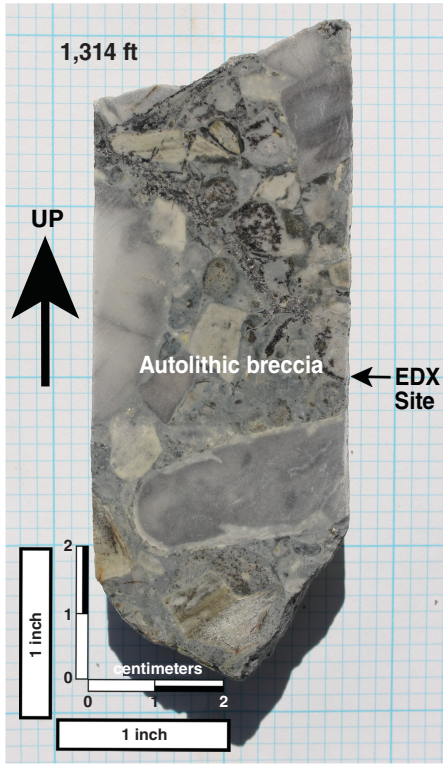


Figure A1 (Continued)

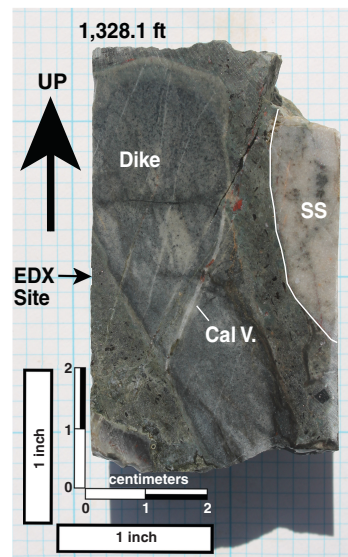
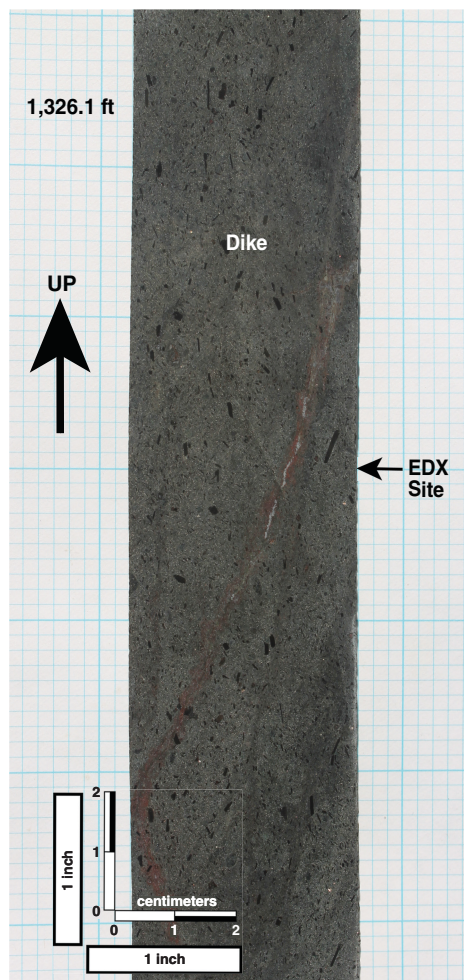
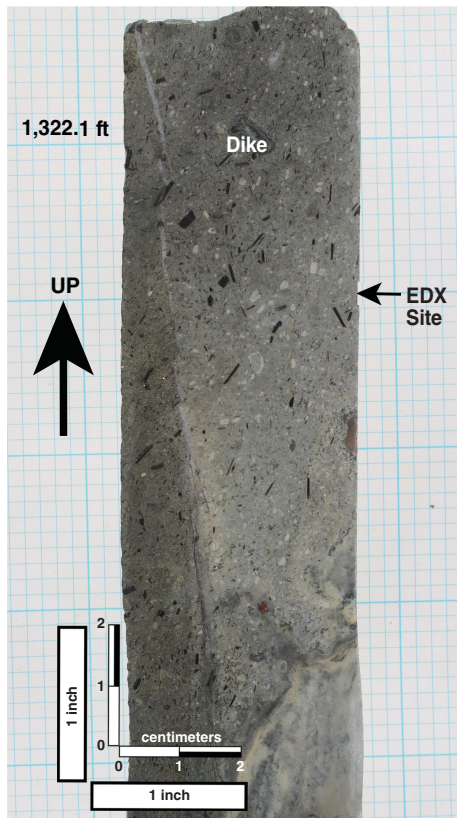


Figure A1 (Continued)

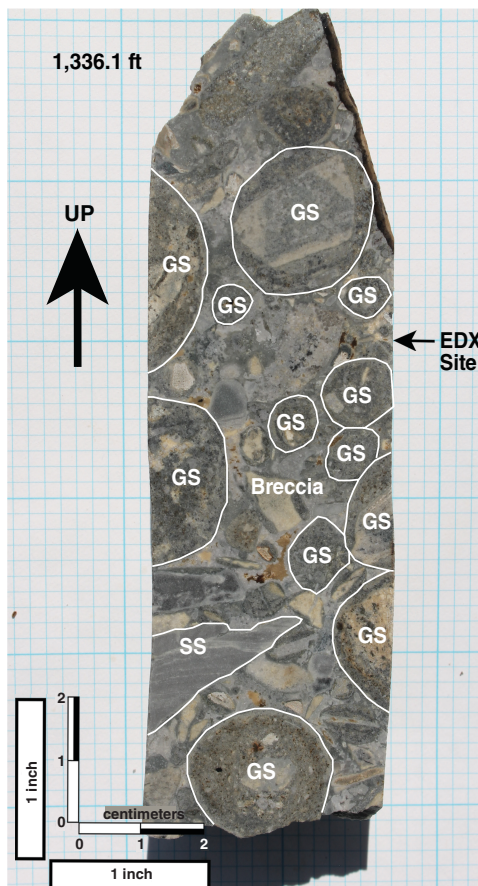
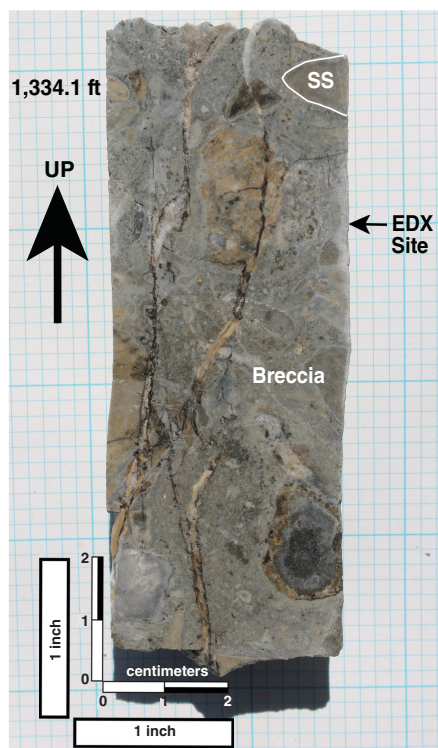
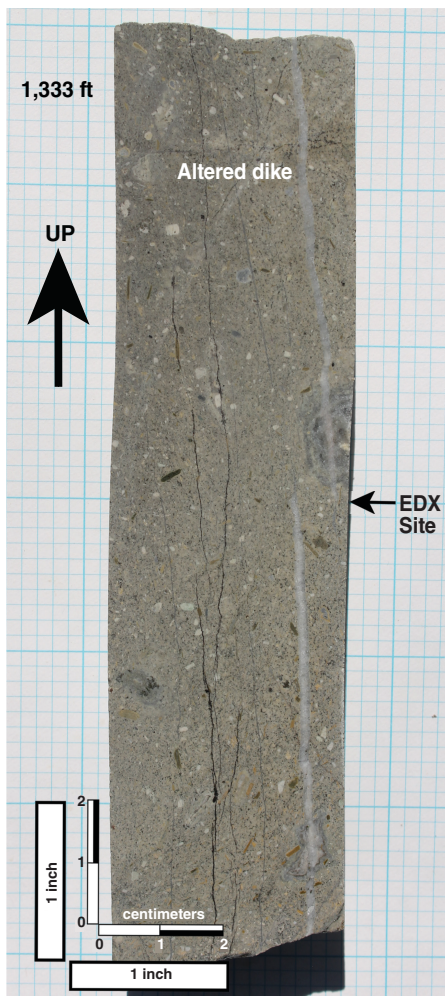
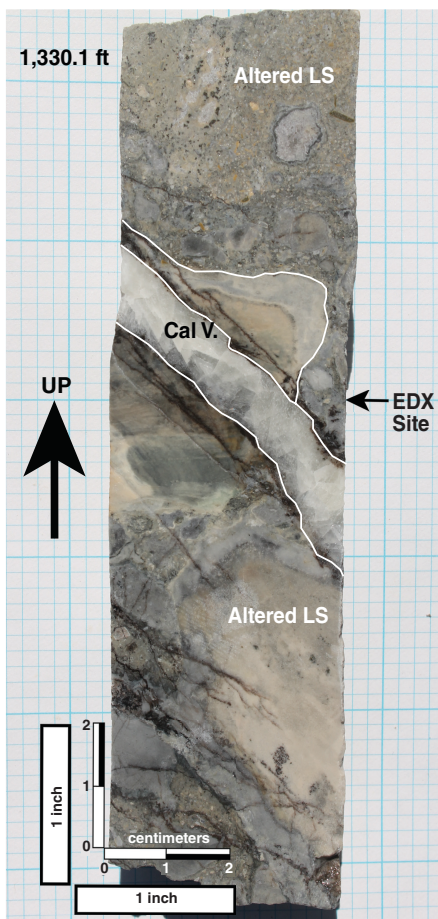


Figure A1 (Continued)

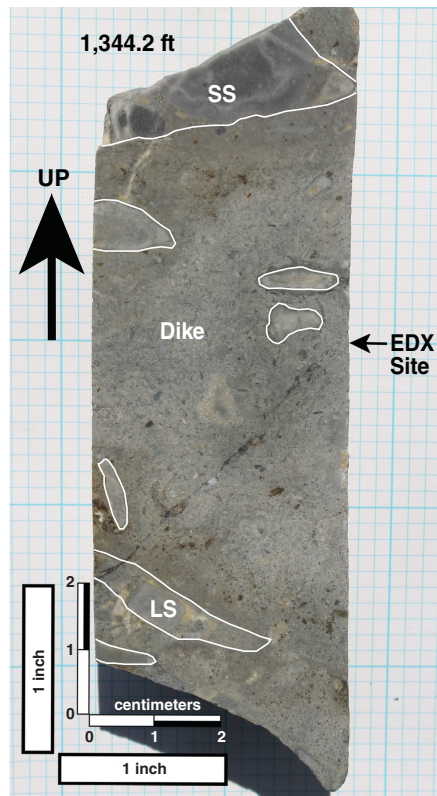
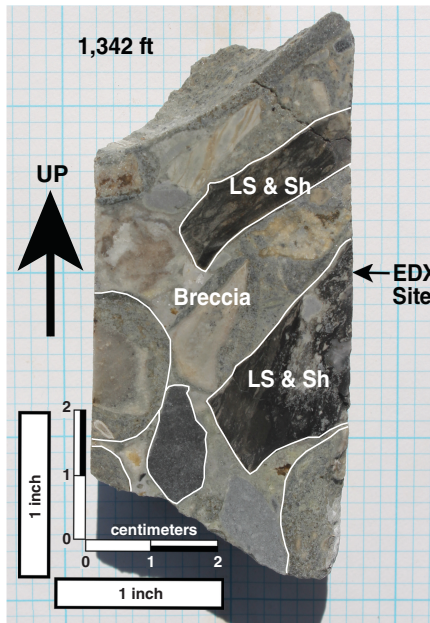
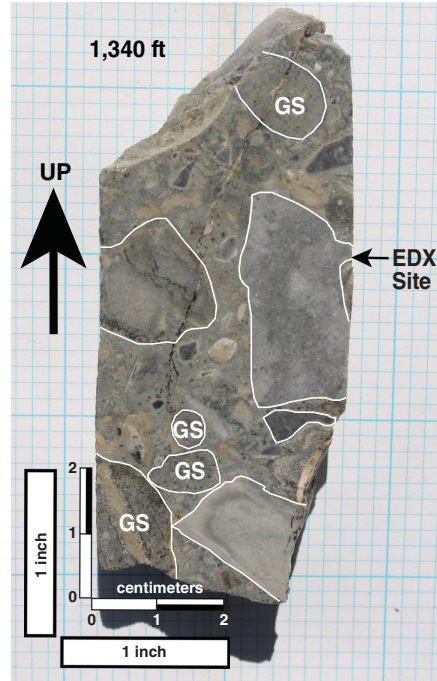
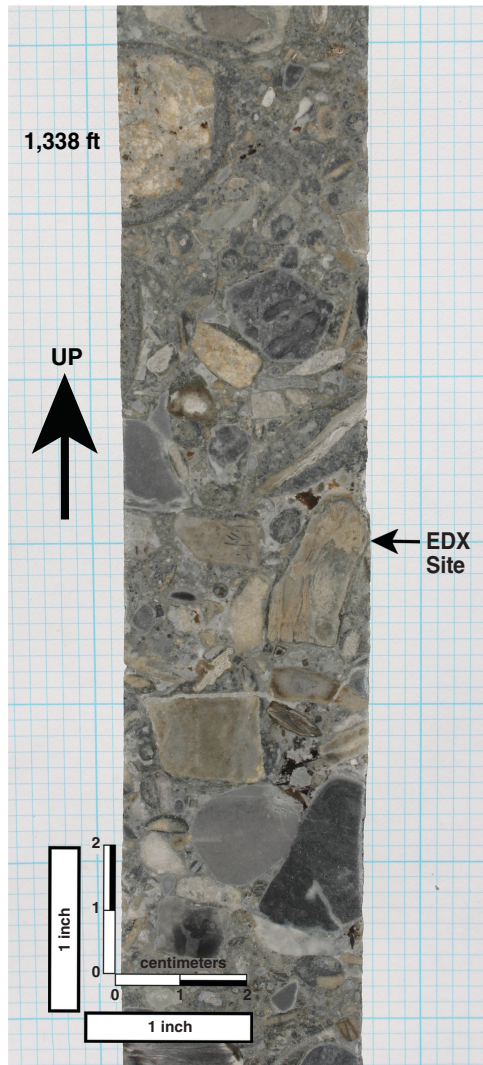


Figure A1 (Continued)

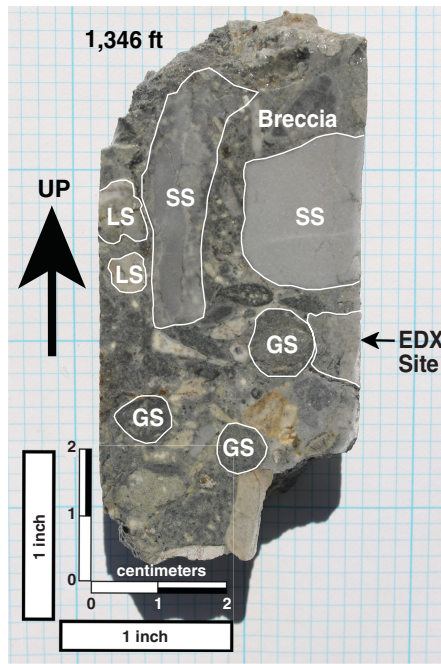


Figure A1 (Continued)

# APPENDIX 2



Figure A2 Graphic log of borehole USSH-3S. Data are from the core description by Ozark Mahoning Inc.



